

Electrospun nanofibers: An alternative sorbent material for solid phase extraction



A thesis submitted to Rhodes University in fulfilment of the requirements for
the degree of

Doctor of Philosophy (Science)

Samuel Chigome

Supervised by

Professor Nelson Torto

Dedication

To my parents Cornelius and Priscilla Chigome.

Acknowledgements

First and foremost, I would like to thank the Almighty God. For it is not because of my own wisdom or strength that I have managed to be where I am today but through his blessings.

I thank Prof Nelson Torto, my supervisor for providing the opportunity and resources to conduct fundamental research, paving the way for me to understand dynamic thinking in research (as you always said “*Research is all about ideas, if you have ideas you can make anything out of nothing*”), teaching me how to write research articles and above all, allowing me to grow as an individual for the benefit of my dream of becoming a world renowned researcher.

I would like to thank Prof Malik Maaza and the Materials research group at iThemba LABS where I started my electrospinning work.

Special thanks are due to the Andrew Mellon Foundation and the Chemistry Department at Rhodes University for funding and support.

I would like to thank past and present members of Prof Torto’s research group as well as all the visiting researchers/collaborators that I worked with.

Finally I would like to thank my family for all the support.

Abstract

The work described in the thesis seeks to lay a foundation for a better understanding of the use of electrospun nanofibers as a sorbent material.

Three miniaturised electrospun nanofiber based solid phase extraction devices were fabricated. For the first two, 10 mg of electrospun polystyrene fibers were used as a sorbent bed for a micro column SPE device (8 mm bed height in a 200 μl pipette tip) and a disk (I) SPE device (5 mm \times 1 mm sorbent bed in a 1000 μl SPE barrel). While for the third, 4.6 mg of electrospun nylon nanofibers were used as a sorbent bed for a disk (II) SPE device, (sorbent bed consisting of 5 \times 5 mm \times 350 μm stacked disks in a 500 μl SPE barrel).

Corticosteroids were employed as model analytes for performance evaluation of the fabricated SPE devices. Quantitative recoveries (45.5-124.29%) were achieved for all SPE devices at a loading volume of 100 μl and analyte concentration of 500 ng ml⁻¹. Three mathematical models; the Boltzmann, Weibull five parameter and the Sigmoid three parameter were employed to describe the break through profiles of each of the sorbent beds. The micro column SPE device exhibited a breakthrough volume of 1400 μl , and theoretical plates (7.98-9.1) while disk (I) SPE device exhibited 400-500 μl and 1.39-2.82 respectively. Disk (II) SPE device exhibited a breakthrough volume of 200 μl and theoretical plates 0.38-1.15. It was proposed that the formats of future electrospun nanofiber sorbent based SPE devices will be guided by mechanical strength of the polymer. The study classified electrospun polymer fibers into two as polystyrene type (relatively low mechanical strength) and nylon type (relatively high mechanical strength).

Publications

1. **Samuel Chigome** and Nelson Torto, “Electrospun nanofiber based solid phase extraction” *Under review to Trends in Analytical Chemistry*
2. **Samuel Chigome** and Nelson Torto, “Synthesis and characterisation of electrospun poly(styrene-co-acrylamide), poly(styrene-co-methacrylic acid) and poly(styrene-co-p-sodium styrene sulphonate) nanofibers” *In preparation for submission to Journal of Materials Chemistry*
3. **Samuel Chigome** and Nelson Torto, “A review of opportunities for electrospun nanofibers in analytical chemistry” *Analytica Chimica Acta* **2011**, 706, 25-36
4. **Samuel Chigome**, Godfred Darko and Nelson Torto, “Electrospun nanofibers as sorbent material for solid phase extraction” *Analyst* **2011**, 136, 2879-2889
5. Godfred Darko, **Samuel Chigome**, Zenixole Tshentu, Nelson Torto, “Enrichment of Cu(II), Ni(II), and Pb(II) in Aqueous Solutions Using Electrospun Polysulfone Nanofibers Functionalized with 1-[Bis[3-(Dimethylamino)-propyl]amino]-2-propanol” *Analytical Letters* **2011**, 44, 1855-1867
6. **Samuel Chigome**, Godfred Darko, Ulrich Buttner and Nelson Torto, “Semi-micro solid phase extraction with electrospun polystyrene fiber disks” *Analytical Methods* **2010**, 2, 623-626
7. **Samuel Chigome**, Adurafimihan Abiona, John Ajao, Jean Kana Kana, Lakhdar Guerbous, Nelson Torto, Malik Maaza, “Synthesis and characterization of electrospun poly (ethyleneoxide)/europium-doped yttrium orthovanadate (PEO/YVO₄:Eu³⁺) hybrid nanofibers” *International Journal of Polymeric Materials* **2010**, 59, 863-872
8. Adurafimihan Abiona, **Samuel Chigome**, John Ajao, Adeniyi Fasasi, Nelson Torto, Gabriel Osinkolu, Malik Maaza, “Synthesis and substrate-aided alignment of porphyrinated poly (ethylene oxide) (PEO) electrospun nanofibers” *International Journal of Polymeric Materials* **2010**, 59, 818-827
9. Adurafimihan Abiona, John Ajao, **Samuel Chigome**, Jean Kana Kana, Gabriel Osinkolu, Malik Maaza, “Synthesis and characterisation of cobalt chloride/ poly (ethylene oxide) (PEO) electrospun hybrid nanofibers” *Journal of Sol-Gel Science and Technology* **2010**, 55, 235-241
10. John Ajao, Adurafimihan Abiona, **Samuel Chigome**, Jean Kana Kana, Malik Maaza, “Preparation and characterization of electrospun poly (2, 5-dicyclohexylphenylene-1, 4-ethynylene) (C₂₄H₃₀)_n /poly(ethylene oxide) (PEO) hybrid nanofibers ” *Journal of Materials Science* **2010**, 45, 713-718
11. John Ajao, Adurafimihan Abiona, **Samuel Chigome**, Adeniyi Fasasi, Gabriel Osinkolu, Malik Maaza, “Electric-magnetic field-induced aligned electrospun poly (ethylene oxide) (PEO) nanofibers ” *Journal of Materials Science* **2010**, 45, 2324-2329

Table of contents

Dedication.....	i
Acknowledgements	ii
Abstract.....	iii
Publications	iv
Table of contents	v
List of Abbreviations.....	vi
List of Figures.....	x
List of Schemes	xiii
List of Tables.....	xiv
Chapter 1	1
1. Analytical chemistry.....	1
1.1 Developmental trends in analytical chemistry	1
Chapter 2	5
2. A review of sorbent based sample preparation techniques.....	5
2.1 Sample preparation.....	5
2.2 Sorption.....	6
2.3 Solid phase extraction (SPE).....	10
2.4 Solid phase micro extraction (SPME).....	28
Chapter 3	41
3. A review of electrospun nanofibers as sorbent material for solid phase extraction ...	41
3.1 Optimal sorbent and sorbent fabrication technique	41
3.2 Electrospinning	43
3.3 Scope of the thesis.....	68
Chapter 4	70
4. Experimental.....	70
4.1 Materials and equipment.....	70
4.2 Electrospinning set-ups	72
4.3 Copolymerisation	72
4.4 Electrospinning	73
4.5 Fabrication of SPE devices	77
4.6 SPE experiments	79
Chapter 5	82
5. Results and discussion	82
5.1 Electrospinning set-up designs.....	82
5.2 Copolymer synthesis and characterisation	95
5.3 Electrospinning of copolymers	110
5.4 Solid phase extraction devices	121
Chapter 6	161
6. Conclusions and further work.....	161
6.1 Conclusions	161
6.2 Further work.....	162
References	164

List of Abbreviations

ACNFs	Activated carbon nanofibers
ATR	Attenuated Total Reflection
BSA	Bovine Serum Albumin
CAR	Carboxen
CFs	Carbon fibers
CD	Cyclodextrin
CB	Cibacron blue F3GA
CNFs	Carbon nanofibers
CNTs	Carbon nanotubes
CW	Carbowax
DAD	Diode Array Detector
DC	Direct Current
DCM	Dichloromethane
DPX	Disposable pipette tip extraction
DVB	Divinylbenzene
DADPA	Diaminodipropylamine
DMF	<i>N,N</i> -dimethylformamide

DMSO	Dimethylsulfoxide
2,4-D	2,4-dichlorophenoxyacetic acid
EDC s	Endocrine disrupting compounds
FTIR	Fourier Transform Infrared
GPC	Gel permeation chromatography
GC	Gas Chromatography
GCB	Graphitized Carbon Black
GC-MS	Gas chromatography-Mass spectrometry
HPLC	High Performance Liquid Chromatography
LLE	Liquid-Liquid Extraction
LSE	Liquid Solid Extraction
LC	Liquid Chromatography
MALDI	Matrix assisted laser desorption
MS/MS	Tandem mass spectrometry
MEPS	Micro extraction packed sorbent
MISPE	Molecularly Imprinted Solid Phase Extraction
MIPs	Molecularly imprinted polymers
MWCNTs	Multiwalled Carbon nanotubes
NMR	Nuclear Magnetic Resonance

NTD	Needle trap devices
PA	Polyacrylate
PAN	Polyacrylonitrile
PET	Polyethylene terephthalate
PEO	Polyethylene oxide
PDMS	Polydimethylsiloxane
PGC	Porous Graphitic Carbon
PS-DVB	Polystyrene divinyl benzene
PLA	Polylactic acid
PS	Polystyrene
PSU	Polysulfone
PMCM	Poly [3-(trimethoxysilyl) propylmethacrylate]
PTFE	Polytetrafluoroethylene
PVA	Polyvinyl alcohol
PU	Polyurethane
PVC	Polyvinyl chloride
RAMs	Restricted access materials
SEM	Scanning electron microscope
SBSE	Stir bar sorptive extraction

SME	Solid Membrane Extraction
SPDE	Solid phase dynamic extraction
SPE	Solid Phase Extraction
SPME	Solid Phase Micro extraction
SIMS	Secondary ion mass spectrometry
S/N	Signal to Noise ratio
SWNTs	Single walled carbon nanotubes
TEOS	Tetraethyl orthosilicate
TFME	Thin Film Membrane Extraction
TGA	Thermogravimetric Analysis
ToF	Time of flight
TPR	Template resin
TLC	Thin layer chromatography
UV	Ultraviolet
VOCs	Volatile organic compounds
XPS	Xray photoelectron spectroscopy

List of Figures

Fig.1.1	Block diagram of an instrumental analytical chemistry process.....	2
Fig.2.1	Schematic representation of an extraction processes.....	7
Fig.2.2	Schematic representation of porous regions of a sorbent.	10
Fig.2.3	Representation of an unbounded silica particle.	14
Fig.2.4	Cross-linked polystyrene divinylbenzene copolymer.....	16
Fig.2.5	Schematic representation of a restricted access material sorbent particle	18
Fig.2.6	Schematic representation of an immunosorbent binding an analyte.....	19
Fig.2.7	Schematic representation of the preparation of molecular imprints.	21
Fig.2.8	Schematic diagrams of cartridge SPE devices.....	22
Fig.2.9	Schematic diagrams of disk sorbent beds.	23
Fig.2.10	Schematic representation of flow paths through sorbent beds.....	24
Fig.2.11	Schematic diagram of disk microtiter plates.....	25
Fig.2.12	Representation of a MEPS syringe from SGE Analytical Science.....	26
Fig.2.13	Schematic diagram of a disposable pipette tip extraction device	28
Fig.2.14	Schematic representation of the components of a fiber SPME device	29
Fig.2.15	Schematic representation of the three modes of SPME operation.....	31
Fig.2.16	Schematic diagram of a SBSE device.....	37
Fig.2.17	Schematic diagram of a SPDE device.....	38
Fig.2.18	Schematic representation of a blunt tip needle trap device.....	39
Fig.2.19	Schematic representation of a TFME device	40
Fig.3.1	Schematic representation of the basic components of an electrospinning set-up ...	43
Fig.3.2	Schematic representation of the Taylor cone formation	44
Fig.3.3	Schematic diagram of a bottom up multiple needle electrospinning set-up	45
Fig.3.4	Free liquid surface electrospinning from a rotating electrode	46
Fig.3.5	Large scale production of a nanofiber sheet by nozzle-less electrospinning line...	46
Fig.3.6	TEM image showing a SWNT bundle embedded in a PS nanofiber.....	52
Fig.3.7	TEM images of carbon nanotube embedded electrospun PAN and PLA nanofibers	53
Fig.3.8	Schematic representation of the electrospun PSU nanofiber surface modification procedure	61
Fig.3.9	SEM image of MIP nanoparticle embedded electrospun PET nanofibers.....	62
Fig.3.10	Schematic representation of molecularly imprinted nanofibers with binding sites specific for 2,4-D template molecules	63
Fig.3.11	Electrospun fiber disk SPE device connected to a vacuum manifold.....	64
Fig.3.12	The fiber-filter solid-phase extraction device	65
Fig.3.13	Representation of a micro-column SPE device	66
Fig.3.14	Schematic diagram of a micro column SPE device connected to a vacuum manifold.....	66
Fig.3.15	SEM image of a electrospun fiber coated SPME device	67
Fig.4.1	Photograph of boiling medium emulsion polymerisation set-up.....	73
Fig.4.2	Representation of the disk (II) SPE device fabrication process	78
Fig.4.3	Representation of solvent flow through SPE sorbent beds.	79
Fig.4.4	Syringe pump driven semi-automated system.	81
Fig.5.1	Numerical model simulation of an electrospinning jet	83
Fig.5.2	Schematic representation of the magnetic field effect electrospinning set-up.....	85
Fig.5.3	Schematic representation of the proposed electric field profile.....	87

Fig.5.4 Schematic representation of a collector geometry effect electrospinning set-up....	89
Fig.5.5 Representation of rotating collector electrospinning set-ups.....	91
Fig.5.6 Deposition patterns on rotating collectors.....	93
Fig.5.7 SEM images of electrospun nanofibers collected at different rotation speeds.....	94
Fig.5.8 FTIR comparison of polystyrene copolymers synthesised from different mole ratios of styrene: methacrylic acid.....	102
Fig.5.9 FTIR comparison of polystyrene copolymers synthesised from different mole ratios of styrene: acrylamide.....	104
Fig.5.10 FTIR comparison of polystyrene copolymers synthesised from different mole ratios of styrene: <i>p</i> -sodium styrene sulfonate.....	106
Fig.5.11 TGA thermograms of different mole ratios styrene:acrylamide.....	108
Fig.5.12 TGA thermograms of different mole ratios of styrene: <i>p</i> -sodium styrene sulphonate.....	109
Fig.5.13 TGA thermograms of different mole ratios of styrene:methacrylic acid.....	110
Fig.5.14 SEM images for fibers spun from different mole ratios of styrene:methacrylic acid.....	111
Fig.5.15 SEM images for β -cyclodextrin treatment of poly (styrene-co-methacrylic acid) fibers.....	113
Figure.5.16 Representation of β -cyclodextrin cross linked.....	114
Fig.5.17 SEM images of electrospun poly (styrene-co-methacrylic acid) fibers spun from different concentrations.....	117
Fig.5.18 Effect of polymer solution concentration on fiber diameter.....	118
Fig.5.19 SEM images for fibers spun from different mole ratios of styrene: <i>p</i> -sodium styrene sulphonate.....	119
Fig.5.20 SEM images for fibers spun from different mole ratios of styrene:acrylamide.....	121
Fig.5.21 Representation of micro column SPE device and sorbent bed.....	124
Fig.5.22 Representation of disk (I) SPE device and sorbent bed.....	125
Fig.5.23 Chemical structures of corticosteroids and Polystyrene.....	127
Fig.5.24 Effect of sorbent packing format and sorbent mass on recoveries in water for disk (I) and micro column SPE devices.....	128
Fig.5.25 Disk sorbent bed recoveries in plasma at different concentrations.....	129
Fig.5.26 Breakthrough curves determined for four steroids on the electrospun polystyrene fiber disks plotted using the Boltzmann model.....	135
Fig.5.27 Breakthrough curves determined for the four steroids on the electrospun polystyrene fiber disk sorbent bed presented lines of best fit using sigmoid three parameter model.....	138
Fig.5.28 Chemical structures for corticosteroids polystyrene.....	140
Fig.5.29 Comparison of breakthrough curves for disk (I) and micro column sorbent bed formats.....	141
Fig.5.30 Breakthrough curves determined for two steroids on electrospun polystyrene fibers packed in micro column sorbent bed format presented as lines of best fit using the sigmoid Weibull five parameter model.....	144
Fig.5.31 Breakthrough curves determined for two steroids on electrospun polystyrene fibers packed in micro column sorbent bed format presented as lines of best fit using the sigmoid Boltzmann model.....	146
Fig.5.32 Photograph of an electrospun nylon 6 nanofiber mat showing regions from which disks were cut out.....	148
Fig.5.33 Chemical structures for corticosteroids and Nylon 6.....	150
Fig.5.34 Representation of disk (II) SPE device and SEM images of electrospun nylon nanofiber polyamide filtration membrane sorbent beds.....	151

Fig.5.35 SPE curve profile and analyte recoveries for a polyamide filtration membrane disk sorbent bed arranged in sandwich format.	153
Fig.5.36 SPE curve profile and analyte recoveries for a polyamide filtration membrane disk sorbent bed arranged in base format.	154
Fig.5.37 SPE curve profile and analyte recoveries for a nylon 6 nanofiber disk sorbent bed arranged in sandwich format.	156
Fig.5.38 SPE curve profile and analyte recoveries for a nylon 6 nanofiber disk sorbent bed arranged in base format.	158
Fig.5.39 SPE curve profile and analyte recoveries for a nylon 6 nanofiber disk sorbent bed arranged in base format.	158
Fig.5.40 Breakthrough curves determined for 3 steroids on commercial polyamide membrane disk sorbent bed format represented as lines of best fit using the sigmoid three parameter model.	160
Fig.5.41 Breakthrough curves determined for 3 steroids on electrospun nylon 6 nanofiber disk sorbent bed format represented as lines of best fit using the sigmoid three parameter model.	162

List of Schemes

Scheme.3.1 Schematic representation of synthesis and molecular structure of the porphyrin copolymers.....	58
Scheme.4.1 Flow diagram for the solid phase extraction protocol.	79

List of Tables

Table.2.1 Energies of interaction mechanisms.	8
Table.3.1 Some electrospinning companies established in the last decade.	48
Table.4.1 Electrospinning conditions for poly (styrene-co-methacrylic acid) copolymers at different mole ratios.	74
Table.4.2 Electrospinning conditions for poly (styrene-co-acrylamide) copolymers at different mole ratios.	75
Table.4.3 Electrospinning conditions for poly(styrene-co- <i>p</i> -sodium styrene sulphonate) copolymers at different mole ratios.	76
Table.4.4 Electrospinning conditions for commercial polymers.	77
Table.5.1 Solubility studies of synthesized poly (styrene-co-methacrylic acid) copolymer at different mole ratios of styrene to methacrylic acid.	98
Table.5.2 Solubility studies of synthesized poly (styrene-co-acrylamide) copolymer at different mole ratios of styrene to acrylamide.	99
Table.5.3 Solubility studies of synthesized poly (styrene-co- <i>p</i> -sodium styrene sulphonate) copolymer at different mole ratios of styrene to <i>p</i> -sodium styrene sulphonate.	100
Table.5.4 SEM results summary for electrospun poly (styrene-co-methacrylic acid) fibers at different mole ratios.	114
Table.5.5 Summary of the behaviour of β -cyclodextrin doped poly (styrene-co-methacrylic acid) fibers in methanol and water.	115
Table.5.6 Behaviour of selected mole ratios of electrospun poly (styrene-co-methacrylic acid) fibers in SPE solvents.	115
Table.5.7 SEM results summary for electrospun poly (styrene-co- <i>p</i> -sodium styrene sulphonate) fibers at different mole ratios.	119
Table.5.8 Behaviour of selected mole ratios of electrospun poly (styrene-co- <i>p</i> -sodium styrene sulfonate) fibers in SPE solvents.	120
Table.5.9 SEM results summary for electrospun poly (styrene-co-acrylamide) fibers at different mole ratios.	122
Table.5.10 Behaviour of selected mole ratios of electrospun poly (styrene-co-acrylamide) fibers in SPE solvents.	122
Table.5.11 Analytical parameters for polystyrene microfiber disks.	130
Table.5.12 Chromatographic parameters of the electrospun polystyrene fiber based disk sorbent bed derived from the Boltzmann model.	136
Table.5.13 Chromatographic parameters of the electrospun polystyrene fiber based disk sorbent bed derived from the sigmoid three parameter model.	139
Table.5.14 Chromatographic parameters of the electrospun polystyrene fiber based micro column sorbent bed format derived from the sigmoid Weibull five parameter model.	145
Table.5.15 Chromatographic parameters of the electrospun polystyrene fiber based micro column sorbent bed format derived from the sigmoid Boltzmann model.	147
Table.5.16 Chromatographic parameters for the polyamide filtration membrane disk sorbent bed.	161
Table.5.17 Chromatographic parameters for the electrospun nanofiber disk sorbent bed.	163

Chapter 1

1. Analytical chemistry

Summary

This chapter provides a brief overview of the developmental trends in analytical chemistry classified into two as “instrumental analytical chemistry” and “materials analytical chemistry”. It aims to demonstrate the need for more research efforts to be channelled towards the materials analytical chemistry component.

1.1 Developmental trends in analytical chemistry

Analytical chemistry can be viewed from the perspective of an “analytical process” which can be split into three components as; sample preparation (low resolution separation), separation (high resolution) and detection [1]. Over the years, each component has been faced with various challenges associated with analyte and matrix complexities which have driven researchers to continuously seek ways to improve the analytical process [2-11].

Instrumental analytical chemistry can be viewed as being that area of analytical chemistry that relies on analyte or sample perturbation in the form of light (Spectroscopic techniques), heat (Thermal techniques), current or voltage (Mass spectrometry and electrochemical techniques) to derive quantitative or qualitative information. Fig.1.1 shows a schematic representation of an instrumental analytical chemistry process showing the stimuli, sample/analyte and signal processing.

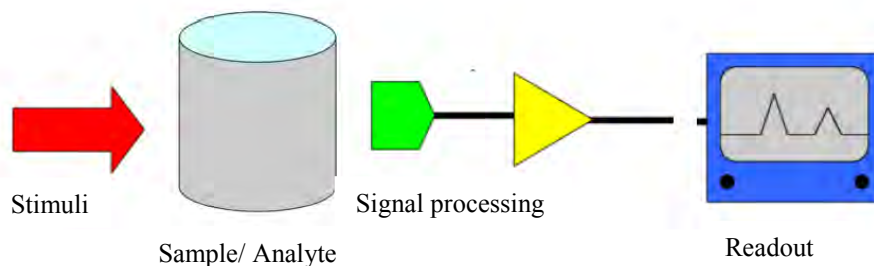


Fig.1.1 Block diagram of an instrumental analytical chemistry process.

Materials analytical chemistry can be viewed as being that area of analytical chemistry that relies on analyte-material structure bonding relationships to derive quantitative and qualitative information. The interaction of the analyte with the material results in a change in a measurable signal which can be electronic, electromagnetic or thermal.

Advances in electronics and computer technologies have led to significant developments in instrumental analytical chemistry research as evidenced by increased automation, fast data processing speeds and highly sensitive detection systems [12]. On the contrary, materials analytical chemistry research seems to have developed at a slower pace.

The advent of nanotechnology was a major leap forward in materials analytical chemistry research as it resulted in a new class of materials with nanodimensions. The main benefit of nanomaterials is their large specific surface area as it provides platforms with an increased number of sites for analyte interaction [13, 14].

In principle, nanoscale phenomena have been employed well before the advent of nanotechnology, a notable example is electrospinning, a nanofabrication technique that is almost a 100 years old [15]. However, what distinguishes the current use of nanoscale phenomena is the level of understanding of the great potential that they hold. This has been

brought about by the need to address new and emerging challenges from all sectors of industry, science and technology.

Nanostructured materials have made it possible to develop miniaturised and more efficient devices for the analytical process. Thus, it is not surprising that over the last decade there have been quite a number of reports on the use of nanostructured materials for different aspects of the analytical process [16-25]. Given the fact that nanostructured materials have demonstrated superior performance, it can be said with some degree of confidence that they will continue to dominate the materials analytical chemistry development sector for an extended period of time. Therefore, the research direction that may be taken could focus on the search for new materials with respect to chemical composition as well as alternative material fabrication techniques at the nanoscale.

This thesis focuses on adding value to the analytical process from the “materials analytical chemistry” perspective; specifically focussing on the use of electrospun nanofibers as an alternative sorbent material for solid phase extraction.

Given the fact that all sorbent-analyte interactions rely on the same intermolecular mechanisms governing chromatographic processes, an in-depth understanding of a sorbent material functionality and morphology is vital for optimal chromatography. Therefore, nanomaterials research from the chromatographer’s perspective could result in useful knowledge for the whole analytical process.

Chapter 2 presents a review of developmental trends in sorbent based sample preparation techniques focussing on solid phase extraction and solid phase microextraction.

Chapter 3 presents a review of literature discussing the potential of electrospinning as a sorbent fabrication technique as well as the potential of the resultant fibers. The chapter

forms the basis upon which the background is provided for setting the specific study objectives.

Chapter 4 presents the experimental protocols employed in the study.

Chapter 5 presents and discusses results obtained in the study.

Chapter 6 concludes the research findings and proposes future experimental approaches in electrospun nanofiber based sorbent research.

Chapter 2

2. A review of sorbent based sample preparation techniques

Summary

This chapter gives an overview of the developmental trends of sorbent based sample preparation techniques. The sorbent based techniques relevant to the thesis have been classified into two as solid phase extraction (SPE) and solid phase micro extraction (SPME). For each class, three aspects are addressed which are; (i) fundamental principles (ii) sorbent material types and (iii) device formats and configurations.

2.1 Sample preparation

The sample preparation step is crucial in the analytical process for two main reasons which are;

1. Transformation of the sample into a form that is suitable for instrumental analysis.
2. Matrix simplification which includes; sample clean up and analyte preconcentration to afford low analyte detection limits.

Despite the fact that the sample preparation step is important, it remains a bottleneck as it accounts for a significant percentage of the time spent on the analytical process. Since sample preparation may not be eliminated, research efforts have been focused on ways to minimise its contribution to the time spent on the analytical process. For example; miniaturisation of sample preparation techniques, development of miniaturised analytical devices that integrate sample preparation, separation and detection on a single platform (lab on chip devices) and the development of analytical systems that achieve direct analyte detection [11].

Recently [26-29], sample preparation trends have been towards:

- Developing the capacity to use smaller initial sample sizes even for trace analyses.
- Greater specificity or selectivity in extraction.
- Increased potential for automation or for online methods.
- Reduction or elimination of organic solvents as an environmental concern.

It is evident that traditional liquid-liquid extraction (LLE) does not fulfil most of the current sample preparation requirements, thus sorbent based sample preparation techniques have become more popular in analytical laboratories. One of the main benefits of sorbent based techniques is the availability of an ever increasing range of sorbent chemistries based on inorganic oxides, bonded phases of polymers, silica and carbon as well as analyte or group selective (ion exchange, mixed mode, restricted access, immunoaffinity and molecularly imprinted polymer) materials [30-36].

2.2 Sorption

Sorption can be defined as a process by which a substance (sorbate) is sorbed (adsorbed or absorbed) on or into another substance (sorbent) [37]. In the sample preparation context, the term sorbent refers to the solid extracting phase, including solid-supported liquid phases upon which an analyte is retained. Schwarzenbach and co-workers [38] make a distinction between absorption meaning into a three dimensional matrix, and adsorption as meaning onto a two dimensional surface. Fig 2.1 shows a schematic representation of analyte adsorption (analyte accumulation onto the sorbent surface) and absorption (analyte accumulation into the bulk of the sorbent) type extraction mechanism.

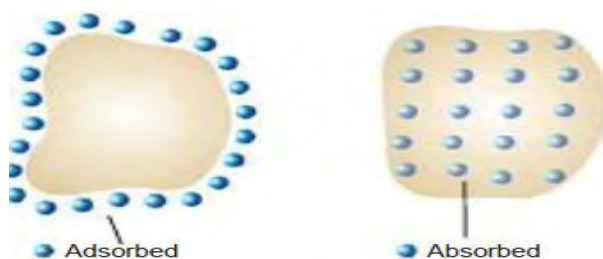


Fig.2.1 Schematic representation of (a) adsorptive and (b) absorptive extraction processes [39].

Although sorbent based extraction techniques can be classified on the basis of either adsorption or absorption, the two processes are not completely separable as they occur concurrently. In principle, what differs is the extent of contribution of the predominant extraction mechanism as that is solely dependent on the nature of the extraction phase. Consequently, it may be difficult to distinguish the two processes experimentally [40] thus the general term *sorption* is often used to refer to a combination of these processes. Despite the uncertainty of the extent of contribution of adsorption or absorption mechanisms in extraction, fundamentally, all sorbent based extraction techniques are guided by the thermodynamic partition or distribution coefficient K which is usually expressed as the ratio of analyte concentration in the sorbent phase, $C_{sorbent}$ to that in the sample phase, C_{sample} ;

$$K = \frac{C_{sorbent}}{C_{sample}} \quad 2.1$$

To predict and optimize extraction, it is important to be aware of the nature of the sorbent used. For adsorption, the most important sorbent characteristics are surface structure (porosity and surface area governing the available sites for analyte retention) and chemical composition. For absorption, the chemical composition (governing the diffusion coefficient of the analyte into the sorbent) of the liquid phase is the most important.

Sorption from the sample phase is essentially a dynamic process in a heterogeneous system in which transport of the analytes between the sorbent and sample phase is achieved. This process proceeds by a decrease in free energy until it reaches the minimum value (that is equilibrium). The mechanism of analyte adsorption or absorption is governed by the characteristics of interactions between the analyte and active sites of the sorbent. Therefore, sorbent selection is based on the binding mechanisms between the sorbent and analyte of interest. Table 2.1 shows different interaction mechanisms with their corresponding energies.

Table.2.1 Energies of interaction mechanisms [30].

Interaction mechanism	Energy (kJ/mol)
Dispersive	1-5
Dipole-induced dipole	2-7
Dipole-dipole	5-10
Hydrogen bonding	5-10
Ionic	50-200
Covalent	100-1000

The process of analyte sorption can be assumed to consist of multiple steps. Any of the steps may become rate limiting in controlling sorption of an analyte. The analyte may interact with a solid phase sorbent in at least four ways:

1. Through absorption, the analyte may interact with the sorbent by penetrating its three dimensional structure. Three dimensional penetrations into the sorbent is a particularly dominating process for solid supported liquid phases. In the absorption process, analytes do not compete for sites; therefore, absorbents can have a high capacity for the analyte.
2. The analyte may interact two dimensionally with the sorbent surface through adsorption due to intermolecular forces [41]. Surface interactions may result in displacement of water or

other solvent molecules by the analyte. In the adsorption process, analytes may compete for sites; therefore, adsorbents have limited capacity. Three steps occur during the adsorption process on porous sorbents; (i) *film diffusion* (when the analyte passes through a surface film to the solid phase surface), (ii) *pore diffusion* (when the analyte passes through the pores of the solid phase), and (iii) *adsorptive reaction* (when the analyte *binds, associates* or *interacts* with the sorbent surface) [42].

3. If the analyte is ionisable in aqueous solution, there may be an electrostatic attraction between the analyte and charged sites on the sorbent surface. Sorbents specifically designed to exploit these types of ionic interactions are referred to as *ion-exchange* (either anion or cation exchange).

4. It is possible that the analyte and the sorbent may be chemically reactive toward each other such that the analyte becomes covalently bonded to the solid phase sorbent. This type of sorption is generally detrimental to analytical recovery and may lead to slow or reduced recovery [38, 42].

For porous sorbents, most of the surface area is inside the nanopores of the sorbent (see Fig. 2.2.). Nanopores of the sorbent are classified into three as; *micropores* (diameters smaller than 2 nm), *mesopores* (2 to 50 nm), and *macropores* (greater than 50 nm) [43]. Most of the surface area is derived from the small diameter micropores and the medium diameter mesopores. Porous sorbents vary in pore size, shape and tortuosity and are characterised by properties such as particle diameter, pore diameter, pore volume, specific surface area, and particle distribution.

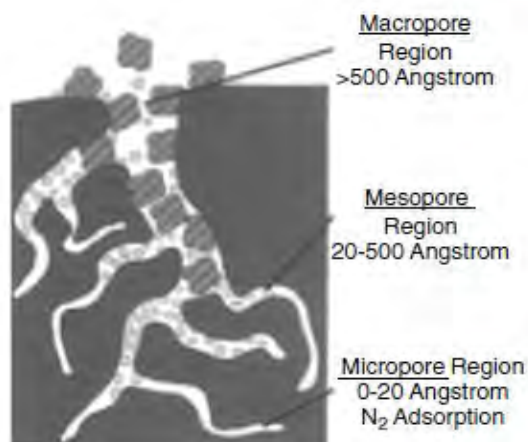


Fig.2.2 Schematic representation of porous regions of a sorbent [44].

2.3 Solid phase extraction (SPE)

Classically, batch-mode liquid solid extractions (LSE) were used in which the liquid sample was placed in contact with the bulk free flowing solid extracting phase. An equilibrium between the two phases was allowed to occur, followed by physical separation (by decanting or filtering) of the solid and liquid phases. One of the first applications of packed sorbent SPE was reported in 1951 where Braus and co-workers packed 1200-1500 g of granular activated carbon into an iron cylinder for the isolation of organics [45]. Since then, there has been significant progress in SPE technology as seen by the development of new formats and sorbents of a wide range of morphologies and chemistries [46].

Although SPE can be defined as a physical extraction process involving a liquid and a solid phase (which can be a packed or free flowing sorbent), the increased use of packed sorbent formats seems to have led to a bias towards packed sorbent SPE devices [47].

Even though extraction mechanisms for SPE are in principle similar to those for HPLC stationary phases, mathematically, the packed sorbent SPE process is different. This is due to the fact that K approaches infinity at the loading step, representing total sorption of the

analyte and K approaches zero during subsequent elution [44]. For this reason, SPE is sometimes referred to as digital chromatography, indicating the all-or-nothing extremes in the sorptive nature of process.

2.3.1 Sorbents for SPE

Sorbent selection for SPE is mainly guided by the ability of a material to rapidly retain analytes selectively as well as facilitate rapid and complete elution. That is, the sorption process must be reversible [48, 49]. In addition to reversible sorption, SPE sorbents should possess a large specific surface area as well as exhibit stability in the sample matrix and elution solvents. Lastly, a sorbent material with a good surface contact with the sample solution would be most preferred.

Poole and co-workers [50] categorized SPE sorbents into three as; (i) general purpose, (ii) class specific and (iii) analyte specific. The most common retention mechanisms in SPE are based on van der Waals forces, π - π interactions, hydrogen bonding, dipole-dipole interactions and ion exchange interactions. As a result, sorbents can be classified into three classes on the basis of retention mechanisms as; (i) reversed phase (ii) normal phase and (iii) ion exchange. From the materials perspective, sorbents can be classified into three as; (i) carbon based (ii) inorganic based and (iii) polymer based.

2.3.1.1 Carbon based

Development of carbon based sorbents was initiated through the use of activated carbons for the extraction of medium to low polarity organic analytes from water [51]. Although activated carbons exhibited a large specific surface area due to their micropores, the presence of polar groups on their surfaces resulted in poor SPE performances [52]. This led to the development of graphitized carbon blacks (GCBs). GCBs are obtained from heating carbon blacks at 2700-3000 °C in an inert atmosphere. The first GCBs were non porous with low

specific surface area estimated at 100 m²/g. Generally, GCB based sorbents are characterized by various functional groups at the surface following oxygen chemisorptions. The surface framework of GCBs used in SPE was shown to be contaminated by oxygen complexes, having a structure similar to hydroquinone, quinines, chromene and benzopyrylium salts. These groups interact so strongly with sufficiently acidic compounds such that conventional solvent systems are not able to desorb them [53].

Despite these limitations, the sorbents still found use for polar molecules with high solubility in water as these types of analytes are the most difficult to extract because of their low affinity for most reversed phase sorbents [54, 55]. The high potential of graphitized carbons for trapping polar analytes was then confirmed by the availability of porous graphitic carbon (PGC), a material with a highly homogeneous structure made of large graphitic sheets [56-62].

PGC was the first material to be described as a more retentive reversed phase sorbent than C₁₈ silica. The retention mechanism was shown to be very different and its ability to provide higher retention for polar and water soluble analytes was reported [63]. The flat homogeneous surface of the PGC is responsible for its unique selectivity to geometrical isomers. The large layers of carbons containing delocalized π electrons and the high polarizability are responsible for a different retention mechanism [64]. Although GCB and PGC were shown to offer improved performance, they had a disadvantage of high retention thus making it difficult to elute some of the analytes [49].

The development of carbon nanotubes (CNTs) by Sumio Iijima in 1991 [65] was a major leap forward in carbon based SPE sorbent research. Carbon nanotubes (CNTs) are fullerene structures that consist of graphene cylinders end capped with pentagonal rings. CNTs possess a large surface area, ability to establish π - π interactions, excellent chemical and mechanical stability. These properties make CNTs attractive as SPE sorbent material for the extraction of

either non-polar (in the case of non-functionalised CNTs) and polar compounds for which functionalisation of the tubes plays a key role in selectivity [66-69].

A change in selectivity has been achieved by covalently functionalizing the surface of CNTs as they can incorporate hydroxyl or carbonyl groups on to their side walls [70]. On the other hand, non-covalent side-wall functionalisation of CNTs also provides a change in selectivity. In this case functionalisation is achieved via ionic interactions, π - π stacking, hydrogen bonds, electrostatic forces, van der Waals forces, dative bonds and hydrophobic interactions. All these interactions that CNTs exhibit have made it possible for them to be applied as SPE material for a wide range of analytes thus making a substitute for carbon based sorbents such as activated carbon, GCB and PGC. For example, Cai and co-workers employed CNTs as an SPE sorbent for extracting organic analytes, in particular EDCs and phthalates [71, 72]. Their studies showed that MWCNTs are similar to or more effective than silica-based sorbents.

2.3.1.2 Inorganic based

The most common inorganic based sorbents for SPE are silica (SiO_2)_x, alumina (Al_2O_3), and Florisil (magnesium silicate/ MgSiO_3). Silica is the most popular inorganic based sorbent.

Porous silica (Fig. 2.3.) is an inorganic polymer (SiO_2)_x which consists of a directly accessible external surface and internal pores accessible only to molecules approximately less than 12000 Da [44].

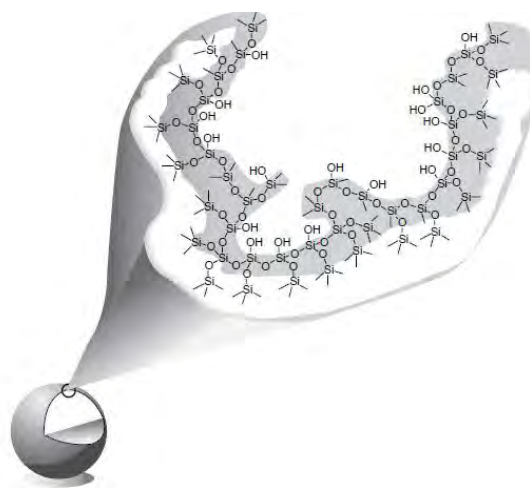


Fig.2.3 Representation of an unbounded silica particle [44].

Use of bare silica as a SPE sorbent predominantly relies on hydrogen bonding as the extraction mechanism. In an effort to increase the applicability of silica, covalent bonding between silica and organosilanes via the silanol groups on the silica surface was employed. This resulted in chemically stable Si-O-Si-C covalent linkages from a variety of organosilanes. Consequently, a new class of sorbents referred to as bonded silicas emerged, which widened the sorbent chemistries. [44].

Although bonded silicas became very popular as SPE sorbents, they possess two disadvantages that led to the search for alternative sorbent materials. Firstly, they were only applicable within a limited pH range as silica experiences hydrolysis below and above pH 1 and 8.5 respectively. Secondly, it was observed that free silanol groups resulted in low recoveries for polar analytes due to irreversible adsorption [31].

2.3.1.3 Polymer based

The development of organic polymer based sorbents addressed the two limitations of silica based sorbents as they are stable over a wide pH range and they do not possess any free silanol groups.

The most widely used polymeric sorbents are the polystyrene divinylbenzene (PS-DVB) copolymers [73]. Bare PS-DVB sorbents extract analytes on the basis of the π - π interactions as a result of their aromatic rings (Fig. 2.4).

One way of improving the retention of these PS-DVB based sorbents would be to increase the specific surface area, and so increase the π - π interactions, creating what is generally known as a highly crosslinked sorbent. Highly crosslinked sorbents can be obtained using conventional methods for preparing macromolecular porous resins with a high content of crosslinking agent. Surface areas of up to $800 \text{ m}^2\text{g}^{-1}$ can be achieved [74].

Alternatively, the specific surface area can be improved (up to $2000 \text{ m}^2\text{g}^{-1}$) using the method developed by Davankov and Tsyurupa [75]. This method consists of the post-crosslinking of linear or slightly crosslinked styrene chains in the swollen state in the presence of a Friedel Crafts catalyst, producing methylene bridges between the neighbouring aromatic rings. Hence, the hypercrosslinked network created shows a considerable increase in the microporous structure and the surface area. The sorbents obtained by the Davankov procedure, which have a large specific surface area, are specifically recognized as hypercrosslinked resins [75-77]. Sorbents with a high specific surface area have numerous sorption sites which are mainly responsible for the interactions between the polymeric sorbent and the analytes.

Therefore, thanks to the π - π interactions, polymeric sorbents can perform better than silica and carbon based sorbents at extracting polar analytes [78-80]. However, the recoveries are still low for most polar analytes. The poor retention towards polar analytes is attributed to the hydrophobic character of these styrene based sorbents. To overcome the hydrophobicity of the resins, some companies have developed hydrophilic resins. The resins can be classified according to the procedure by which they are synthesized; the copolymerization of a hydrophilic monomer with a crosslinking agent or the chemical modification of the existing PS-DVB polymer with a polar moiety. In synthesising copolymers, it is important to control the initial ratio of monomers as it influences the degree of hydrophilicity and specific surface area, which are inversely related in hydrophilic copolymeric sorbents, is acceptable [81]. In the latter half of the 1990s, porous highly cross-linked PS-DVB resins with spherical shapes were made available.

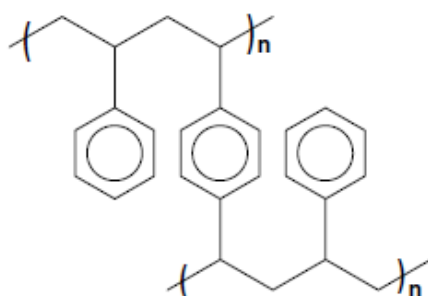


Fig.2.4 Cross-linked polystyrene divinylbenzene copolymer [81].

Adding polar functional groups to crosslinked apolar polymeric resins by covalent chemical modification has developed particularly for generation of SPE sorbents suitable for recovery of polar compounds. Hydrophilic functional groups such as acetyl, benzoyl, *o*-carboxybenzoyl, 2-carboxy-3/4-nitrobenzoyl, 2,4-dicarboxybenzoyl, hydroxymethyl, sulfonate, trimethylammonium and tetrakis *p*-carboxyphenyl) porphyrin have been chemically introduced into the structural backbone of PS-DVB copolymers [82]. Generation

of a macroporous copolymer consisting of two monomer components, divinylbenzene (lipophilic) and N-vinylpyrrolidone (hydrophilic), produced a hydrophilically-lipophilically balanced SPE sorbent [79]. Chemically modifying apolar polymeric sorbents in this way improves wettability, surface contact between the aqueous sample, sorbent surface and mass transfer by making the surface of the sorbent more hydrophilic.

Higher breakthrough volumes (indicating greater attraction of the sorbent for the analyte) for selected polar analytes have been observed when the hydrophilic functionalised polymeric resins are used as compared to classical hydrophobic bonded silicas or nonfunctionalised, apolar polymeric resins. In addition to having a greater capacity for polar compounds, functionalised polymeric resins provide better surface contact with aqueous samples. The bonded silica sorbents and polymeric resins (discussed earlier) have hydrophobic surfaces and require pretreatment, or conditioning with a hydrophilic solvent to activate the surface to sorb analytes. Using covalent bonding to incorporate hydrophilic character permanently ensures that it will not be leached from the sorbent as are the common hydrophilic solvents used to condition bonded silica sorbents and polymeric resins [79].

2.3.1.4 Improvements in SPE sorbent selectivity

2.3.1.4.1 Restricted Access Materials

In order to improve selectivity of sorbents towards target analytes, restricted access materials (RAMs) were developed. Because of their biporous structure, they have reversed phase interactions with the analytes, but exclude high-molecular-weight compounds by size exclusion (see Fig. 2.5.). However, RAMs do not always act selectively and, when they do, their selectivity is low [83]. They are well suited for handling of biological samples as they exclude the access by matrix components such as proteins while retaining the analytes of interest in the interior of the sorbent [30]. Smaller drug molecules can penetrate into the pores

and be retained by specific bonded phases (non-polar or ion exchange). The RAM technique provides safer handling of hazardous clinical samples and has been successfully applied for on-line sample clean-up prior to the determination of acidic compounds [84], basic drugs [85, 86] and verapamil [87] in different biological matrices.

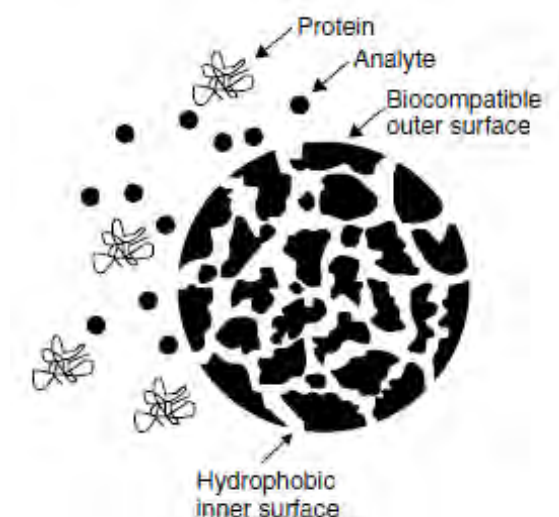


Fig.2.5 Schematic representation of a restricted access material sorbent particle [88].

2.3.1.4.2 Immunosorbents

These sorbents are based on molecular recognition as they employ antibodies. A high degree of molecular selectivity is achieved because the immunosorbents, with their immobilized antibody, present specific and selective interactions for the target analyte (Fig.2.6). Immunosorbents are obtained by covalently binding antibodies onto appropriate sorbents. The ideal support for an immunoaffinity sorbent is rigid and porous to facilitate high flow rates.

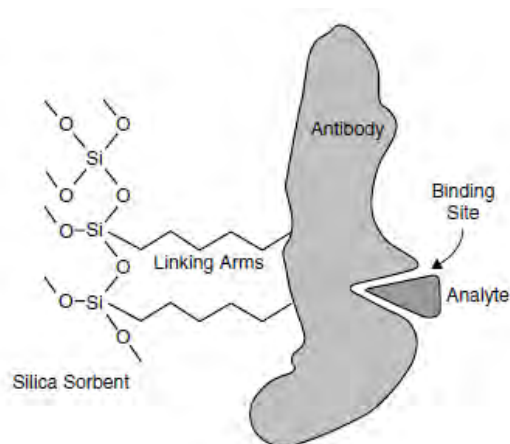


Fig.2.6 Schematic representation of an immunosorbent binding an analyte [89].

Likewise, it should provide functional groups to enable appropriate coupling with a sufficient number of antibodies as well as being hydrophilic to prevent nonspecific interactions with the analytes and the matrix [90, 91]. The formation of the antibody-antigen complex may be affected by the chemical composition of the sample [91]. The capacity of immunosorbents can be increased by a better selection of the silica used for the bonding procedure [90], and may depend on the orientation and the purity of the immobilized antibodies [92].

Extraction, concentration and isolation are possible in a single step. Single analytes may be targeted but owing to cross reactivity of antibodies, immunoextraction sorbents have been designed to target a group of structurally related analytes. However, they have several drawbacks as they are time-consuming and expensive to prepare; they are irreproducible from batch to batch; they are not very stable; and, they are of limited use in aqueous medium [30, 83].

Few immunosorbents are commercially available thus far, so the number of analytes that can be analyzed is limited. Moreover, it is well known that polyclonal antibodies can be produced and prepared in SPE cartridges and this takes approximately one year in research laboratories.

The costs at this stage are high compared to conventional systems. Only when industry is involved will the costs be reduced due to the production of larger quantities. On the other hand, industry has demonstrated interest in such columns and most probably they will be available at reasonable prices in the near future [93].

2.3.1.4.3 Molecularly imprinted polymeric sorbents

The introduction of MIPs into SPE (MISPE) revolutionized sample preparation technology as it provides tailor-made selectivity and presents a new class of SPE materials that transforms traditional SPE into an analyte specific affinity technique [94]. Because of the retention mechanisms based on molecular recognition, MIPs are selective for only the molecule of interest or some structurally-related compounds. MISPE is prepared by the copolymerization of the template (imprinted) molecules with functional monomers (see Fig. 2.7), for example polyacrylate or polyacrylamide, using a specific cross-linker such as vinyl benzene or ethylene glycol dimethacrylate. The template is subsequently removed from the polymer and leaves specific three dimensional polymeric networks which are capable of recognizing the template molecules. The resulting MISPE therefore exhibits high affinity and selectivity for the template compound. The MISPE binding mechanism is similar to the binding affinity of antibody-antigen and enzyme (lock and key) reactions [83].

The advantages of MISPE are the binding specificity for trace analytes and their stability towards extreme pH as well as a wide range of organic solvents. Andersson compared MISPE with normal C₁₈ SPE and liquid-liquid extraction (LLE) methods for extracting bupivacaine from plasma and showed that MISPE produced the purest extract [95]. Although the absolute response signal of the target analyte in MISPE was smaller than SPE and LLE techniques, the relative sensitivity was much higher as a result of cleaner extracts. More recently, MISPE technology has also been applied in a 96 well block configuration to allow high throughput analysis of new pharmaceutical compounds using HPLC with fluorescence

detection [96]. The study reported much cleaner baselines obtained for the template compounds using the MISPE approach as compared to C₁₈ SPE cartridge and therefore, higher sensitivity of the target analyte was achieved even with lower analyte recovery. There have been some reports on the application of MISPE for extracting plasma phenytoin [97], serum theophylline [98], urinary clenbuterol [99] and plasma caffeine [100]. All these examples demonstrated the potential of MISPE to become more widely used in sample clean up procedures [101]. Certainly MISPE provides a cheaper equivalent to immunosorbents.

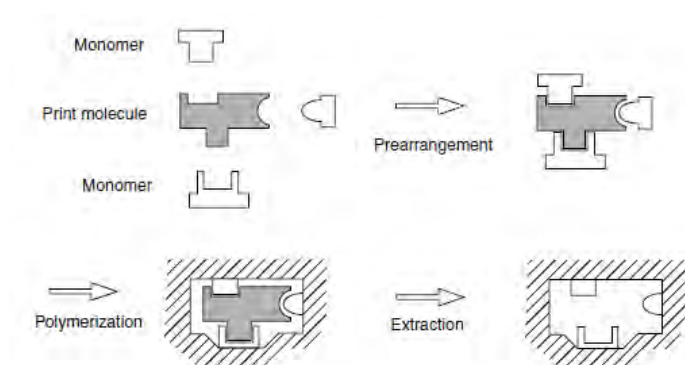


Fig.2.7 Schematic representation of the preparation of molecular imprints [102].

2.3.2 SPE formats and configurations

In packed sorbent SPE there are four general types of formats that exist; cartridges, disks, packed syringes and/or capillaries and pipette tips [35].

2.3.2.1 Cartridge

The cartridge is the main format for SPE and it typically consists of 40-60 μm diameter particles packed between polyethylene or stainless steel frits in a glass or polypropylene barrel. SPE cartridges are available in a wide range of sizes, with volumes ranging from 1 ml to 50 ml. A disadvantage of the cartridge design is that due to its small cross-sectional area, sample processing rates are slow and the tolerance to blockage by particles and adsorbed

matrix components is low, thus channelling reduces the capacity to retain analytes. Nevertheless, with proper sample filtration prior to SPE, the cartridge format achieves good recoveries, furthermore it is easy to pack sorbents manually thus the widespread use of the cartridge format. Operationally SPE cartridges are typically loaded on vacuum manifolds. Fig.2.8. shows a schematic representation of the two popular cartridge designs.

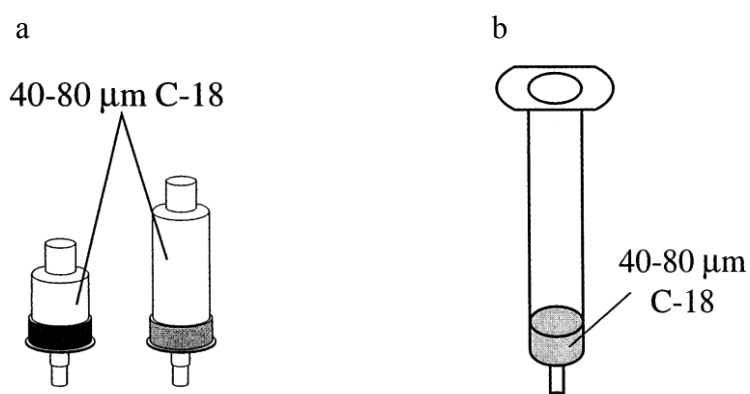


Fig.2.8 Schematic diagrams of SPE (a) cartridges and (b) barrel type packed with silica microparticles [103].

2.3.2.2 Disk

SPE disk fabrication involves a multistep process where microparticles (8-12 μm) are tightly held within or between an inert fiber matrix such as glass or PTFE [103]. Fig. 2.9 shows diagrammatically a configuration of a 10 μm C₁₈ SPE disk compared to a conventional SPE cartridge (typically a syringe barrel).

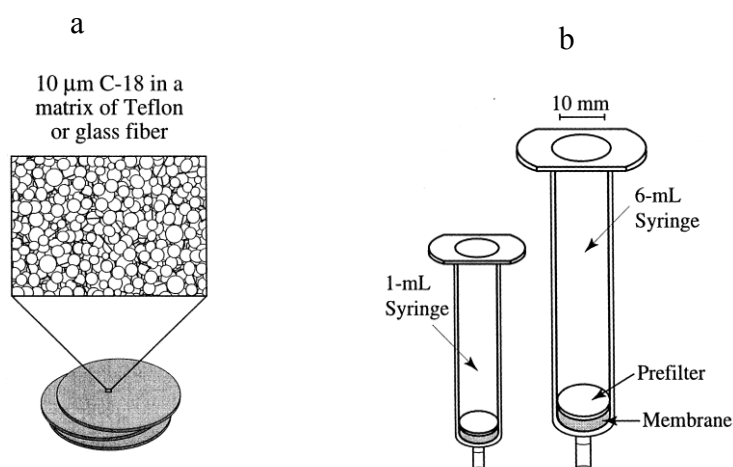


Fig.2.9 Schematic diagrams of SPE (a) Free disks and (b) syringe barrel disk cartridges [103].

The short sample path and small particle size allows efficient trapping of analytes with a relatively high flow rate through the sorbent as compared to the cartridges. The disks are primarily used to reduce analysis time when handling large volumes of aqueous environmental samples. Because the disks use the same chromatographic material as conventional cartridges, the chromatography is similar to that in cartridges. The difference lies in the particle size as shown in Fig. 2.10. For the same bed height between a disk and a cartridge, the disk has many more particles and a much more tortuous path of flow, which means that there is considerably more surface area available and the kinetics of sorption is much quicker for the disk than the cartridge [103].

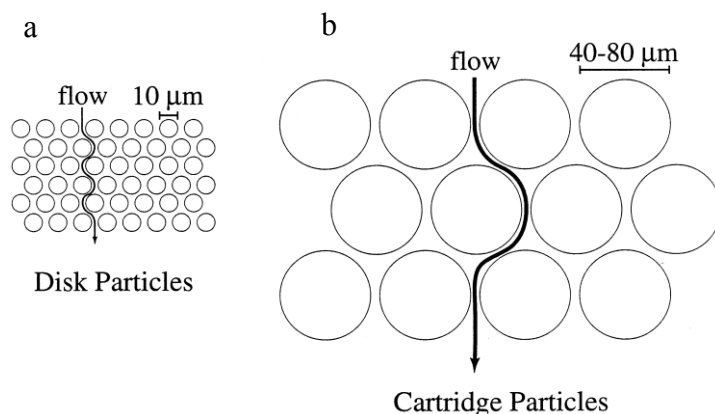


Fig.2.10 Schematic representation of flow paths within (a) disk and (b) cartridge microparticle sorbent beds [103].

One of the disadvantages of using disks as compared to cartridges is the decrease in the breakthrough volume. For this reason, disks are used when there is a strong interaction between the analyte and the sorbent [104].

For small sample sizes (100 μl or less), it is easier to miniaturize disks than cartridges, the ability to fabricate disk devices that contain only a few milligrams of sorbent facilitated the development of the 96-well plate SPE disk configuration (see Fig. 2.11) [105]. The 96-well plate format is based on the standard 96-well microtiter plate format. Parallel sample processing allows 96 samples to be extracted in approximately one hour or less. Processing 96 samples simultaneously reduces handling errors and limits labour input. Each of the 96 wells has a small 1 or 2 ml SPE column with 3-10 mg of packing material. Each individual cartridge has top and bottom frits and a stationary phase packing, as used in the fixed 96-well SPE plate design. A vacuum manifold is often used to pull liquids through a flexible well plate, and users can plug the unused holes of the base plate with plug strips if only a portion of the 96 wells is needed.

384-well SPE plates also exist and have the same external dimensions as the current 96-well SPE plates, so SPE wells would be very tightly sandwiched together.

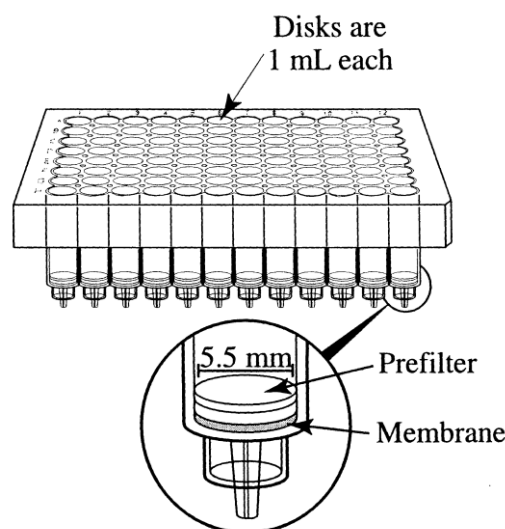


Fig.2.11 Schematic diagram of disk microtiter plates [103].

Disks have two distinct advantages over conventional SPE cartridges. Firstly, they often can be operated with smaller elution volumes and higher flow rates. The improved performance of the disk can be attributed to the smaller particle size (8-12 μm) of the sorbent embedded in the PTFE, compared to 40-80 μm in a conventional cartridge. The decrease in void volume and increase in surface area associated with the small particles promote partitioning. Hence, a smaller mass of sorbent is required to process a similar volume of sample, permitting the use of smaller volumes of solvent for elution. Secondly, the increase in density and uniformity of packing provided by the smaller particles mitigates breakthrough and channelling, which permits the use of higher flow rates and reduces extraction times [30, 78]. For the same bed height between a disk and a cartridge, the disk has many more particles and a much more tortuous path of flow, which means that there is considerably more surface area available and the kinetics of sorption are much quicker for the disk than the cartridge.

2.3.2.3 Micro extraction in a packed syringe (MEPS)

Micro extraction by packed sorbent is a new format for solid phase extraction that can be said to be a miniaturized version of the cartridge SPE format. In MEPS the sorbent, 1-2 mg is either inserted into the syringe (100-250 μl) barrel as a plug or between the needle and the barrel as a cartridge (Fig.2.12).

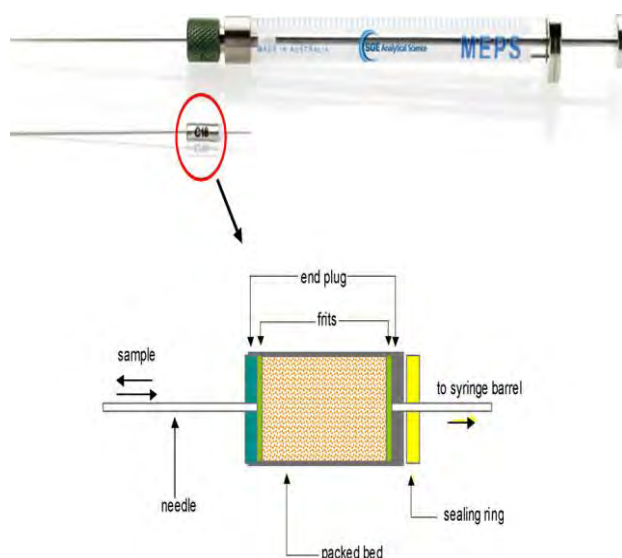


Fig.2.12 Representation of a MEPS syringe from SGE Analytical Science [106].

The cartridge bed can be packed with a sorbent or coated to provide selective and suitable sampling conditions. Any sorbent material can be packed into the syringe. The MEPS was invented and developed at AstraZeneca Sweden [107].

Operationally, the sample is drawn through the sorbent and ejected to waste. This draw and eject process is repeated several times depending on the desired preconcentration. The solid phase is then washed once by water (50 μl) to remove the proteins and other interfering material. The analytes are then eluted with an organic solvent such as methanol or the LC mobile phase (20-50 μl) directly into the instrument's injector GC or LC. An advantage of MEPS over conventional SPE is that the conditioning step is not necessary [106].

2.3.2.4 SPE pipette tips

Pipette tip extraction represents a simple and rapid method of solid phase extraction. The solid phase sorbent is positioned inside a pipette tip, held in place by a screen and filter. Because the stationary phase is mixed with the sample, the conditioning step necessary for conventional solid-phase extraction is not required. The sample is subsequently sent to a waste container and the stationary phase is washed only with 1 ml of water or buffer. After the washing step, the solvent is sent to waste and the adsorbed analytes are eluted by drawing up only 0.1-0.3 ml of solvent and transferring the solution to GC or HPLC. The time consuming concentration step is not required because of the small volume of solvent. Pipette extraction has some advantages; faster extraction time (1-2 min), one extraction method for all analytes, clean extracts, less sample volume (200-400 μ l) and less solvent waste.

Several companies began to manufacture pipette tips, each with a different twist for example Millipore introduced the Zip Tip 4 pipette tip and EST Analyticals introduced disposable pipette tip extraction (DPX)(see Fig 2.13) (provided a pipette designed to extract drugs of abuse from small volumes of urine or serum). In this configuration, the sorbent is placed loosely between two frits inside the pipette tip; the sample is drawn and mixed with the stationary phase. The matrix is sent to waste and the adsorbed drugs are eluted with the small amount of solvent and analyzed by GC-MS [78].

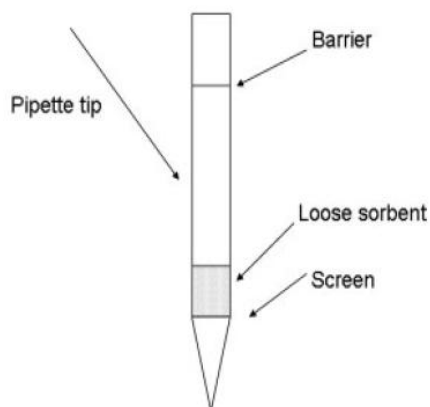


Fig.2.13 Schematic diagram of a disposable pipette tip extraction device [108].

2.4 Solid phase micro extraction (SPME)

The introduction of SPME was a significant step towards miniaturisation of sorbent based sample preparation techniques [109]. SPME which is not a miniaturised version of SPE was a welcome addition to sorbent based sample preparation techniques due to the fact that it integrates sampling, extraction, concentration and sample introduction into a solvent free process at the micro scale [109-112]. Among sample preparation techniques, SPME nearly fulfils all the requirements for the driving forces of current sample preparation trends.

In principle, similarities between SPME and SPE are in twofold; firstly, they both rely on a solid or solid supported sorbent as the extracting phase and secondly, the efficiency of extraction is dependent on the distribution of the analyte between the solid phase and the liquid sample although SPME has an added advantage in that analytes can be extracted from the gas phase. The fundamental difference is that, for SPME, analysis is carried out after equilibrium is reached or at a specified time prior to reaching equilibrium. Therefore, SPME operationally encompasses non-exhaustive equilibrium and pre-equilibrium, batch and flow through sorbent based microextraction techniques.

The fiber SPME device is the most widely used SPME format (see Fig. 2.14). It is based on a modified syringe, which contains a stainless steel microtube within its syringe needle. The microtube has a 1 cm fused silica fiber tip which is coated with an organic polymer. The syringe is designed to move the fiber in and out of the needle, which allows exposure of the fiber during extraction and desorption and its protection during transfers and storage [113].

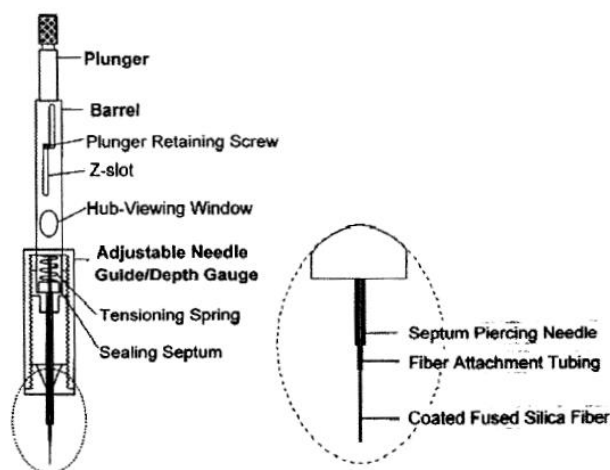


Fig.2.14 Schematic representation of the components of a commercially available fiber SPME device [113].

There are three common modes of SPME: direct extraction, headspace extraction and membrane protected extraction. In direct extraction mode, the fiber is placed directly into the sample and analytes are transferred from the matrix to the coating. Agitation, stirring or sonication can significantly decrease the equilibration time. For gaseous samples, convection is sufficient to facilitate short extraction times.

In headspace mode, the analytes are transported to the fiber through the headspace. This approach is necessary for sample types such as biological matrices or humic matter, where the fiber is protected from damage by high molecular weight interferences. In headspace analysis, the fiber is protected from harsh extraction conditions such as extreme pH and high

salt concentrations. The issue of cross contamination is also minimized with headspace SPME because the fiber does not come in contact with the sample.

In membrane extraction mode, the membrane acts as a barrier to prevent detrimental matrix materials from destroying the fiber. This mode of extraction is advantageous for higher boiling point compounds that cannot be extracted by headspace SPME. In membrane extraction, the extraction time can be significantly longer than direct or headspace SPME, because analytes need to first penetrate the membrane before they can be absorbed or adsorbed to the fiber coating [114]. The three modes of extraction are shown schematically in Fig. 2.15.

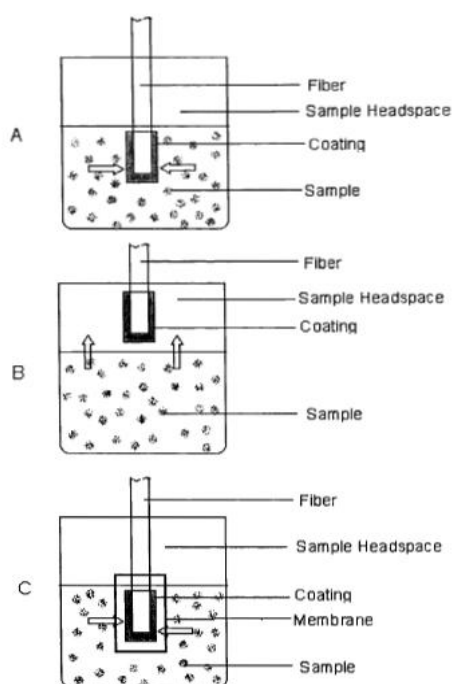


Fig.2.15 Schematic representation of the three modes of SPME operation: (A) Direct Extraction, (B) Headspace Extraction (C) Membrane Extraction [47].

During extraction, analytes migrate between the three phases; sample, headspace and fiber coating until equilibrium is reached. The equilibrium of analytes in the three phases, where the mass remains constant in the system, can be described using equation 2.2:

$$C_o V_s = C_f^\infty V_f + C_h^\infty V_h + C_s^\infty V_s \quad 2.2$$

Where C_o is the initial concentration of the analyte in the matrix, C_f^∞ , C_h^∞ and C_s^∞ are the equilibrium concentrations of analyte in the coating, the headspace and the sample respectively; V_f , V_h , and V_s are the volumes of the coating, headspace and the matrix respectively. The fiber coating/gas distribution constant can be described as $K_{fh} = \frac{C_f^\infty}{C_h^\infty}$, and the gas/sample distribution constant as $K_{hs} = \frac{C_h^\infty}{C_s^\infty}$. The mass of analyte in the coating, $n = C_f^\infty V_f$ can be expressed as in equation 2.3:

$$n = \frac{K_{fh} K_{hs} V_f C_o V_s}{K_{fh} K_{hs} V_f + K_{hs} V_s} \quad 2.3$$

Since the fiber/headspace distribution constant, K_{fh} , can be estimated by the fiber/gas distribution constant K_{fg} , and the headspace/sample distribution constant by the gas/sample distribution constant, K_{gs} , the following equation can be deduced:

$$K_{fs} = K_{fh} = K_{fg} K_{gs} \quad 2.4$$

Equation 2.3 can be rewritten as:

$$n = \frac{K_{fs}V_fC_0V_s}{K_{fs}V_f+K_{hs}V_h+V_s} \quad 2.5$$

If there is no headspace in the sample, the term $K_{hs}V_h$ in the denominator can be eliminated, giving rise to:

$$n = \frac{K_{fs}V_fC_0V_s}{K_{fs}V_f+V_s} \quad 2.6$$

Equation 2.6 depicts the relationship of the analyte mass that is extracted by the fiber coating after the system has reached equilibrium. In most applications, K_{fs} is relatively small compared to the phase ratio of the sample matrix to coating volume ($V_f \ll V_s$) resulting in a state where the capacity of the sample is much larger than the capacity of the fiber. Equation 2.6 can therefore be simplified to:

$$n = K_{fs}V_fC_0 \quad 2.7$$

The simplified equation 2.6 demonstrates that in SPME it is not necessary to determine the sample volume as long as ($K_{fs}V_f \ll V_s$).

Equation 2.7 assumes that the system exists as a single homogeneous phase and there is no headspace present. The distribution constant has also been correlated with the octanol/water distribution coefficient, K_{ow} , since this is a classical and general measure of the affinity of analytes to the organic phase.

2.4.1 Sorbents for SPME

The selection of the sorbent material used in SPME is based primarily on the polarity and volatility characteristics of the analyte. SPME sorbents can be classified into two as liquid or solid coatings.

2.4.1.1 Liquid coatings

The liquid coatings are those which are either a high viscosity rubber liquid, deposited on the solid support, or a crystalline solid at room temperature which transforms into a liquid at the elevated temperatures necessary for desorption. These coatings extract analytes via an absorption mechanism and are the homogeneous pure polymer coatings of poly (dimethyl siloxane) (PDMS) and poly (acrylate) (PA).

PDMS is a nonpolar liquid absorbent phase coated on fused silica commercially in thick film thicknesses. The thickest coating, 100 μm is used for volatile compounds by headspace procedures. The intermediate coating level, 30 μm is appropriate for use with nonpolar semivolatile organic compounds while the smallest diameter coating 7 μm is used when analyzing nonpolar high molecular weight compounds. The use of PDMS fibers is restricted to a sample pH between 4 and 10 [115].

PA is a polar absorbent coating commercially available in a film thickness of 85 μm . The sorbent is suitable for extraction of polar semivolatile compounds.

2.4.1.2 Solid coatings

The second type of solid fiber coating, primarily extract analytes via adsorption. These typically consist of multiple component phases where solid particles are suspended in a liquid phase to coat it onto the fiber. Multicomponent phases that are commercially available contain either DVB and/or Carboxen (CAR) particles suspended in either PDMS (nonpolar phase) or Carbowax (CW) a moderately polar phase [44] and on a smaller scale TPR (template resin) particles suspended in CW.

These include PDMS/DVB, CAR/PDMS, DVB/CAR/PDMS, and CW/TPR. The intermolecular forces involved are the same as those responsible for adsorption and absorption processes in SPE [116].

PDMS-DVB is a multicomponent bipolar sorbent coating that is applicable for the extraction of amine or nitroaromatic analytes [117]. CW-DVB is a multi-component polar sorbent coating appropriate for the extraction of alcohols and polar analytes [118]. CAR/PDMS is a multiple component bipolar sorbent used for extraction of gases and low molecular weight compounds [119]. Among the SPME coatings commercially available, the 85 μm CAR/PDMS sorbent is the best choice for extracting analytes having molecular weights of less than 90 regardless of functional groups present with the exception of isopropylamine.

DVB/CAR/PDMS is a multicomponent bipolar phase that contains a combination of a DVB-PDMS (50 μm) layered over Carboxen-PDMS (30 μm) [120]. The multicomponent phase expands the analyte molecular weight range, because larger analytes are retained in the meso and macropores of the outer DVB layer, while the micropores in the inner layer of Carboxen retain smaller analytes. The dual layered phase is used for extraction of odor compounds and volatile and semi volatile flavour compounds. DVB sorbents have a high affinity for small

amines; consequently the combination coating of DVB over Carboxen is the best sorbent of choice for extracting isopropylamine [121].

CW/TPR is used for analysis of surfactants by HPLC. The template resin in CW/TPR is a hollow, spherical DVB formed by coating DVB over a silica template. When the silica is dissolved, the hollow spherical DVB particle formed has no micro or mesopores [122]. Development of different types of coatings has resulted in an increasing number of SPME methods for environmental applications [110, 123].

2.4.1.3 Improvements in SPME sorbents

To date only a limited number of coatings are commercially available for SPME, notably pure polymeric phases such as PDMS and PA and dispersions of solid sorbents such as CAR and DVB in polymeric agglutinants.

Apart from the reduced assortment of coatings with different properties, these materials may present some limitations depending on its nature and film thickness. The limitations include instability and swelling towards direct exposure to organic solvents, reduced operating temperature and mechanical fragility of the fused support. Therefore, the search for new SPME coatings that overcome these challenges is an important research direction. One of the goals is the investigation of sorbent films with strong adhesion with the base substrate. An interesting alternative SPME coating approach is that which involves coatings prepared through sol-gel synthetic routes. The first description of sol-gel technology for preparation of SPME coatings was presented by Chong and co-workers in 1997 [124]: the organic modifier was hydroxyl-PDMS, and the resulting chemically bound film was an organically modified silica (ormosil).

Sol-gel technology has also been applied with success to prepare a broad range of coatings which include polyethylene glycol for the extraction of alcohols, phenols and amines [125] and PDMS/PVA for the extraction of polychlorinated biphenyls (PCBs) [126], hydroxyfullerene for the extraction of PCBs. among others.

Mullet and co-workers [127] in 2001, developed a MIPs based SPME device which consisted of packing a capillary with the MIP particles for in-tube SPME and was used for the selective determination of propranolol in serum samples. The developed method was successfully applied and the advantages of in-tube SPME were obvious (high enrichment factors provided by multiple draw/eject cycles, ease of automation and fast operation). However, this methodology is not free of some important drawbacks such as the lack of compatibility between the solvent needed to desorb analytes from the MIP and the mobile phase used (typical drawback of online MISPE protocols) and the necessity of extra instrumentation (pump, multiport valves). Thus, the preparation of silica fibers coated with an MIP to perform SPME would be the best option. The suitability of the approach was demonstrated by Koster and co-workers [128] in 2001 reporting the preparation of the first MIP coated silica fiber for the SPME of brombuterol from human urine.

2.4.2 SPME formats and configurations

2.4.2.1 Stir bar sorptive extraction (SBSE)

In 1999, Baltussen and co-workers introduced stir bar sorptive extraction (SBSE), a method based on the same principles as SPME where a magnetic stirring bar is incorporated into a glass jacket and the outer surface is coated with a layer of PDMS [129]. However, a relatively large quantity of extracting phase is coated on a stir bar as compared to SPME. Solutes are extracted into the coating based upon their octanol-water partition coefficient and upon the sample-sorbent medium phase ratio. The coating material used in SBSE is the same as that of

SPME, but the quantity used is 50 to 250 times greater than SPME. The stir bars are made up of three essential components. The first and innermost is a magnetic stirring rod, which is necessary for rotation above a stirring plate. The second component is a thin layer of glass jacket that covers the magnetic core. This layer acts as a barrier between the PDMS and the metal to prevent decomposition of the coating. The third and outermost component is the PDMS coating where analytes are extracted. Fig. 2.16 shows a schematic of a stir bar showing the essential components.

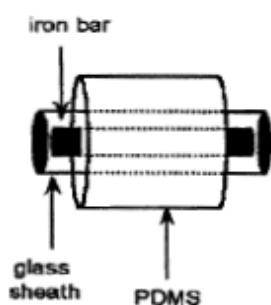


Fig.2.16 Schematic diagram showing the three essential components of a SBSE device [130].

Because of the increased film thickness in SBSE compared to conventional SPME, the sensitivity is increased by a factor of 100 to 1000.

Operationally, the stir bar is introduced into an aqueous sample and the extraction takes place during stirring. After extraction, the stir bar is removed from the sample and placed in a thermal desorption unit where the analytes are thermally desorbed. Alternatively, liquid desorption can be used to transfer the analytes to the instrument.

2.4.2.2 Solid phase dynamic extraction (SPDE)

SPDE [131, 132] is an in needle technique for vapour and liquid sampling. In SPDE, the analytes are concentrated onto the inner wall of a stainless steel needle coated with a 50 μm film of PDMS and 10% activated carbon used as the extracting phase (Fig. 2.17)

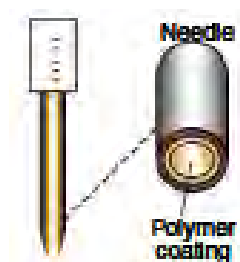


Fig.2.17 Schematic diagram of a SPDE device [132].

Dynamic sampling is performed automatically by passing the headspace through the tube using a syringe. The volume of the stationary phase of the SPDE needle is approximately 5.99 mm^3 , whereas a $100 \text{ }\mu\text{m}$ PDMS SPME fiber has a volume of 0.94 mm^3 which has an effect of improving sensitivity. Operationally, analytes are accumulated in the polymer coating of the inner wall of the needle by pulling in and pushing out a fixed volume of the sample headspace in an appropriate number of times. Thus, SPDE sampling permits operation under dynamic conditions while retaining a constant headspace volume. The trapped analytes are recovered by heat desorption directly into the GC injector body. The most significant advantages of SPDE over SPME are the larger coating volume and the shorter extraction time [132].

2.4.2.3 Needle trap devices (NTD)

In response to the demand for more robust SPME systems, the needle trap device (NTD) technique was introduced [133, 134]. Blunt-type hypodermic needles, packed with a proper sorbent, are used for extraction followed by thermal desorption into GC systems. Fig. 2.18 shows the structure of the latest design of NTD [135].

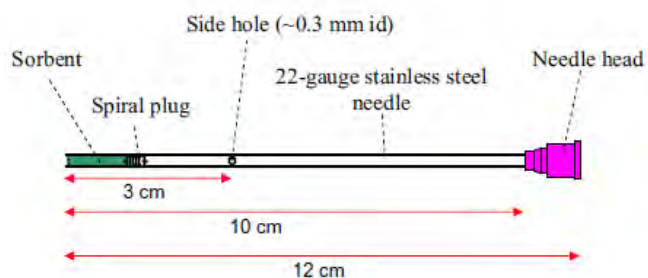


Fig.2.18 Schematic representation of a blunt tip needle trap device [110].

The extraction phase is packed into a needle with a side hole. The analytes are trapped on the sorbent by passing the gaseous sample through the needle. Different types of packing materials have been used in NTD, including quartz wool packing for sampling particulate matter and aerosol [133], a single layer of carboxen or multi layers of PDMS, DVB and carboxen for sampling volatile organic compounds (VOCs) [134]. After sampling, the needle is inserted into the hot injector of a gas chromatograph, blocking the narrow neck liner which is used for injection of NTD. The carrier gas flows into the needle through the side hole (on the needle), passes through the sorbent and carries the thermally desorbed analytes into the column. NTD is more robust than SPME and has a high sorbent capacity which makes it capable of performing exhaustive extraction [110].

2.4.2.4 Thin film microextraction (TFME)

TFME is another sampling device that has been developed to achieve higher extraction efficiency and sensitivity for SPME [136].

A thin film of PDMS is cut into a pentagon shape and mounted on a stainless steel wire for support (Fig. 2.19.)

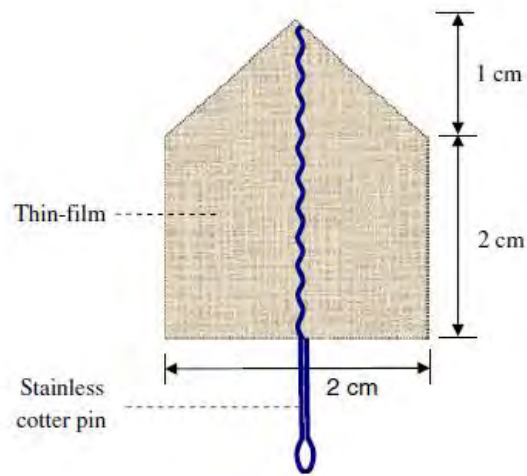


Fig.2.19 Schematic representation of a TFME device [110].

After conditioning and baking out, the device can be used for both active and passive sampling. TFME can also be used for extraction of organic contaminants in water samples, especially for onsite sampling [137]. The main benefit of TFME is the shorter equilibrium time which can be explained by higher surface area to volume ratio of the thin film.

Chapter 3

3. A review of electrospun nanofibers as sorbent material for solid phase extraction

Summary

This chapter gives an overview of some of the developments in electrospinning research that could contribute towards the development of sorbent based sample preparation techniques. The main objective is to demonstrate with some recent examples how through electrospinning two important parameters of a sorbent material (selectivity and sorptive capacity) can be addressed. In addition, a discussion of the potential for miniaturising SPE devices is discussed.

3.1 Optimal sorbent and sorbent fabrication technique

Over the years, significant progress has been made in the search of new materials (with respect to chemical composition) for SPE [66, 73, 138, 139]. On the contrary, the development of new SPE formats has been very slow. The fact that the shape or form of a sorbent material plays a vital role in the development of new SPE formats or configurations implies that alternative sorbent fabrication techniques would be vital for the development of SPE technology.

The SPE sorbent fabrication technique of choice can be viewed as one that produces material that exhibits chemical and morphological properties that can be easily modified. Similarly, an optimal SPE sorbent material combines the following benefits: (i) small diameter, (ii) large specific surface area, (iii) simplified fabrication/synthesis, (iv) ability to be modified in order

to incorporate all sorbent chemistries/functionalities, (v) ability to be modified in order to incorporate all sorbent morphologies and (vi) a material that can be packed in the lower (less than 10) mg range without presenting a back pressure limitation or low analyte recoveries. Developing an ideal sorbent fabrication technique and sorbent material seems to be a mammoth task that can only remain a dream, needless to say, it is expected that with improved technology and the ability to handle and characterise the material, the dream might be realised.

The development of nanomaterials was a major leap forward in the research area of sorbent based sample preparation techniques as it opened up possibilities for a class of materials with a large specific surface area that could be used in SPE applications. Thus it is not surprising that over the last 10 years there have been quite a number of reports on the use of nanoparticles for sample preparation as evidenced by a comprehensive review article presented in 2011 by Lucena and co-workers [18]. Although nanoparticles offer improved performance as sorbent material, they inherently exhibit some limitations. One of the main challenges is associated with their handling in packed SPE formats.

Given the fact that nanoparticles have shown excellent properties as sorbent material, it would seem prudent to focus developmental efforts on nanostructured materials. Therefore, an alternative sorbent fabrication approach that carries with it the benefits of nanoparticles at the same time addressing some (if not all) of their limitations would be ideal. The use of electrospun nanofibers as sorbent material is seen as a possible way of improving upon the use of nanoparticles as sorbent material for SPE.

This is based on the fact that through electrospinning, the benefits of nanoparticles can be incorporated in nanofibrous form at the same time addressing some (if not all) of their

limitations. Further, as a result of their fibrous and continuous nature, electrospun nanofibers may expand possibilities for the analytical process beyond their nanoparticle counterparts.

3.2 Electrospinning

Electrospinning is a technique that relies on repulsive electrostatic forces to draw a viscoelastic solution into nanofibers [140]. In simple terms, the electrospinning set-up consists of three basic components: a high voltage power supply, a mode to deliver a viscoelastic solution and a means of collecting the fibers (Fig. 3.1).

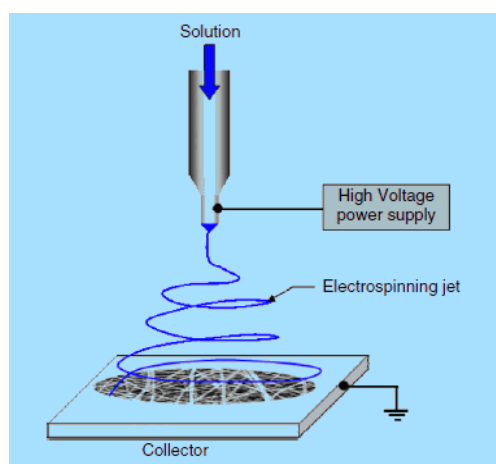


Fig.3.1 Schematic representation of the basic components of an electrospinning set-up [140].

When a high voltage is applied to the needle tip, surface charges accumulate and they lead to the deformation of the spherical droplet to a Taylor cone (Fig. 3.2.).

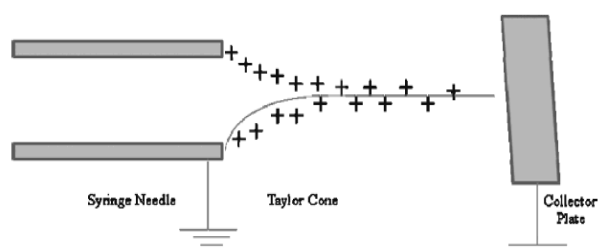


Fig.3.2 Schematic representation of the Taylor cone formation [141].

If the applied voltage is increased beyond this point, a jet will be ejected from the apex of the cone [141, 142]. As the jet travels towards the collector, tensile forces brought about by surface charge repulsion lead to a bending motion. It is at this stage that polymer chains within the jet stretch and orient to form a nanofiber that is deposited on a collector.

Besides electrospinning, there are other methods that are used for nanofiber fabrication which include drawing [143], template synthesis [144], phase separation [145] and self assembly [146]. Even though each method carries along its advantage(s), electrospinning is the most flexible. One of the unique benefits of electrospinning is that it is able to easily control the orientation of the nanofibers [140], which is important because fiber arrangement has a significant effect on the performance of the subsequent SPE devices.

Although production rate of fibers through electrospinning is relatively low in comparison to conventional textile processes, various strategies have been implemented towards scaling up the electrospinning set-up [147], the predominant strategy being the multiple spinneret electrospinning set-up which can be divided into two types as; linear arrays [148, 149] and two dimensional arrays [150, 151]. Fig 3.3 shows a schematic representation of a linear array multiple needle electrospinning set-up.

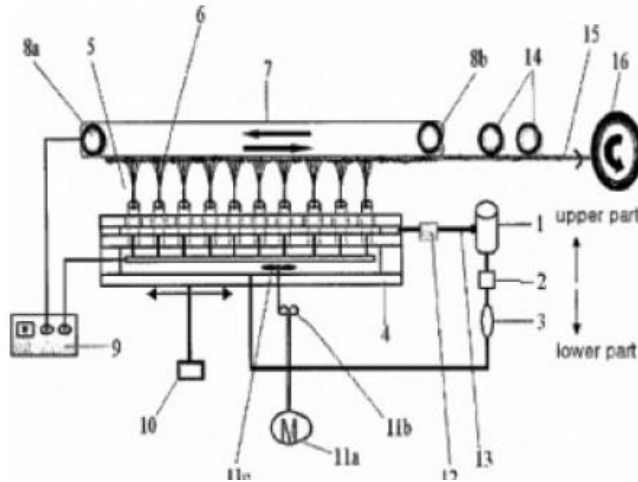


Fig.3.3 Schematic diagram of a bottom up multiple needle electrospinning set-up [152].

Initially the thinking regarding efforts to scale up the electrospinning set-up to an industrial production level was biased towards multiplication of the jets using multi-nozzle constructions [147]. However, this approach posed a challenge associated with the number of jets needed to reach economically acceptable productivity, typically thousands. Furthermore, challenges associated with reliability, quality consistency, and machine maintenance (especially cleaning) also surfaced.

A welcome development to electrospinning technology was nozzle-less electrospinning reported in 2004 by Jirsak and co-workers [153]. The nozzle-less electrospinning solves most of the limitations associated with multiple needle electrospinning due to its mechanical simplicity. However, the process itself is more complex because of its spontaneous multi-jet nature.

The main difference between nozzle-less electrospinning and conventional electrospinning is that multiple electrospinning jets are ejected from a free liquid surface where the voltage is applied. This means that the number of electrospinning jets is solely dependent on the available liquid surface area unlike conventional electrospinning which is dependent on the

number of needles.

Fig. 3.4 shows nozzle-less electrospinning in which a rotating drum is used as the substrate for the free liquid surface.



Fig.3.4 Free liquid surface electrospinning from a rotating electrode [154].

Fig. 3.5 shows an industrial scale set-up for nozzleless electrospinning for production of nanofiber sheets at Elmarco.



Fig.3.5 Large scale production of a nanofiber sheet by nozzle-less electrospinning line (Nanospider™) [154].

With the increase in the number of electrospinning companies (see Table. 3.1) over the last decade, electrospinning is expected to progressively move from a laboratory bench process to an industrial scale process. On the basis of the development of electrospinning companies, it may be said that in the near future, large scale production of electrospun fiber based sorbent material will be possible and thus paving way for industrial scale production of electrospun nanofiber based analytical devices.

Table.3.1 Some electrospinning companies established in the last decade (refer to web references).

Company Name	Country
Applied Sciences, Inc. (ASI)	United States of America
Elmarco	Czech Republic
eSpin Technologies, Inc	United States of America
Fibertex Nonwovens	Denmark
Finetex Technology	USA
IME Technologies	Netherlands
NanoFMG	Turkey
Neotherix	United Kingdom
Nicast	Israel
SNS Nanofiber Technology, LLC	United States of America
Zeus	United States of America
Electrospinz nanofibre engineering	New Zealand
Fuence	Japan
KES Kato Tech, Co., Ltd	Japan
Mechanics Electronics Computer Corporation	Japan
NanoNC	Korea
Yflow technology	Spain
The Electrospinning Company	United Kingdom
PolyNanotech	Germany
Fanavaran Nano-Meghyas	Tehran
ANSTCO	Turkey
Fiber Materials Electrospinning Laboratory	Russia

3.2.1 Range of materials that can be electrospun for SPE

The primary requirement for fiber formation through electrospinning is the viscoelasticity of the spinning solution. Solutions based on high molecular weight polymers possess the requisite viscoelasticity due to their long chains, hence making them the most popular electrospun material [155]. However, there is a wide range of pre- and post-electrospinning

modification processes that have made it possible to broaden the range of materials that can be electrospun [156, 157]. This means that it should be possible, through electrospinning to fabricate almost all classical SPE sorbent material (carbon based, polymeric and inorganic based) to form nanofibrous sorbents.

3.2.1.1 Carbon based

Over the years there have been several developments to carbon based materials for SPE, with the latest being carbon nanoparticles like fullerenes and carbon nanotubes (CNTs) [158]. The current focus on carbon nanoparticles for SPE has made other carbon based materials such as activated carbon almost obsolete. However, through electrospinning, a renewed interest in these materials has been realised.

Commercial polyacrylonitrile (PAN) based carbon fibers account for nearly 90% of the total carbon fiber output worldwide due to the high carbon yield and easy carbonisation process. Therefore, PAN is mostly chosen as the precursor polymer for the preparation of electrospun carbon nanofibers (CNFs) [159].

Electrospun nanofibers are generally reported to have a large specific surface area and this brings about three questions:

- 1) How large is large?
- 2) To what extent does the specific surface area of the respective electrospun nanofibrous materials affect their sorbent characteristics?
- 3) What methods are available for controlling the specific surface area of electrospun nanofibers?

Porous carbon nanofibers fabricated by thermal activation of electrospun PAN based CNFs have improved sorptive properties due to their large specific surface area. In a report by Oh

and co-workers, a study was carried out to determine the toluene adsorption capacity for PAN based steam activated carbon nanofibers (ACNFs) [160]. The CNFs were activated between 800 °C and 1000 °C in order to evaluate the effect of activation temperature on fiber porosity. A relatively large adsorption capacity (65 g toluene/100 g ACNFs) was achieved by ACNFs (activated at 1000 °C) with a specific surface area of 1403 m²g⁻¹ as compared to (40 g toluene/100 g ACNFs) that was achieved for ACNFs (activated at 800 °C) with a lower specific surface area of 853 m²g⁻¹. The results obtained in the study clearly demonstrated the great potential of steam activation as a post electrospinning modification approach for the fabrication of carbon nanofibers with large sorptive capacity that could be used as sorbent material for SPE.

Shim and co-workers compared the adsorption properties of electrospun steam activated carbon nanofibers and commercially available carbon fibers (CFs) [161]. Although there was a significant attenuation in the average fiber diameter from 20 μm (CFs) to 250 nm (ACNFs), the change in specific surface area was not significant (1015 m²g⁻¹ for CFs to 1193 m²g⁻¹ ACNFs). Nevertheless, ACNFs exhibited a much larger adsorption capacity and faster adsorption/desorption kinetics due to their large number of shallow micropores and a more homogeneous surface, all these properties brought about by their nanoscale size. As demonstrated by the results obtained in this study, it is interesting to note that, besides the specific surface area, the pore structure and surface homogeneity also play a significant role in improving sorptive capacity.

Bui and co-workers explored an alternative approach for fabricating porous carbon nanofibers in which PAN/pitch blends were electrospun with steam activation [162]. The specific surface area of the fabricated ACNFs increased from 723 m²g⁻¹ (activation temperature 700 °C) to 1877 m²g⁻¹ (activation temperature 900 °C). This was attributed to an increase in the mesopore fraction as the micropore fraction decreased. Given the fact that a

specific surface area of $1877 \text{ m}^2\text{g}^{-1}$ is among the highest ever reported for nanostructured materials, it is expected that carbon nanofibers fabricated as described would exhibit an excellent sorptive capacity.

Carbon nanotubes, besides their large adsorption surface, also possess excellent mechanical and electrical properties among others. Hence, electrospinning of polymer/CNT composites has become a broad field of research that aims to harness the superior properties of CNTs into fibrous structures [163].

Electrospinning has the capacity to align CNTs within a nanofiber matrix [164], thus allowing exposure of the CNT surface for sorptive interactions. It is due to the alignment ability of electrospinning that an interest has been developed for the use of electrospun polymer/CNT nanofiber composites for SPE.

A typical fabrication approach involves the integration of CNTs into the precursor solution and in some cases; heat treatment of the electrospun polymer/CNT composite fibers follows. The diameters of the electrospun fibers decrease with an increase in CNT content due to improved electrical conductivity brought about by the CNTs therefore increasing the specific surface area. Haddon and co-workers reported the fabrication of single walled carbon nanotubes (SWNTs) filled polystyrene (PS) nanofibers [165]. The distribution of the SWNTs was studied and no agglomeration within the polystyrene nanofibers was observed. Although the specific alignment of the individual SWNTs with respect to each other was not discerned, the incorporated nanotube bundles were straight and aligned along the fiber axis (Fig. 3.6).

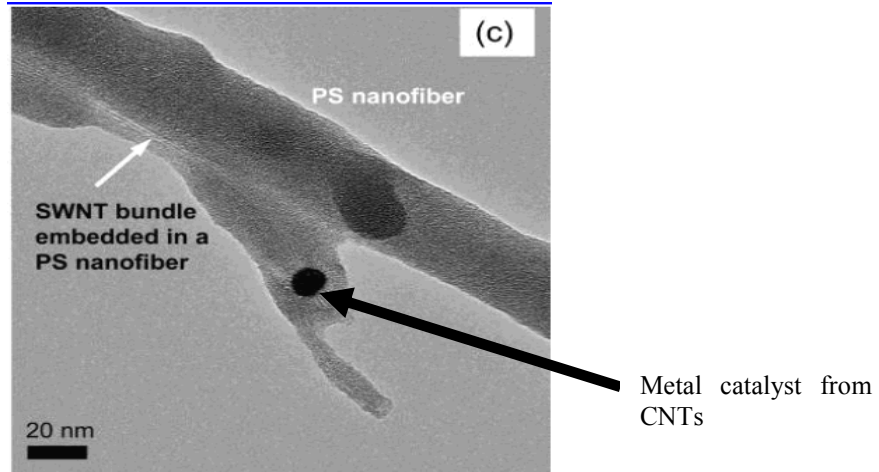


Fig.3.6 TEM image showing a SWNT bundle embedded in a PS nanofiber [165].

In another report that demonstrated the ability of electrospinning to align CNTs within polymer fibers, Ko and co-workers fabricated composite fibers of polylactic acid (PLA)/SWNT and PAN/SWNT [166]. TEM analyses revealed that the SWNTs were not distributed homogeneously in PLA fibers as the nanotubes were highly tangled forming spherical agglomerates (Fig. 3.7 (b)). In contrast, the SWNTs in PAN nanofibers maintained their straight shape and were parallel to the axis direction of the fibers (Fig. 3.7 (a)). One of the possible reasons could be that agglomeration was hindered by the smaller diameter (50-200 nm) of PAN fibers compared to about 1000 nm for PLA fibers. Furthermore, the differences in conductivity and wetting ability of the two polymers could also have had a significant effect.

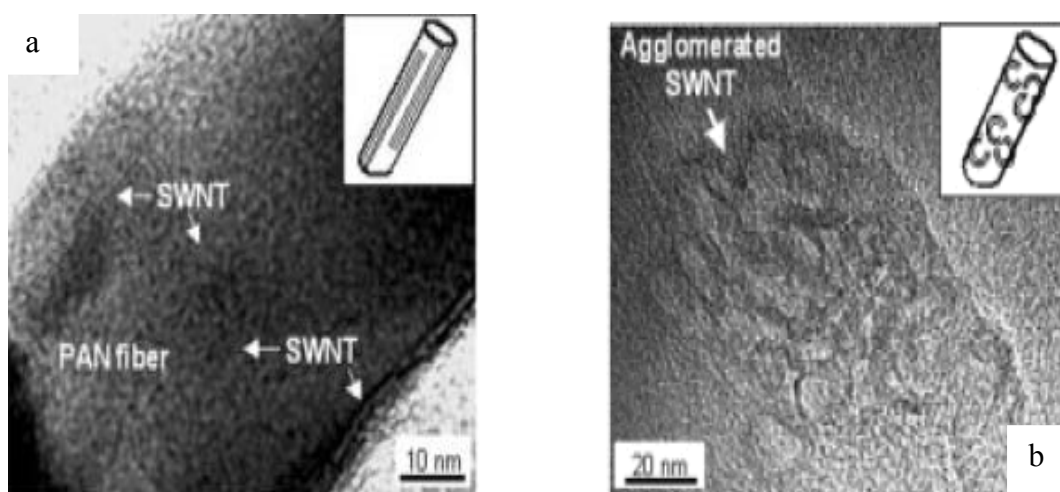


Fig.3.7 TEM images of (a) aligned SWNTs in electrospun PAN and (b) agglomerated SWNTs in PLA nanofibers [166].

3.2.1.2 Inorganic based

Over the years, silica microparticles have been used widely as sorbents for solid phase extraction. Recently, the focus has shifted to the use of silica nanoparticles due to their large specific surface area and intrinsic surface reactivity [18]. However, the use of silica nanoparticles for packed sorbent SPE still remains a challenge chiefly because of high back pressure, which explains why to date the smallest micro particle that has been used for packed sorbent SPE has a diameter of 8 μm [78]. Due to the fact that the simplest electrospinning set-up allows the collection of nanofibers in the form of a porous nonwoven mesh, it follows that porous electrospun nanofiber based SPE sorbent formats could be easily fabricated. Therefore, it is anticipated that electrospun silica nanofibers will be used for packed sorbent SPE, thus overcoming the high back pressure limitation associated with silica nanoparticles.

The fabrication of inorganic nanofibers typically involves the electrospinning of a polymer/sol composite and subsequent calcination of the electrospun fibers. In 2002, Shao

and co-workers were the first to report the fabrication of silica nanofibers [167]. The experimental approach involved first the preparation of a silica sol from tetraethyl orthosilicate (TEOS), H_3PO_4 , H_2O followed by electrospinning of a PVA/silica sol. The PVA/silica fibers were calcined to remove PVA resulting in amorphous silica fibers.

In 2003, Choi and co-workers reported a simplified approach in which silica nanofibers were fabricated directly from a silica sol [168]. Their fabrication method involved the preparation of a silica sol from TEOS, distilled water, ethanol and HCl with subsequent electrospinning. An interesting aspect of the fabrication approach was the fact that unlike in the first report by Shao and co-workers [167], TEOS did not contain a polymer to help with the spinnability, thus there was no need for the calcinations step. Spectroscopic characterisation of the silica nanofibers confirmed the extensive hydrolysis of the TEOS suggesting the availability of a substantial amount of silanol groups for silylation [168].

A way of improving the adsorption capacity of silica nanofibers could be to increase the specific surface area as a function of the pore volume. Patel and co-workers fabricated porous silica nanofibers containing catalytic silver nanoparticles [169]. TEOS, poly [3-(trimethoxysilyl)propylmethacrylate] (PMCM) and $AgNO_3$ were used as precursors for the production of silica/polymer hybrid nanofibers. On heat treatment of the electrospun fibers, degradation of the PMCM polymer resulted in pores that led to the increase in specific surface area from $11\text{ m}^2\text{g}^{-1}$ to $600\text{ m}^2\text{g}^{-1}$. The porous fibers exhibited an improved catalytic activity due to increased surface area. Therefore, it is expected that a similar approach could be used to improve the adsorptive capacity of silica fibers in SPE applications.

There is a wide range of other inorganic salts or particles that have been incorporated into nanofibers, the most popular being alumina [170-173]. Alumina has been widely used for adsorption of heavy metal ions such as arsenic. Due to the fact that adsorption depends on the

exposed surface area, it is expected that electrospun alumina nanofibers will exhibit an excellent sorptive capacity. Panda and Ramakrishna studied the effect of different precursors on the morphology of electrospun alumina nanofibers [174]. Their experimental approach employed a combination of PVA and PEO as the polymer precursor, aluminium acetate and aluminium nitrate as the alumina precursor. The PVA/aluminium acetate composite solution was found to be most suitable for fabricating alumina nanofibers. It is expected that the knowledge gained from the modification approaches for fabricating porous fibers of carbon and silica will be useful for the production of large specific surface area fibers of a whole range of other inorganic materials.

3.2.1.3 Polymer based

Synthetic polymers are the most popular class of materials that have been electrospun for SPE applications. Some of these polymers include polystyrene or polystyrene copolymers [175-184], nylon 6 [185-187], and polyethylene terephthalate [188]. Other reports have appeared in the Chinese database, unfortunately the polymeric material was not described in English [189-191]. It is expected that synthetic polymers will continue to be the most popular class of electrospun materials for use as SPE sorbents. This is due to the fact that, of all the materials that have been electrospun, polymers show the greatest potential for tuning of the sorptive chemistries.

Sorptive capacity of polymer nanofibers can be improved by increasing the pore volume. There are several methods that have been reported for introducing porous structures in nanofibers which include electrospinning of polymer blends [192], controlled humidity [193], the salt induced process [194] and silica nanotemplating [195]. Silica nanotemplating is a relatively simple process compared to the other methods as they require handling of complicated interactions between the polymer matrix and pore generator. In addition,

porosity and pore size of the resultant porous nanofibers may be controlled easily by adjusting the content and size of silica nanoparticles.

Shi and co-workers fabricated porous nylon 6 nanofibers using silica nanoparticles as the nanotemplate [195]. The experimental approach involved the fabrication of nylon 6/silica nanofiber composites, followed by removal of the silica nanoparticles through treatment with hydrofluoric acid. After the removal of the silica nanoparticles, the specific surface area and pore volume increased from $4.68 \text{ m}^2\text{g}^{-1}$ to $8.31 \text{ m}^2\text{g}^{-1}$ and $0.0133 \text{ cm}^3\text{g}^{-1}$ to $0.0250 \text{ cm}^3\text{g}^{-1}$ respectively. The increase in specific surface area demonstrated that the approach could be used to improve the sorptive capacity of nylon nanofibers for SPE applications.

Although all the examples that appear in literature have not been listed, it can be said with confidence that through electrospinning, all classical SPE sorbent material can be fabricated in their fibrous form. Some of the challenges that are likely to be encountered in the application of the electrospun fibers for SPE will be discussed in chapter 5.

Questions raised are:

- 1) What is the mechanical stability of these nanofibers?
- 2) Are they not brittle?
- 3) How does the introduction of pores affect the mechanical properties of the nanofibers?
- 4) What is the impact of packing on the morphology of the fibers?

It is expected that some of these questions will be answered in the near future after more experimental work has been carried out on the use of electrospun nanofibers as SPE sorbent material. For all these to be achieved, the process has to be initiated, which is the

primary objective of this thesis, as it is hoped it will stimulate the interest of those working towards better extraction processes.

3.2.1.4 Improvements in selectivity of electrospun nanofiber sorbents

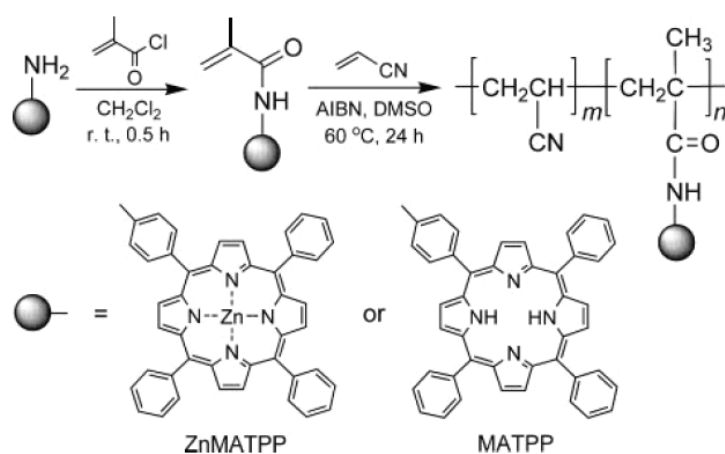
Selectivity of sorbent material is a parameter of great concern in current SPE applications. Due to the availability of a wide range of pre and post electrospinning modification processes, it is possible to impart selectivity on electrospun nanofibers based on all fundamental interaction mechanisms of all sorbents (microparticles to nanoparticles) which include; basicity, acidity, polarity, size and more recently, molecular recognition [31, 196, 197]. In the following section relevant examples will be used to highlight some of the successes of electrospinning towards selective SPE sorbents.

In 2007, Kang and co-workers were the first to report the use of electrospun polymer nanofibers for packed sorbent SPE [177]. Polystyrene nanofibers were employed for the extraction of trazodone (a basic analyte) from plasma. The predominant interactive forces were hydrophobic, thus inducing selectivity for trazodone in its unionised form. The objective of the study was to explore the feasibility of using electrospun nanofibers as sorbent material for SPE. Although polystyrene nanofibers may be regarded as a general purpose sorbent due to the fact that they rely on hydrophobic forces, the successes achieved in the study created a platform for further research.

At the beginning of 2008, the same research group reported a comparative study of the performances of poly (styrene-co-methacrylic acid), poly (styrene-co-*p*-sodium styrene sulfonate) and polystyrene nanofibers for the extraction of steroidal compounds [178]. Of the three kinds of nanofibers, those of poly (styrene-co-*p*-sodium styrene sulfonate) exhibited the highest extraction efficiencies, while those of polystyrene were the least efficient. The trend was attributed to the fact that the polar model analytes favoured the polar sorbent. With

respect to applications, the study provided a platform for different chemistries that could introduce selectivity based on hydrophobicity (polystyrene nanofibers) for non polar analytes, strong cation exchange properties (poly (styrene-co-*p*-sodium styrene sulfonate) nanofibers) for basic and neutral analytes and weak cation exchange properties (poly (styrene-co-methacrylic acid) nanofibers) for strongly basic analytes. Due to the ease of spinnability of polystyrene copolymers and the demonstrated performance of the resultant fibers as SPE sorbents, a wide range of functionalities can be introduced on the polystyrene backbone by an experimental approach that involves copolymerisation and electrospinning. It is expected that in the near future, SPE sorbents based on electrospun polystyrene copolymers will increase as there is a wide range of vinylic monomers that can be copolymerised with styrene.

Besides the conventional small functional groups like sulfonates and carboxylic acids, macromolecules can be incorporated into polymer nanofibers to improve their selectivity as SPE sorbents. Wan and co-workers reported the fabrication of porphyrinated nanofibers by copolymerisation and electrospinning [198]. The fabrication approach involved solution copolymerisation of acrylonitrile with vinyl porphyrins (see scheme. 3.1.) and subsequent electrospinning of the resultant porphyrin copolymers.



Scheme.3.1 Schematic representation of synthesis and molecular structure of the porphyrin copolymers [198].

Porphyrins have been used as the bonded phase in conventional SPE to improve the recovery of analytes such as phenols and polycyclic aromatic hydrocarbons [199-201]. The improved extraction efficiency was mainly due to the increased π - π interactions between the porphyrin molecules and the analytes. Furthermore, the increase in surface area due to the porphyrin macromolecule may be another factor. It is therefore anticipated that a wide range of porphyrin functionalised nanofiber sorbents will be fabricated as the chemistry of porphyrins is well known.

Cyclodextrin bonded phase materials are among some of the highly selective chiral stationary phases for thin layer chromatography (TLC) and high performance liquid chromatography (HPLC). Cyclodextrin molecules are able to effect selective separations due to their ability to form inclusion complexes with selected organic and inorganic molecules [202]. Therefore, an approach in which nanofibers are functionalised with cyclodextrins is seen as possible way of fabricating highly selective SPE sorbent material.

Uyar and co-workers reported the incorporation of β -cyclodextrin (β -CD) into electrospun polystyrene fibers for use as molecular filters [203]. They investigated the adsorptive capability of β -CD functionalised nanofibers by using phenolphthalein as the model analyte. It was observed that the rate of phenolphthalein adsorption increased with β -CD content. Although this functionalisation approach raises questions with respect to the sort of bonds formed between the functional molecules and polymer support, it provides a platform for fabricating selective nanofiber sorbents for SPE. A possible way forward could be to consider a method that immobilises β -CD at the surface of the nanofibers by covalent bond formation.

In another modification approach, Yao and co-workers reported the fabrication of quaternary amine functionalised polyurethane (PU) fibers for use as novel antibacterial material. They

used a process which involved plasma pretreatment, UV-induced graft copolymerisation of 4-vinylpyridine, and quaternisation of the grafted pyridine groups with hexylbromide [204]. The modified PU fibers exhibited highly effective antibacterial activities due to the availability of the quaternary amine functional groups at the surface. Quaternary amine modification of nanofibers using the reported experimental approach could offer a possibility for fabricating a sorbent material that may exhibit both anion exchange and reversed phase properties. This sort of material would be applicable for the selective retention of acidic and neutral analytes.

In chromatographic separation, dye ligands for protein purification have been developed extensively because they offer opportunities for simple and rapid isolation of proteins. To the best of our knowledge, as of 2006 there were about 30 different types of dyes available for purification of a great variety of protein molecules [205]. A modification approach that can allow surface attachment of the dye ligands on the nanofibers would open up possibilities for a wide range of selective sorbent materials for SPE.

Ma and co-workers reported the fabrication of Cibacron blue F3GA (CB) functionalised electrospun polysulfone (PSU) fibers for use as an affinity membrane [205]. They used a process which involved graft polymerisation of methacrylic acid onto the air plasma treated PSU surface. This was then followed by the introduction of amino groups via the reaction of diaminodipropylamine (DADPA) in the presence of carbodiimide (coupling agent). Finally, CB was attached onto the PSU fiber surface by covalent bond formation with the amino groups (Fig. 3.8).

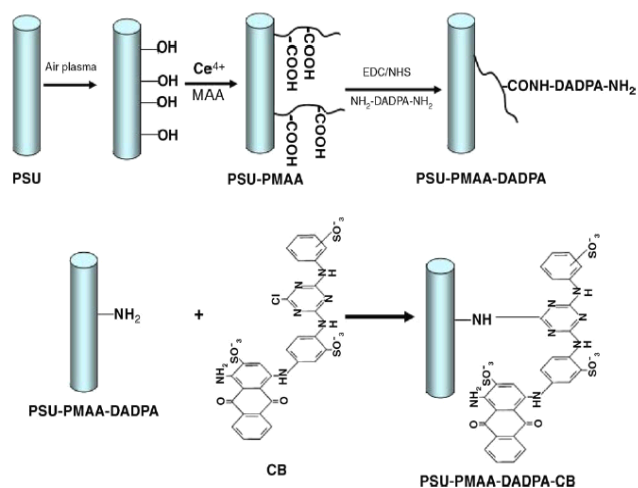


Fig.3.8 Schematic representation of the electrospun PSU nanofiber surface modification procedure [205].

CB was selected due to its widespread use as a dye ligand for purification of many enzymes and blood proteins, among which the most popular is bovine serum albumin (BSA) [206]. The novel PSU nanofiber mat showed higher water permeability than commercially available microporous membranes as well as good capturing for BSA. Although our main interest in the study was driven by the need to demonstrate the capability of the electrospinning technique to fabricate selective sorbent material for biomolecules, it opens up possibilities for fabricating sorbent material in which hydroxyl (normal phase property for polar analytes), carboxyl (weak cation exchange property for strong bases) and amino (weak anion exchange property for strong acids) functionalities are of interest.

Of all SPE sorbent materials that have been reported to date, those fabricated via the molecular imprinting technology have shown the best selectivity after immunosorbents [139]. Through electrospinning it is possible to incorporate the selectivity of MIPs either by encapsulating MIP nanoparticles into electrospun nanofibers or by imprinting the electrospun fibers.

Yoshimatsu and co-workers encapsulated molecularly imprinted nanoparticles into poly (ethylene terephthalate) (PET) nanofibers through electrospinning [188]. The composite nanofibers (Fig. 3.9) were used as sorbent material for batch solid phase extraction of propranolol. As confirmed by radio ligand binding analysis, the specific binding sites in the composite nanofibers remained easily accessible and were chiral selective. Furthermore, it was demonstrated that without the electrospun nanofiber based solid phase extraction step, the existence of propranolol residues in water could not be confirmed even with the sensitivity of HPLC-MS/MS analysis [188].

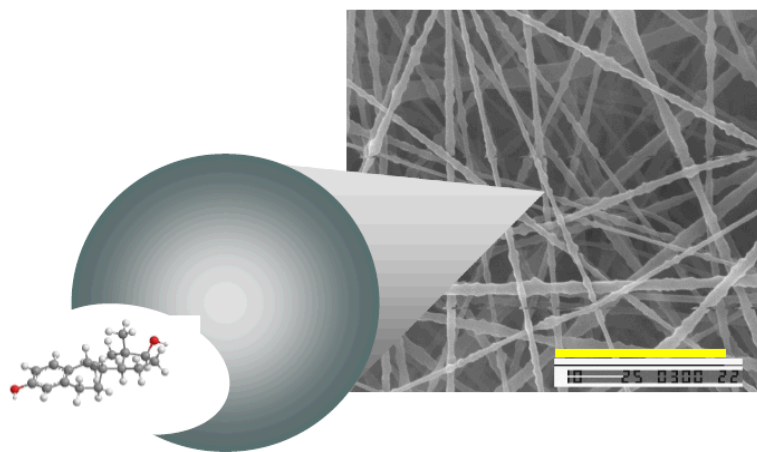


Fig.3.9 SEM image of MIP nanoparticle embedded electrospun PET nanofibers [188].

Chronakis and co-workers reported a simplified approach that allowed the generation of template defined sites directly during electrospinning [207]. The electrospun nanofibers were prepared from a solution mixture of PET and polyallylamine in the presence of a template molecule, 2,4-dichlorophenoxyacetic acid (2,4-D). Polyallylamine was used to provide functional groups that interacted with the template during the electrospinning process, and PET was used as the supporting matrix to ensure easy fiber formation and to minimise the conformational change of the polymers when the nanofibers were subjected to different solvent treatments. Fig. 3.10 shows a schematic representation of a possible binding site model for the reported 2,4-D imprinted nanofibers. The results obtained demonstrated for the

first time that electrospun template directed molecular imprinting is a viable method for creating robust molecularly imprinted nanofibers that can selectively rebind the target molecule.

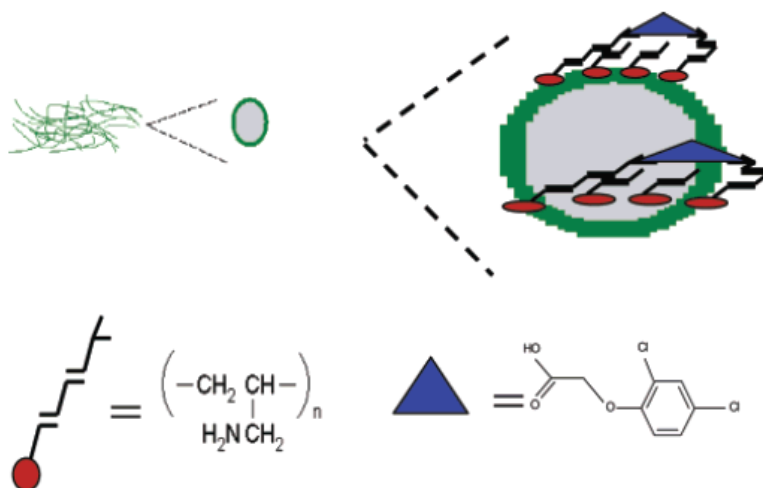


Fig.3.10 Schematic representation of molecularly imprinted nanofibers with binding sites specific for 2,4-D template molecules [207].

3.2.2 Electrospun nanofiber based SPE formats and configurations

Two important aspects in the development of SPE technology are simplicity of sorbent fabrication and miniaturization of devices. It is a fact that electrospun fibers can be packed in all existing formats and configurations for both SPE and SPME. Furthermore, the use of electrospun fibers introduces an aspect of simplicity and miniaturization to the fabrication of SPE devices.

To date, methods of SPE disk fabrication involve a complicated multi step process in which microparticles are tightly held together within an inert fiber matrix, such as polytetrafluoroethylene [208]. This has limited the range of disk sorbent chemistries that are available. Two possible ways of simplifying the disk sorbent fabrication process would be; (i) to incorporate nanoparticles into nanofibers and pack the fibers in disk format or (ii) to

fabricate nanofibers of the material with the chemistry of interest and pack them in disk format.

Chigome and co-workers fabricated a solid phase extraction device based on electrospun polystyrene fibers packed in disk format [180]. The experimental approach consisted of copolymerization with subsequent electrospinning of the resultant polymer. 10 mg of electrospun polystyrene fibers were packed in a disk format (5 mm × 1 mm) as shown in Fig. 3.11. The study clearly demonstrated how the use of electrospun fibers can simplify SPE disk fabrication as the sorbent material was packed using simple homemade tools. It is expected that in the near future, a wide range of chemistries will be introduced on disk SPE devices fabricated using a similar approach that will ultimately lead to a routine disk fabrication technology.

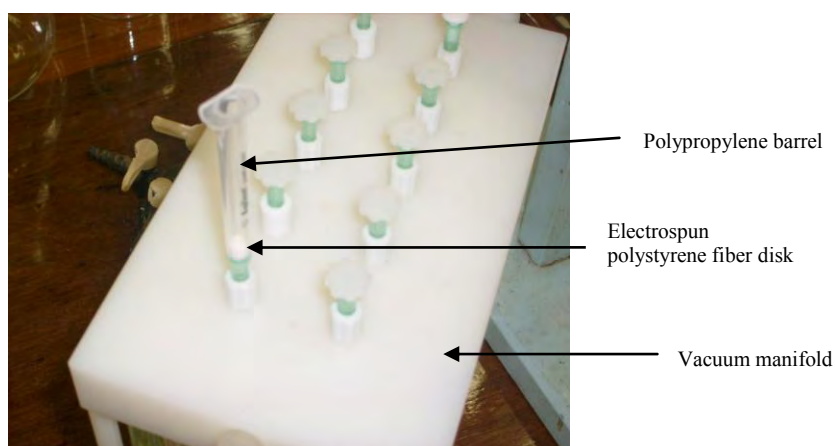


Fig.3.11 Electrospun fiber disk SPE device connected to a vacuum manifold [180].

In another SPE disk fabrication approach, Xu and co-workers reported the use of Nylon 6 nanofibers as sorbent material for what they referred to as solid membrane extraction (SME) [185]. A Nylon 6 nanofiber sheet was cut in the form of disks of 1.5 cm diameter, 120–150 μm thickness and 1.5 mg mass (Fig. 3.12).

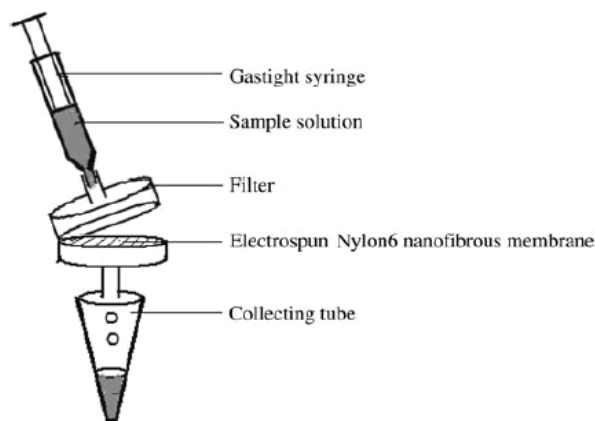


Fig.3.12 The fiber-filter solid-phase extraction device [185].

The success achieved with the reported electrospun fiber based disk formats demonstrates that in future, it will be possible to fabricate miniaturized disk SPE variants like the 96 well plate configurations or large scale disk SPE devices like the Buchner funnel format. Therefore, the use of electrospun nanofibers might overshadow the complicated multi-stage particle embedded or particle loaded disk fabrication processes.

The micro column configuration is the third electrospun nanofiber based SPE device that has been reported. Kang and co-workers were the first to report the fabrication of this type of SPE device [177]. They manually packed 1 mg of polystyrene nanofibers into the tip end of a 200 μ L micropipette tip to form a micro column as shown in Fig. 3.13 (a). Solvents were pushed through the electrospun nanofiber based SPE device manually by the pressure of air forced by a gas tight plastic syringe (2 mL) as shown in Fig. 3.13 (b). The device demonstrated a leap forward regarding the use electrospun nanofibers for miniaturized SPE devices. Although the packing process involved the use of simple homemade tools, it seems the packing operation is not that simple as reproducibility relies very much on operator experience. Nevertheless, the study created a platform for further research as it clearly demonstrated that nanofibers allowed the miniaturization of SPE devices without compromising the extraction efficiency.

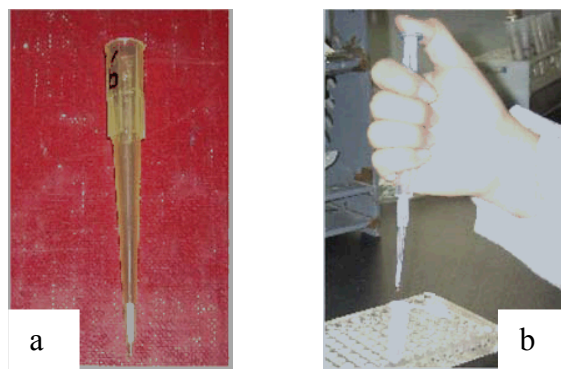


Fig.3.13 Photograph of (a) micro-column SPE device and (b) manual SPE operation [209].

In an effort to simplify SPE operation, Zhang and co-workers fabricated the micro column SPE device in the same way as reported by Kang and co-workers, their modification being the use of a vacuum manifold to easily control flow rate (Fig. 3.14) [178].

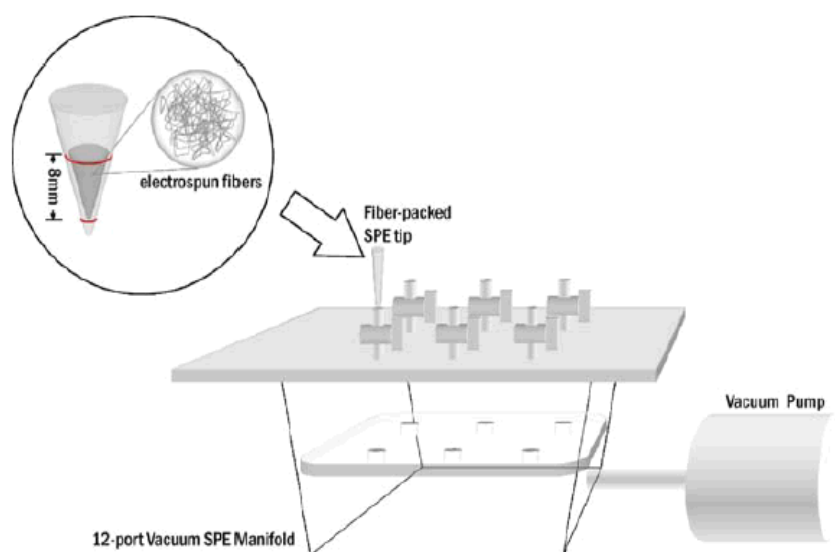


Fig.3.14 Schematic diagram of a micro column SPE device connected to a vacuum manifold. [178].

Innovations employing electrospun nanofibers as a chromatographic sorbent bed besides SPE have also been demonstrated. Susan Olesik's research group was the first to report other chromatographic applications of electrospun nanofibers besides SPE. Olesik and co-workers electrospun SU-8 2100 (a negative photoresist) nanofibers onto stainless steel wires with

subsequent pyrolysis to form carbon nanofiber based coatings [210]. Fig. 3.15 shows the SEM image of an electrospun fiber coated SPME device. An interesting aspect of the fabrication approach is that the fibers were attached to the stainless steel wires without the use of a binder. The extraction efficiencies of the resulting SPME device were enhanced or comparable to commercially available SPME fibers. Fabrication of SPME devices using electrospinning as a sorbent coating technique is a viable alternative as it presents a platform for improved sorptive and selectivity characteristics due to the available electrospun nanofiber modification and/or functionalisation approaches.

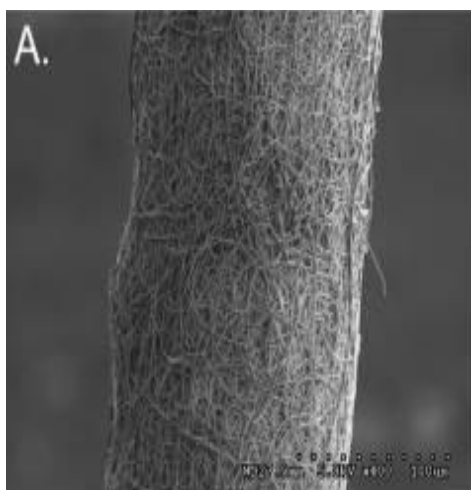


Fig.3.15 SEM image of a electrospun fiber coated SPME device [210].

Another benefit of the electrospinning technique is that, besides fibers, SPME coatings of nano to micro particles can be fabricated by simply reducing the viscosity of the dope solution. The technique is referred to as electro spraying [211-213]. It is expected that through electro spraying, besides improved sorptive and selectivity characteristics, SPME applications will expand due to the wide range of available nanoparticles.

3.3 Scope of the thesis

The driving forces for the research work reported in this thesis are in twofold;

1. To get a better understanding of the experimental aspects associated with the control of the electrospinning process aimed at electrospun nanofiber based sorbent fabrication.
2. To get a better understanding of the experimental aspects associated with the fabrication and application of electrospun nanofiber sorbent based solid phase extraction devices.

The stimuli for the thought process behind the thesis were aligned in this framework not only because the author has a passion for fundamental research (*Curiosity driven fundamental research is the basis for all discoveries. "It is a profound and necessary truth that the deep things in science are not found because they are useful; they are found because it was possible to find them"-Robert Oppenheimer*) but also due to the need to contribute to knowledge from the nanomaterials perspective. The focus on nanomaterials is due to the fact that they are at the leading edge of all available materials and the only limiting factor from getting the most out of these materials is getting a better understanding of their fabrication and application to address the numerous challenges in science and technology.

The specific focus on using electrospinning for the value addition to SPE as a way of getting a better understanding of nanomaterials fabrication and handling is due to the fact that it is a interdisciplinary area combining analytical chemistry, polymer science, physics and engineering. A researcher in this area is forced to constantly think of strategies for morphological and chemical modification of materials. This is due to the fact that optimal performance of a SPE process is dependent on a total control of the analyte mass transfer kinetics which not only depends on solution properties but also on the sorbent

physicochemical properties as a function of the wide range of analyte and matrix challenges. In the thought process, the researcher would ultimately add value directly or indirectly to all areas of science and technology because all classes of materials would be considered.

Therefore, the main objective of the thesis was to explore the possibility of using electrospun nanofibers as an alternative sorbent material for solid phase extraction. In order to achieve this, specific objectives were split into three as;

1. To explore the possibility of developing an electrospinning set-up for controlled nanofiber deposition.
2. To explore the possibility of developing a synthetic protocol for controlling electrospun nanofiber functionality.
3. To develop miniaturised solid phase extraction devices that use electrospun nanofibers as the sorbent bed.

Chapter 4

4. Experimental

Summary

This chapter presents the experimental details for the study. It has been structured to provide details of the experimental procedures for the three components of the research work which are; (i) Polymer synthesis and characterisation, (ii) Electrospinning procedures and electrospun fiber characterisation, (iii) SPE device fabrication and procedures.

4.1 Materials and equipment

4.1.1 Polymers and related polymerisation materials

Styrene, *p*-sodium styrene sulphonate, methacrylic acid and acrylamide monomers were purchased from Sigma Aldrich (Saint Louis, MO, USA). Potassium persulphate (thermal initiator) was purchased from Saarchem (Johannesburg, South Africa). Nylon 6 (M_w : 10 000), polyethylene oxide (PEO) (M_w : 300 000), and β -cyclodextrin were purchased from Sigma Aldrich (Saint Louis, MO, USA).

4.1.2 Solvents

HPLC grade solvents acetonitrile and methanol were obtained from Sigma Aldrich (Saint Louis, MO, USA). Ultrapure water was obtained from a Milli-Q purification system by Millipore (Molsheim, France). Analytical grade *N,N*-dimethylformamide (DMF), tetrahydrofuran (THF), acetic acid, formic acid, chloroform, dichloromethane (DCM), dimethyl sulfoxide (DMSO), acetone and formic acid were purchased from Merck Chemicals (Wadesville, South Africa).

4.1.3 Standards

Hydrocortisone (98.0%), cortisone acetate (99.0%), 19-nortestosterone (99.0%), prednisone (98%), betamethasone (98%) and dexamethasone (98%) were purchased from Sigma Aldrich (Saint Louis, MO, USA). Stock solutions of each standard ($500 \mu\text{g ml}^{-1}$) were prepared in methanol and working standards were prepared by serial dilutions with water.

4.1.4 Instrumentation

Photographs were taken using a single shot digital camera (Sony DSC-S730 Cyber-shot). An Olympus BX40 optical microscope was used to confirm the formation of fibers before scanning electron microscopy (SEM). The morphology of fibers was determined using a Vega Tescan Scanning Electron Microscope. Fourier transform infrared spectra (FTIR) were obtained from a Perkin Elmer Spectrum 100 ATR (attenuated total reflection)-FTIR spectrometer. Separation and detection of analytes was achieved on an Agilent 1200 high performance liquid chromatograph equipped with a diode array detection (HPLC-DAD) system. A Zorbax Eclipse C₈, $3.5 \mu\text{m} \times 4.6 \text{ mm} \times 100 \text{ mm}$ column was used with subsequent detection at 240 nm. Two HPLC methods were employed; in the first method, isocratic elution was achieved using a methanol-water mixture (58:42 v/v) mobile phase at a flow rate of 1 ml min^{-1} . In the second method, isocratic elution was achieved using a acetonitrile-10 mM formic acid mixture (35:65 v/v) at a flow rate of 0.8 ml min^{-1} . A $\pm 0\text{-}25 \text{ kV}$ high voltage power supply assembled by Ulrich Büttner, (Stellenbosch University, Stellenbosch, South Africa) was used for all electrospinning experiments. Two syringe pumps, an “infusion only” (NE-300) and a “withdraw/ infuse” (NE-1000) from New Era Pump Systems, Inc (Farmingdale, New York, USA) were used. All rotating collectors were driven by a 12 V DC motor that was powered by a stabilized voltage supply (Farnell Instruments Ltd, Type L 30).

Thermogravimetric analyses (TGA) were carried out on a Thermal Analysis (TA) Instruments Q600 SDT using a heating rate of $10\text{ }^{\circ}\text{C min}^{-1}$ and nitrogen as the purge gas.

4.2 Electrospinning set-ups

Three electrospinning set-ups were employed, the first two set-ups which were employed for all the initial controlled deposition experiments consisted of either a pasteur pipette in which a polymer solution was charged by a copper wire [214-218] with a grounded static collector or a polypropylene syringe with a negative counter electrode and rotating collectors. All polymer solutions were driven by gravity.

The third set-up which was employed for the fabrication of all sorbents evaluated in the study was a modification of a rotating collector set-up as reported by Katta and co-workers [219]. In the set-up, a polymer solution was loaded into either a glass (10 ml) or polypropylene (25 ml) syringe. A 21 gauge, 90° blunt end stainless steel needle was connected either directly to the luer tip of the syringe or via a polytetrafluoroethylene (PTFE) tubing. The anode of the high voltage power supply was connected to the stainless steel needle while a sharp edged copper strip placed behind a rotating drum collector was connected to the cathode. All polymer solutions were driven by a syringe pump.

4.3 Copolymerisation

Three copolymers poly (styrene-co-methacrylic acid), poly (styrene-co-*p*-sodium styrene sulfonate) and poly (styrene-co-acrylamide) were synthesized at five mole ratios of their respective comonomers, that is (0:1, 1:10, 1:1, 2:1, 5:1, 10:1, 1:0) for methacrylic acid: styrene and acrylamide:styrene. While for *p*-sodium styrene sulfonate:styrene, mole ratios of (0:1, 1:1, 5:1, 10:1, 15:1, 20:1, 1:0) were employed. Homopolymers of polystyrene, polyacrylamide, polymethacrylic acid and poly (*p*-sodium styrene sulfonate) were synthesized. All copolymers and homopolymers were synthesised by boiling medium

emulsion polymerisation. In a typical polymerisation procedure, a three (with one opening blocked) or two necked flask equipped with a reflux condenser and a magnetic bar placed in an oil bath was used (see Fig. 4.1). Appropriate quantities of the monomers were added into 50-100 ml of water and stirred at a rotation speed of 300 rpm. The mixture was raised to reflux and after the medium had boiled for 30 min, typically at 93-98 °C, 0.2 wt% (with respect to the monomers) of the potassium persulfate initiator dissolved in an appropriate amount of water was added to the boiling medium. The reaction was left to run for 12 h to ensure complete polymerisation before water removal by a rotary evaporator and subsequent oven or air drying of the resultant polymer powders.



Fig.4.1 Photograph of boiling medium emulsion polymerisation set-up.

4.4 Electrospinning

4.4.1 Copolymers

Flow rate, polymer solution concentration, applied voltage and the tip to collector distance are the only parameters that were optimised in the electrospinning of the synthesised polymers. For all polystyrene copolymers, the desire was to use the same solvent system

DMF:THF (4:1), but at some mole ratios either methanol or formic acid were used depending on polymer solubility.

Table.4.1 Electrospinning conditions for poly (styrene-co-methacrylic acid) copolymers at different mole ratios.

Mole ratio	Concentration (wt%)	Solvent	Voltage (kV)	Distance (cm)	Flow rate (ml h⁻¹)
0:1	20	Methanol	+20, -5	10	0.1
1:10/ β -CD	20/10	DMF:THF (4:1)	+20, -5	13	0.3
1:1/ β -CD	20/10	DMF:THF (4:1)	+20, -5	10	0.010
2:1	18	DMF:THF (4:1)	+20, -5	11	0.1
5:1	13	DMF:THF (4:1)	+20, -5	11	0.1
10:1	13	DMF:THF(4:1)	+20, -5	10	0.1

Table 4.1 shows the optimised electrospinning conditions for poly (styrene-co-methacrylic acid) at monomer mole ratios ranging from 0(styrene):1(methacrylic acid) to 10(styrene):1(methacrylic acid). Poly (styrene-co-methacrylic acid) copolymers synthesised from a mole ratio of 1:10 and 1:1 were spun doped with 10 wt% (with respect to the polymer) β -cyclodextrin. The resulting electrospun nanofibers of β -cyclodextrin doped poly (styrene-co-methacrylic acid) were placed in an oven at 140 °C for 1 h to effect heat induced cross linking so as to render the polymer fibers water and methanol insoluble.

Table.4.2 Electrospinning conditions for poly (styrene-co-acrylamide) copolymers at different mole ratios.

Mole ratio	Concentration (wt%)	Solvent	Voltage (kV)	Distance (cm)	Flow rate (ml h⁻¹)
0:1	10	Formic acid	+20, -5	10	0.1
1:10	20	Formic acid	+22.5, -5	10	0.05
*1:1	-	-	-	-	-
*2:1	-	-	-	-	-
5:1	20	DMF:THF (4:1)	+20, -5	10	0.5
10:1	20	DMF:THF (4:1)	+22.5, -5	10	0.05

Table 4.2 shows the optimised electrospinning conditions for poly (styrene-co- acrylamide acid) at monomer mole ratios ranging from 0(styrene):1(acrylamide) to 10(styrene):1(acrylamide). The mole ratios marked with asterix (*), there are no electrospinning conditions because the resultant polymeric materials were not soluble in the tested solvents of interest.

Table.4.3 Electrospinning conditions for poly(styrene-co-*p*-sodium styrene sulphonate) copolymers at different mole ratios.

Mole ratio	Concentration (wt%)	Solvent	Voltage (kV)	Distance (cm)	Flow rate (ml h⁻¹)
0:1	20	Formic acid	-	-	-
1:1	-	-	-	-	-
5:1	-	-	-	-	-
10:1	10	DMF:THF (4:1)	+22.5, -5	10	0.2
15:1	10	DMF:THF (4:1)	+22.5, -5	10	0.2
20:1	20	DMF:THF (4:1)	+20.5, -5	10	0.1

Table 4.3 shows the optimised electrospinning conditions for poly (styrene-co- *p*-sodium styrene sulphonate) at monomer mole ratios ranging from 0 (styrene):1(styrene-co- *p*-sodium styrene sulphonate) to 20 (styrene):1(styrene-co- *p*-sodium styrene sulphonate). The mole ratios marked with asterix (*), there are no electrospinning conditions because the resultant polymeric materials were not soluble in the tested solvents of interest.

4.4.1 Commercial polymers

Table.4.4 Electrospinning conditions for commercial polymers.

Polymer	Concentration (wt%)	Solvent	Voltage (kV)	Distance (cm)	Flow rate (ml h ⁻¹)
Polyacrylic acid/ β -CD	6.6/10-25	Ethanol:Water (4:1)	+15,-5	15	1
Nylon 6	16	Formic acid: acetic acid (1:1)	+20, -5	6	1
Polyethylene oxide	10	Water	+15,-5	15	0.05
Polyethylene oxide	7	Water	+15	15	-

Table 4.4 shows the optimised electrospinning conditions for commercial polymers; polyacrylic acid, polyethylene oxide and nylon 6. β -cyclodextrin doped (10-25 wt%) polyacrylic acid fibers were placed in an oven at 140 °C for 1 h to effect heat induced cross linking so as to render the polyacrylic fibers water and methanol insoluble.

4.5 Fabrication of SPE devices

4.5.1 Micro-column SPE device

The electrospun fibers were divided into three fiber clews then each clew was put into a 200 μ l pipette tip. The clews were made in such a way that the smallest was put first into the pipette tip and forced down (using a 0.5 mm stainless steel rod) to a point 8 mm from the bottom of the pipette tip. The other two clews were placed successively and finally the whole sorbent bed was made firm by a (2 mm diameter) copper wire rod to end up with a bed height of 8 mm (when 10 mg of electrospun fibers were packed).

4.5.2 Disk SPE device (Disk I)

Electrospun fibers were placed at the base of a 1000 μl polypropylene SPE barrel. With the aid of a glass rod (5 mm diameter), the fibers were manually compressed by sandwiching them between polyethylene frits to form a disk (1 mm \times 5 mm in the case where 10 mg of fibers were packed). The electrospun fibers disk sorbent bed was then forced to the base of the SPE barrel with the aid of the glass rod.

4.5.3 Disk SPE device (Disk II)

The second disk SPE device was fabricated manually by a three step process. In the first step, a homemade manual brass cutter was used to cut out 5 mm diameter circular portions directly from an electrospun nanofiber mat deposited on an aluminium foil collector (see Fig. 4.2). The second step consisted of placing the 5 mm diameter portions at the base of a 500 μl polypropylene SPE barrel and supported by a homemade stainless steel frit. Finally, polypropylene tubing with an outside diameter of 5 mm was forced to into the SPE barrel to firmly hold the stainless steel frit and the sorbent bed.

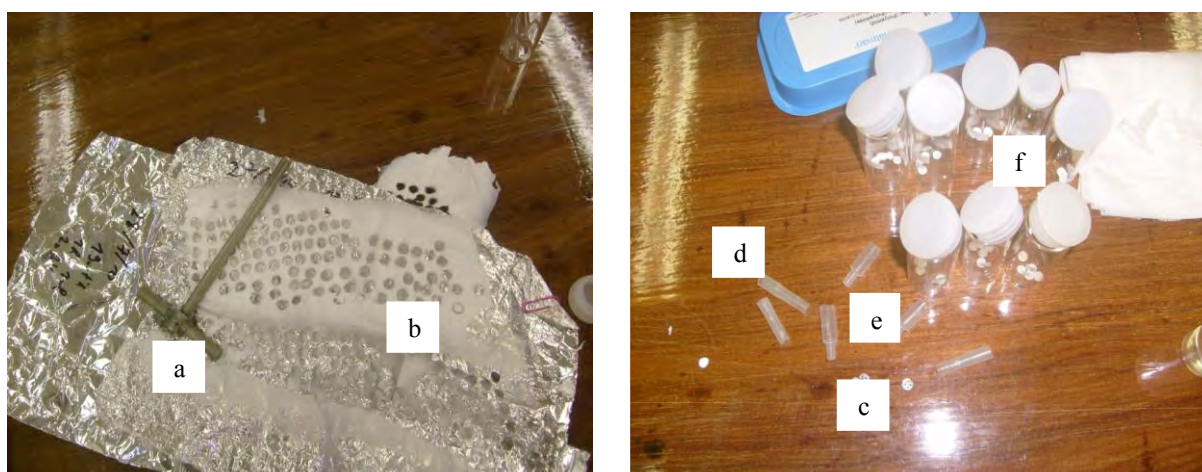


Fig.4.2 Photographs showing the process involved in fabricating the disk (II) sorbent bed (a) brass cutter (b) electrospun nylon nanofiber sheet on aluminium foil with perforated portions (c) stainless steel frit (d) polypropylene tube (e) 500 μl barrel (f) disk sorbent beds in vials.

4.6 SPE experiments

4.6.1 Recoveries

A micro pipette (see Fig 4.3 (a)) was used to control solvent flow through the micro column sorbent bed while a vacuum manifold (see Fig 4.3 (b-c)) was used to control solvent flow for the disk and micro column sorbent beds.

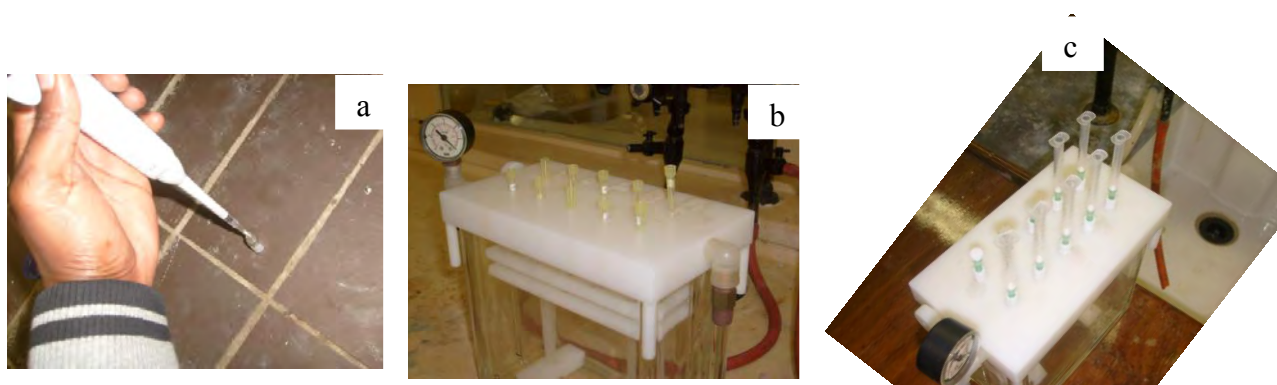
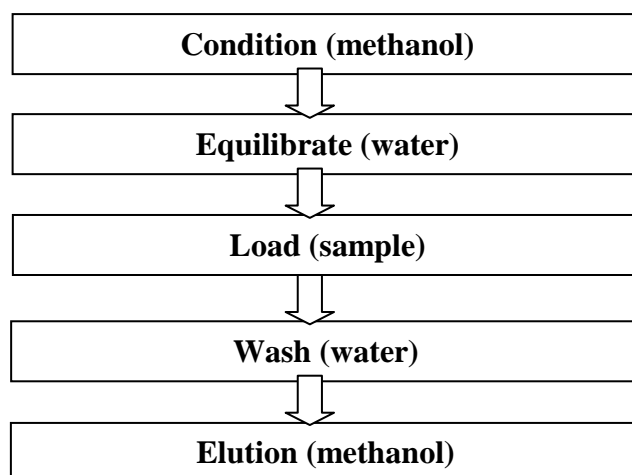


Fig.4.3 (a) Micropipette and (b-c) vacuum manifold control of solvent flow through sorbent beds.

For all SPE steps, 100 μl aliquots were used and the recoveries were established by comparing the signal response (peak area) of the eluted analyte (from spiked plasma, urine or water) to that of the analyte signal prior to SPE. All the initial recovery experiments were conducted using water spiked with 500 ng ml^{-1} of corticosteroids (prednisone, hydrocortisone, cortisone acetate, 19-nortestosterone, betamethasone and dexamethasone). Further recovery experiments in plasma and urine were conducted at three spiking levels (31.23, 125 and 500 ng ml^{-1}).



Scheme.4.1 Flow diagram for the solid phase extraction protocol.

4.6.2 Breakthrough experiments

For all breakthrough experiments the sorbent bed (either disk or micro column format) was activated with 100 μl methanol and subsequently equilibrated with 100 μl water. Initially, the breakthrough experiments were conducted manually (using a vacuum manifold) by continuously loading the sample at a flow rate that corresponds to a pressure of 1mmHg and collecting 100 μl fractions of the eluate. A second manual approach was employed for breakthrough experiments on the micro column SPE device. This consisted of driving the solvent through the sorbent bed with the aid of a micro pipette, 100 μl fractions were collected dropwise as corresponding to 4-5 drops per minute. Lastly, a syringe pump driven semi-automated system (see Fig 4.4) was then developed to allow a continuous flow of the sample at a flow rate of 0.1 ml min^{-1} through the sorbent bed with subsequent collection of 100 μl fractions.

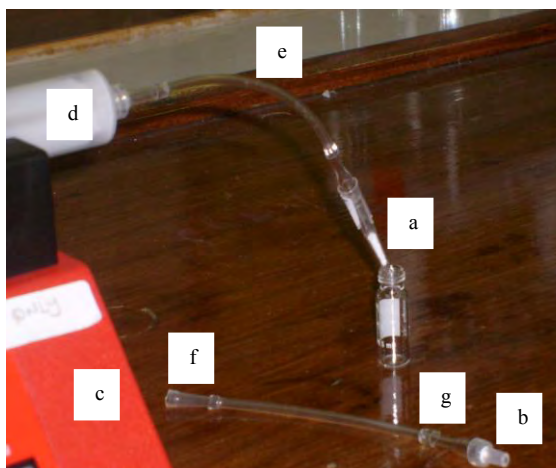


Fig.4.4 Syringe pump driven semi-automated system (a) micro column SPE device (b) modified disk (I) and disk (II) SPE device (s) (c) syringe pump (d) polypropylene syringe (e) PVC tubing (f) polypropylene adaptor (g) glass adaptor.

Breakthrough curves were established by comparing the signal of the analyte in the eluate to that prior to loading. For all syringe pump driven experiments a flow rates of 0.1 ml h^{-1} was used.

4.6.3 Analytical parameters

The linearity of the SPE method was investigated by employing the SPE conditions in clean up of $100 \mu\text{l}$ aliquots of plasma spiked with 12.5 to 400 ng ml^{-1} of the standard mixture (prednisone, hydrocortisone, cortisone acetate, 19-nortestosterone). The limits of detection of the SPE method were defined as the lowest analyte concentrations that could be determined from the sample employing the SPE procedure. They were calculated based on a signal-to-noise (S/N) ratio of 3:1 for individual peaks on the HPLC-DAD after SPE.

Chapter 5

5. Results and discussion

Summary

Reported in this chapter are the results obtained in an effort to address objectives that are in threefold; (i) Control of the electrospinning jet (ii) Control of polystyrene copolymer nanofiber functionality (iii) Fabrication and chromatographic characterisation of electrospun nanofiber based solid phase extraction devices.

5.1 Electrospinning set-up designs

The process of electrospinning is still not fully understood, a major challenge being a complete understanding of the exact details of charge motion of the polymer solution jet as it travels towards the collector. Nevertheless, it is believed that charges accumulate at the surface of the polymer jet such that they are essentially static with respect to the moving coordinate systems of the jet [220]. On that basis, the electrospinning jet can be thought of as a string of charge elements connected by a viscoelastic medium with one end fixed at the point of origin and the other end free. The free end initially follows a stable trajectory until a point where the electrostatic interactions between the charge elements begin to dominate the ensuing motion, initiating and perpetuating a chaotic motion. Fig. 5.1 shows a schematic representation of a simulation of an electrospinning jet based on numerical modelling as proposed by Kowalewski and co-workers [221].

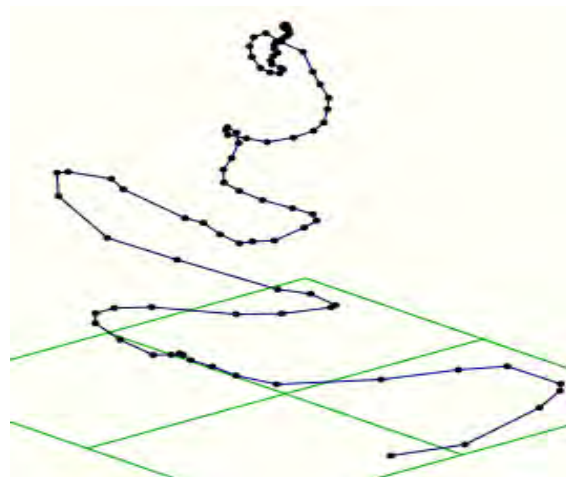


Fig.5.1 Numerical model simulation of an electrospinning jet [221].

If the electrospinning jet is thought of as a moving charged object, then it follows that electric, magnetic and mechanical forces can be employed to control the deposition patterns of electrospun nanofibers.

Given the fact that sorbent based extraction techniques consist of having the extracting phase in one of three ways:

1. Sorbent on a solid support which is typical of SPME devices.
2. Sorbent in a packed format which is typical of SPE devices.
3. Free flowing sorbent which is typical of batch or equilibrium based solid phase extraction.

It was necessary to investigate the parameters governing the deposition pattern of fibers during electrospinning as that has an influence on SPE device fabrication and performance. This is in light of the fact that analyte mass transfer kinetics are influenced by the packing density of the sorbent bed which can be influenced by the electrospinning deposition pattern. At this stage it was postulated that packed sorbent SPE device fabrication could proceed via two possible routes; the first route could consist of removing electrospun nanofibers from the collector and manually forcing them into either disk or micro column sorbent bed shapes

(extraction efficiency of the sorbent bed would be independent of fiber orientation as packing density would be solely dependent on the force applied), while the second route could consist of cutting out a disk sorbent shape directly from the fiber mat on the collector (extraction efficiency would be dependent on fiber orientation as packing density would be solely dependent on the inter-fiber distance as a function of the fiber deposition process).

On that basis, preliminary experiments were conducted to investigate the effect of the magnetic field, electric field and mechanical force on fiber orientation. In an effort to investigate the effect of the magnetic field on the electrospinning jet, a magnet was placed on a grounded aluminium plate (see Fig.5.2). It was observed that the fibers were well aligned on the top side of the magnet while a non woven mesh deposition pattern was observed on the sides of the magnet. A possible explanation for the observed phenomena could be related to a theoretical report by Wu and co-workers [222]. They proposed that fiber alignment could be induced by shrinking of the radius of the whipping circle as a result of a centripetal force produced by a current in the electrospinning jet under the magnetic field. In addition, the fact that the magnetic force acts in a direction that is perpendicular to the direction of the electric current implies that it would have an influence on minimising bending instability.

The influence of the magnetic field was more pronounced on the top side of the magnetic compared to the sides because the poles are the points of the strongest magnet field. This explains the nonwoven mesh deposition patterns on the sides of the magnets as compared to the top side where fibers were aligned. The results obtained demonstrated that the magnetic field could be employed to control fiber orientation which could be useful in controlling inter-fiber porosity within a sorbent bed.

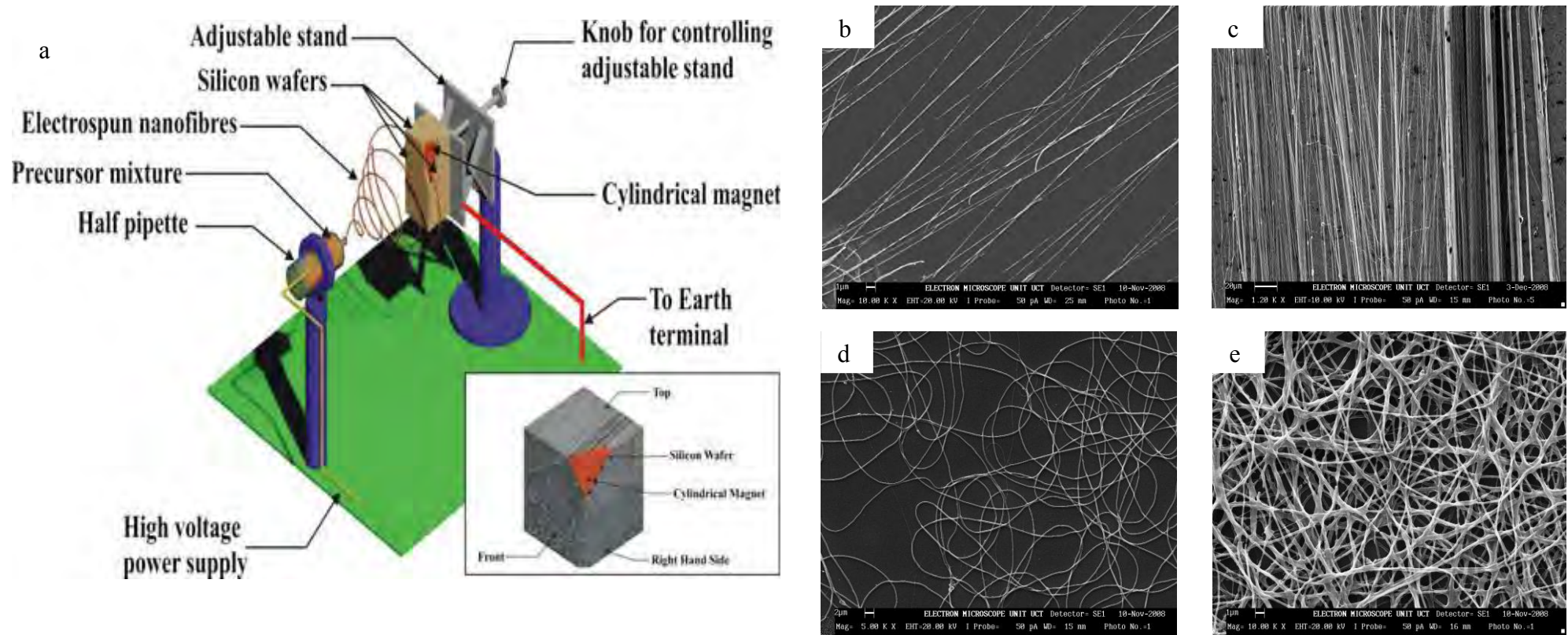


Fig.5.2 (a) Schematic representation of the electrospinning set-up employed to investigate the effect of the magnetic field on nanofiber deposition (b) and (c) SEM images for the fibers deposited top side of the magnet (d) and (e) SEM images for fibers deposited on the sides of the magnet [214].

In the first attempt to investigate the effect of the electric field and mechanical force on the electrospinning jet, electrospun nanofibers were collected onto a spring placed on a grounded aluminium plate (see Fig.5.4). It was observed that the fibers were well aligned on all parts of the spring. A possible explanation for the observed phenomenon could be that, by virtue of the nanofibers being positively charged, they tended to deposit in such a manner that they would span the gap between the spring wires and that way induce stretching. The fact that the spring is a conductor meant that each of the wires was a point of strong electric field strength in comparison to the flat aluminium plate. Therefore, there was a stronger pull of fibers to the spring.

The observed deposition pattern can be related to that observed by Li and co-workers [223] who deposited uniaxially aligned nanofibers onto two pieces of electrically conducting substrates. Based on their explanation, it can be said that unlike a flat grounded aluminium collector where there are uniform electric field lines [224], in the vicinity of the spring wires, electric field lines were split into two fractions pointing toward opposite edges of the gap between the wires. Fig 5.3 (a) shows a proposed cross sectional view of the electric field strength vectors between the spinneret and the spring wires.

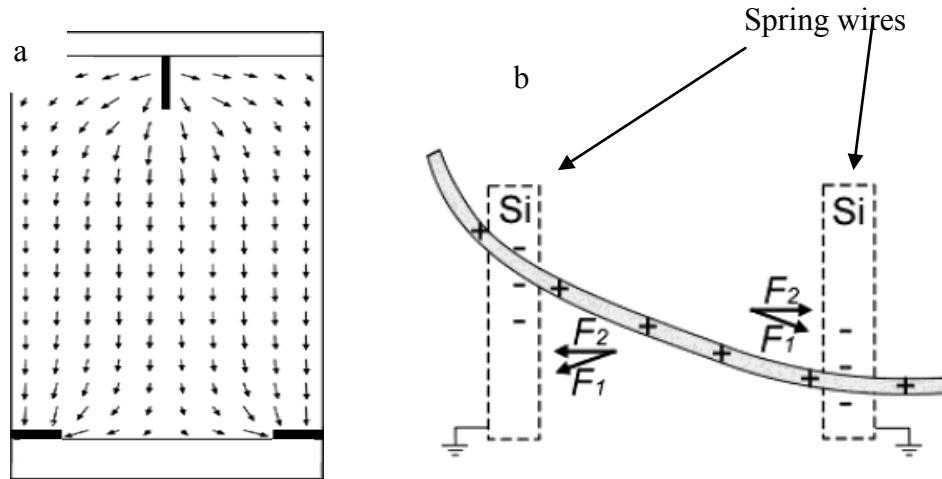


Fig.5.3 (a) Schematic representation of the proposed electric field strength vectors in the region between the spinneret and the spring collector (b) electrostatic force analysis of a charged nanofiber spanning across the gap between two spring wires [223].

Fig 5.3 (b) illustrates the proposed electrostatic forces acting on the positively charged nanofiber spanning the gap between the spring wires. It can be said that the charged nanofiber experiences two sets of electrostatic forces; the first set (F_1) originating from the splitting electric field and the second one (F_2) between the charged nanofiber and the negative charges induced on the surface of the spring wires. Once the charged fiber has moved into the vicinity of the spring wires, charges on the surface of the fiber will induce opposite charges on the surfaces of the spring wires. Considering that coulomb interactions are inversely proportional to the square of the separation between charges, the two points of the fiber closest to the spring wires should generate the strongest electrostatic force (F_2) which would stretch the nanofiber across the gap to have it positioned perpendicular to the edge of the wire.

In addition, unlike fibers directly deposited on a flat aluminium foil where they can be immediately discharged by virtue of the whole fiber surface coming into contact with the conducting aluminium foil surface, the fibers suspended across the gap between the wires remain highly charged after deposition due to the fact that most of the fiber surface is

exposed to the poor conducting air. More so, the electrostatic repulsion between the deposited and the upcoming fibers can further enhance the parallel alignment. The experimental results obtained led to the conclusion that a combination of a manipulation of electric field lines and introduction of a mechanical force (on the basis of stretching) could be used to control the deposition pattern of electrospun fibers.

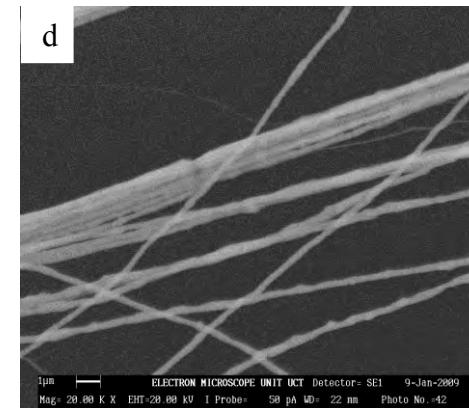
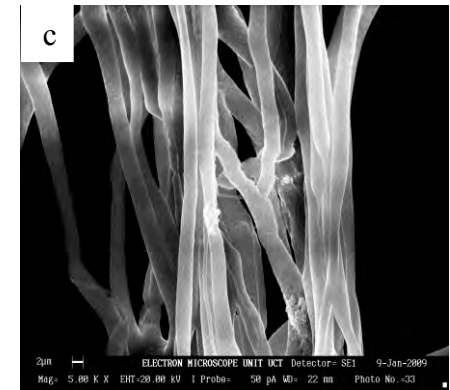
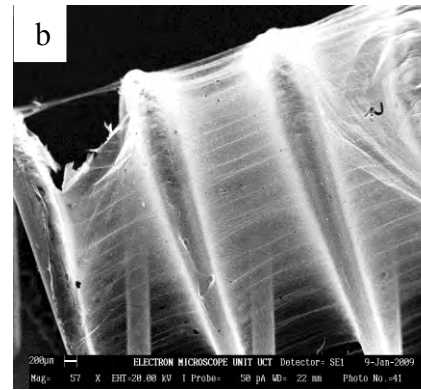
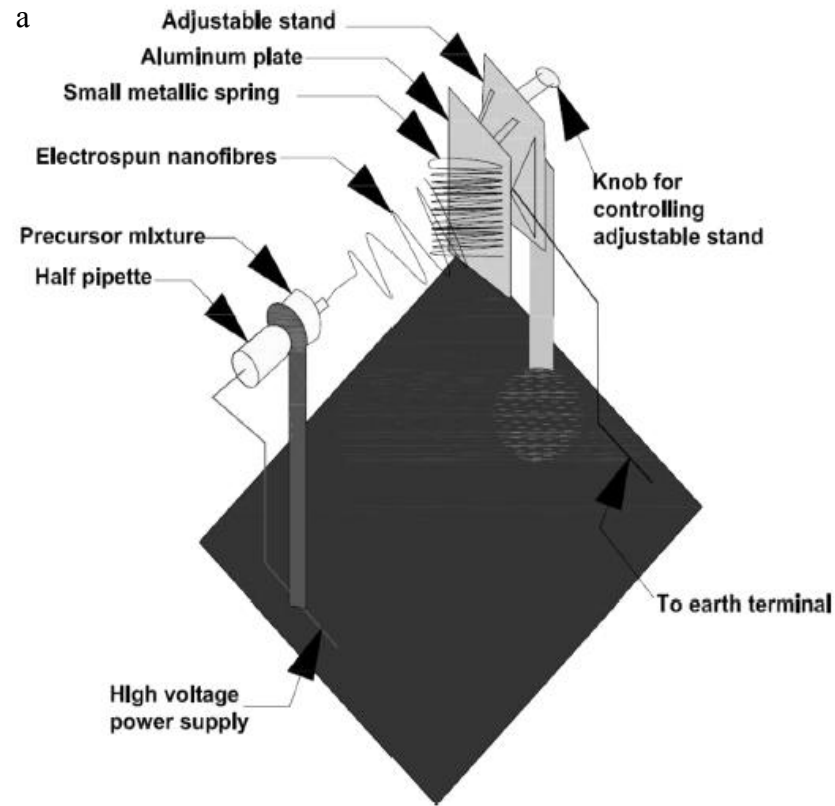


Fig.5.4 (a) Schematic representation of a electrospinning set-up employed to investigate the effect of collector geometry on nanofiber deposition (b-d) SEM images of electrospun fibers collected on a spring [215].

Even though preliminary experiments successfully demonstrated that the electric and magnetic fields could be manipulated to control the pathway of an electrospinning jet, they were based on short deposition times which were not sufficient for sorbent fabrication as large quantities of fibers were desired. In addition, maintaining fiber orientation on removal from a spring collector was a challenge. Therefore, the next stage was to explore the possibility of developing an electrospinning set-up that affords focused deposition of large quantities of fibers in the form of a sheet of controlled orientation.

The experimental designs were based on the proposal that when an auxiliary counter electrode (in this case, a sharp edged copper plate that acted as a point of strong electric field strength resulting in the convergence of electric field lines) is positioned behind a rotating collector, the electrospinning jet would track the converged electric field lines and attempt to attach to the charged counter electrode [224]. The rotating collector would then intercept the jet and the fibers would be taken up on the surface of the collector and wound around it.

The first two rotating collectors employed were designed as shown in Fig.5.5 (a) and (b).

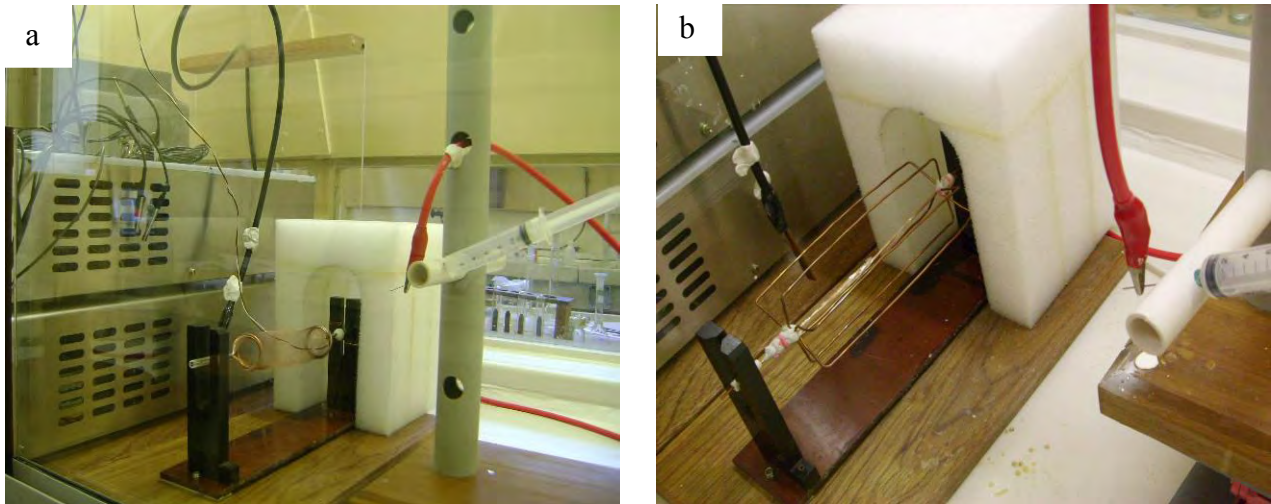


Fig.5.5 (a) Small and (b) big rotating wire collector based electrospinning set-ups.

These proved not to be the optimal designs as the fibers were deposited in the form of a web covering the entire collector, see Fig.5.6 (a). This was not consistent with the expected focused deposition. Covering the rotating wire collector(s) with aluminium foil resulted in a significant improvement as fibers were observed to be confined in the central part of the collector (Fig.5.6 (b)).

These deposition patterns could be due to the fact that when the copper wires of the rotating collector(s) were exposed, they acted as centres of strong electric field attraction that competed with the auxiliary counter electrode. The charged fibers deposited in such a way that they followed the electric field attraction of each copper wire. As the collector rotated, the fibers were stretched to span the gap between the wires and each incoming fiber experienced the repulsion due to the electric field originating from the charged fibers already deposited on the collector. The fibers were therefore forced to deposit on the bare wire portions resulting in them spreading all over the rotating wire collector to form a web. However, when the rotating wire collector was covered with aluminium foil, the strong electric field attraction of the copper wires was significantly reduced thus the collector

approached the properties of a drum that has a surface with uniform weak electric field attraction relative to the auxiliary counter electrode. This resulted in the fibers depositing in a confined area directly opposite the counter electrode due to the converging electric field lines that exerted a strong pull on the fibers. Based on the observed deposition patterns, the development of a rotating drum collector with a bare surface seemed to be a plausible experimental approach. This led to the development of a drum collector that consisted of the following components; (i) two polyvinylchloride (PVC) disks of 7.6 cm diameter with a 0.6 cm diameter hole cut in the centre, (ii) the disks were mounted on a stainless rod spaced 25 cm apart and enclosed in a 7.4 cm (inside diameter)*25 cm (length) PVC cylinder that joined up the disks and (iii) the rotating collector was mounted onto a wooden base (Fig. 5.6 (c)).

The initial experiments conducted using the rotating PVC drum collector were based on the electrospinning of 10 wt% PEO in deionised water. It was observed that after a deposition time of 10 min, nanofiber sheets of 50 mm width were formed in the central part of the collector (Fig.5.6 (d)). In addition, the nanofiber sheet was thick and dry enough such that it could be easily peeled off. This led to the conclusion that this experimental approach not only facilitated controlled deposition but the rotating effect introduced an enhanced solvent drying.

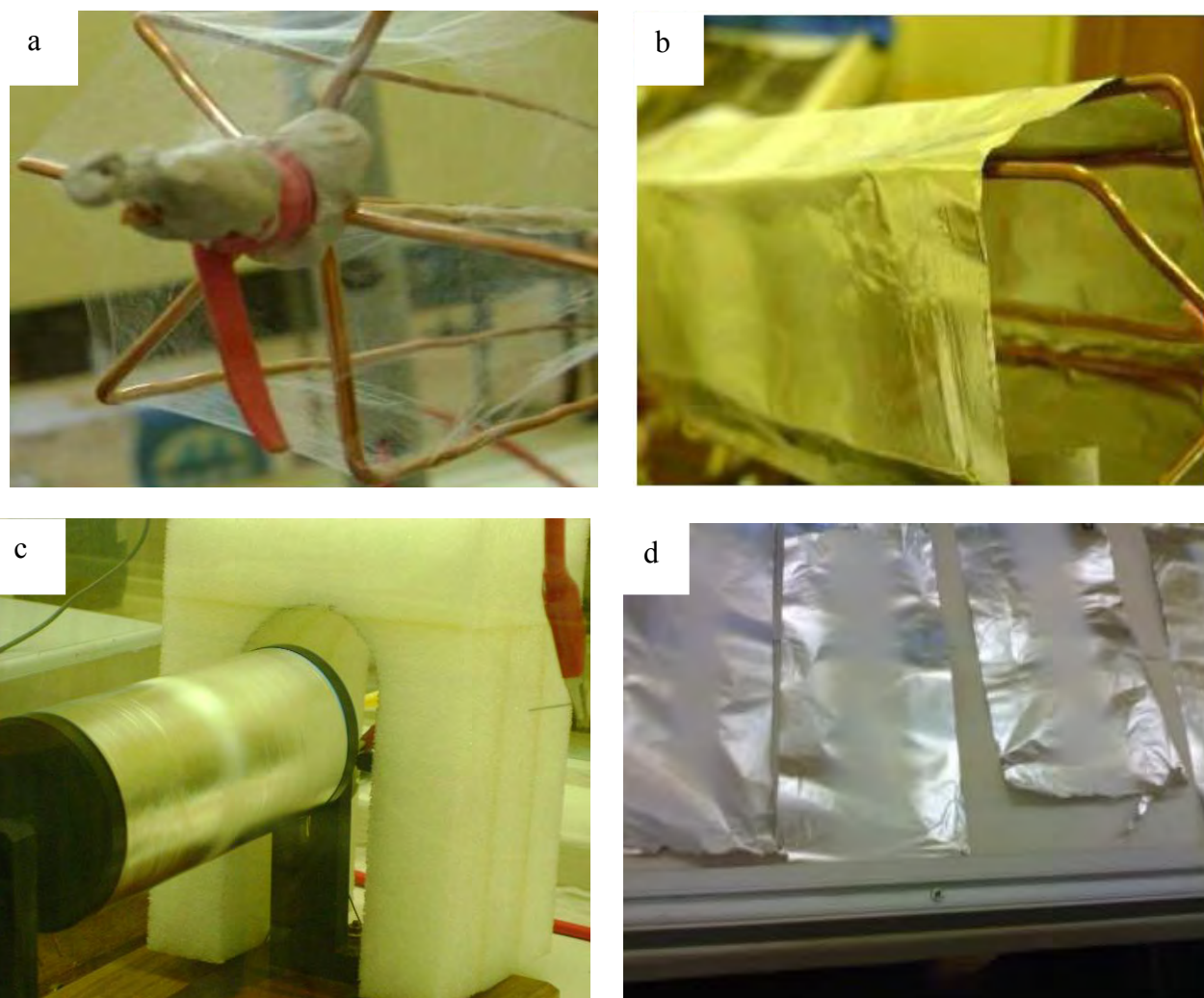


Fig.5.6 Deposition patterns on rotating collectors (a) Nanofiber web on bare wires (b) nanofiber sheet on bare wires wrapped with aluminium foil (c) nanofiber sheet on PVC drum and (d) nanofiber sheets on peeled off aluminium foil.

Investigation of the effect of the rotating collector of fiber orientation was conducted by varying the rotation speed as function of the power supply voltage sufficient to induce rotation. Fig.5.7 shows the SEM images of fibers collected at the minimum (2 V) and maximum (8 V) rotation speeds at 1 min and 15 min respectively. A nonwoven mesh collection pattern was obtained in all cases which suggests that the electric field manipulation

was not the predominant factor inducing fiber alignment. Therefore, it is proposed that for this particular electrospinning set-up, employing a higher rotation speed may induce fiber alignment on the basis of matching the electrospinning jet velocity. Nevertheless, the experimental design was employed for all the subsequent electrospinning procedures aimed at SPE device fabrication where fiber orientation was not controlled.

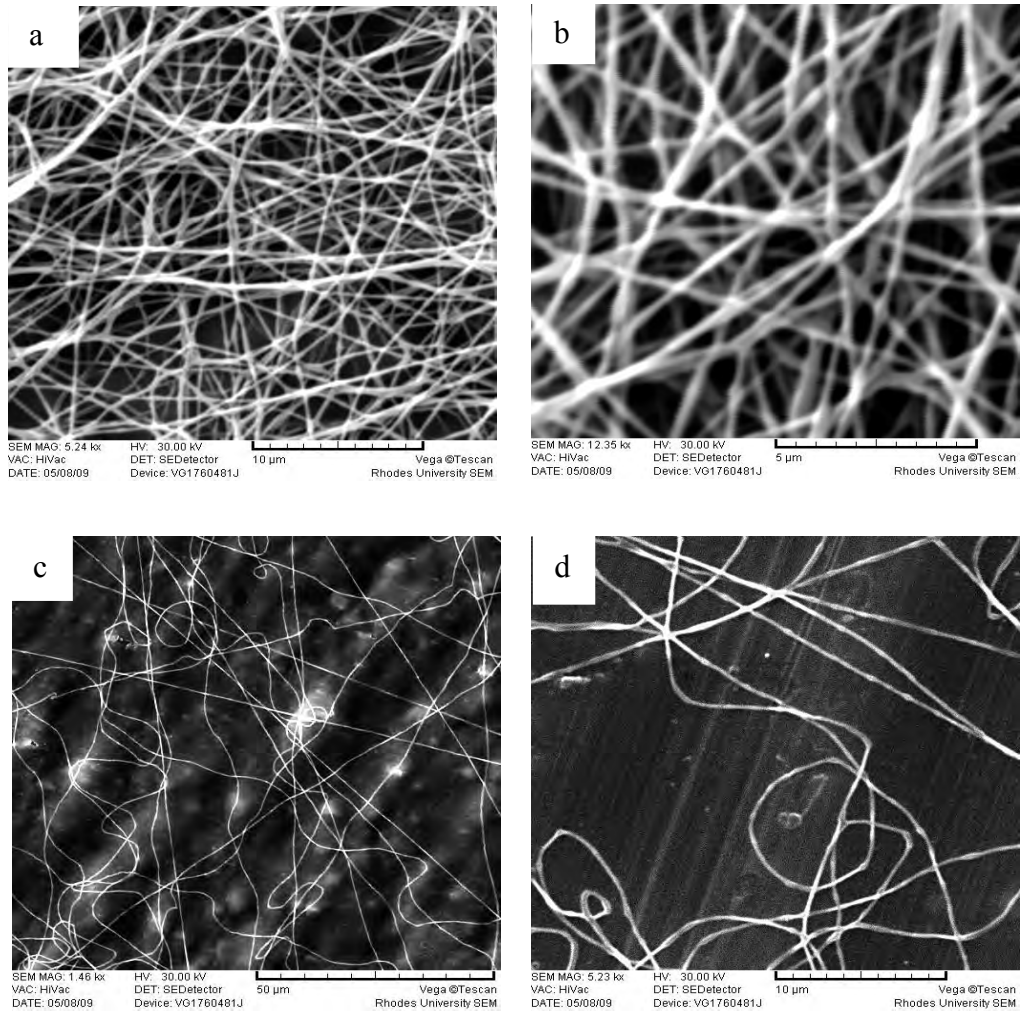


Fig.5.7 SEM images of electrospun nanofibers collected at different rotation speeds and collection time on the PVC drum collector (a) 2V and 15 min (b) 8V and 15 min (c) 8 V and 1 min and (d) 2 V and 1 min.

5.2 Copolymer synthesis and characterisation

A simplified boiling medium surfactant free emulsion polymerisation procedure based on a report by Gu and co-workers [225] was employed. The emulsion polymerisation technique was chosen over other free radical polymerisation techniques like conventional bulk and solution because of its ability to produce high molecular weight polymers at high polymerisation rates. This is due to the fact that during the polymerisation process, the concentration of the growing chains within each polymer particle is very low resulting in a longer polymer chain length unlike the other techniques where a high concentration of polymer chains in the growing polymer particle leads to termination by coupling which ultimately results in shorter polymer chains [226, 227].

The primary objective of the copolymerisation experiments was to explore the possibility of employing a pre-electrospinning functionalisation protocol based on introducing a vinylic monomer with a functional group of interest to a styrene monomer. This was driven by the need to bridge the gap between crosslinked polystyrene microparticle based sorbents and electrospun polystyrene nanofiber based sorbents.

The most widely used copolymerisation model is the Mayo Lewis model which describes the copolymer composition as a function of monomer feed concentration and reactivity ratio [228] as seen in equation 5.1.

$$\frac{d[M_1]}{d[M_2]} = \frac{[M_1](r_1[M_1]+[M_2])}{[M_2]([M_1]+r_2[M_2])} \quad 5.1$$




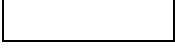
Where $[M_1]$ and $[M_2]$ are concentrations of monomers in the feed while r_1 and r_2 are the respective reactivity ratios. Therefore, the copolymerisation experiments were conducted on the basis of varying the monomer mole ratio in the feed [229]. The intention was to

investigate the effect of the copolymer composition on the spinnability of the polymer as well as compatibility of the resultant fibers with targeted SPE solvents.

5.2.1 Solubility studies

In an effort to establish the effect of monomer mole ratio on the solvent compatibility properties of the resultant polymers, six solvents were employed. It was expected that as the polymer feed composition tended towards 100% of either of the co-monomers, the behaviour of the resultant copolymer would closely resemble that of the respective homopolymer.

Due to the complexity of polymer behaviour in solution, the observations were classified into four categories as; completely soluble, sparingly soluble, swollen or shrunken and completely insoluble (see key below)

	Completely soluble
	Sparingly soluble
	Swollen or shrunken
	Completely insoluble

As shown in Tables 5.1 to 5.3, the solvent compatibility properties tended towards the properties of the homopolymers. This could be attributed to the increased homopolymerisation in comparison to copolymerisation as a result of the increased reactivity ratio with increased monomer feed concentration [230].

In addition to copolymer stability in water, it was a desire to use an electrospinning solvent system of DMF:THF (4:1) thus solubility in DMF or THF was used as a guide for optimal copolymer mole ratio selection. This was in light of the assumption that solubility in the same electrospinning solvent as polystyrene, in addition to water insolubility served as a way of confirming that the comonomers were incorporated on the polystyrene backbone.

On the basis of preliminary experiments conducted, it was proposed that there was a limit regarding the extent of functionalisation (dependent on copolymer composition as a result of monomer mole ratio) for which the resultant copolymers would be spinnable and also insoluble in water. Guided by water insolubility and DMF or THF solubility, mole ratios (10:1) for poly (styrene-co-methacrylic acid), (10:1) for poly (styrene-co-acrylamide) and (10:1 to 20:1) for poly (styrene-co-*p*-sodium styrene sulfonate) were selected as the most suitable for electrospinning and potential SPE application.

Table.5.1 Solubility studies of synthesized poly (styrene-co-methacrylic acid) copolymer at different mole ratios of styrene to methacrylic acid.

Solvent	Mole ratio						
	0:1	1:10	1:1	2:1	5:1	10:1	1:0
Chloroform					Yellow	Yellow	Black
Acetonitrile				Grey	Grey		Yellow
Formic acid							
Acetic acid							
DMSO	Black	Black	Black	Grey		Grey	
Water	Black	Grey					
DMF			Black	Black	Black	Black	Black
Methanol	Black	Black	Grey	Grey	Grey		
Acetone					Grey		Yellow
THF		Yellow	Black	Black	Black	Black	Black

Table.5.2 Solubility studies of synthesized poly (styrene-co-acrylamide) copolymer at different mole ratios of styrene to acrylamide.

Solvent	Mole ratio						
	0:1	1:10	1:1	2:1	5:1	10:1	1:0
Chloroform					Yellow	Yellow	Black
Acetonitrile					Grey		Yellow
Formic acid	Black		Grey	Grey	Grey		
Acetic acid			Grey	Grey	Grey		
DMSO				Grey	Grey		
Water	Black		Yellow				
DMF					Black	Black	Black
Methanol							
Acetone							Yellow
THF							Black

Table.5.3 Solubility studies of synthesized poly (styrene-co-*p*-sodium styrene sulphonate) copolymer at different mole ratios of styrene to *p*-sodium styrene sulphonate.

Solvent	Mole ratio						
	0:1	1:1	5:1	10:1	15:1	20:1	1:0
Chloroform							Black
Acetonitrile				Grey	Grey		Yellow
Formic acid	Black	Grey	Grey	Grey	Grey		
Acetic acid							
DMSO		Grey	Grey		Grey	Grey	
Water	Black	Grey	Grey				
DMF			Yellow	Black	Black	Black	Black
Methanol							
Acetone							Yellow
THF							Black

5.2.2 Fourier Transform Infrared Spectroscopy

The FTIR spectra of polystyrene copolymers synthesized from mole ratios ranging from 0:1 (styrene: methacrylic acid) to 1:0 (styrene: methacrylic acid) are shown in Fig.5.8. A characteristic peak around 1698 cm^{-1} is attributed to the carbonyl stretching vibration of the carboxyl groups in the methacrylic acid component of the polymers [231]. With the increase in the methacrylic acid content in the feed, the intensity of the peak was observed to gradually increase which provided confirmatory evidence of the successful incorporation of the carboxyl group onto the polystyrene backbone. In addition the well defined peaks around 2924 cm^{-1} ($-\text{CH}_2$ asymmetric stretching) and 3026 cm^{-1} (aromatic CH stretching) from a mole ratio of 5:1 confirmed the predominance of the polystyrene backbone [232]. Most importantly, the presence of the carbonyl stretch at the mole ratio 10:1 confirmed the incorporation of the carboxylic acid functionality onto the polystyrene backbone, which was consistent with the prediction from the solubility experiments.

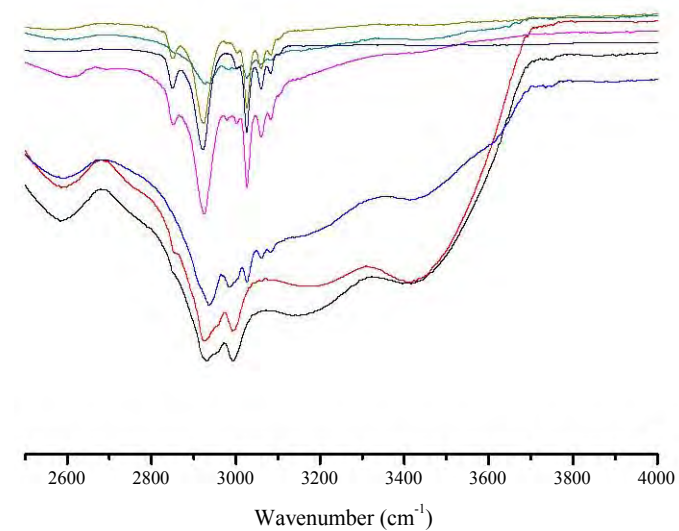
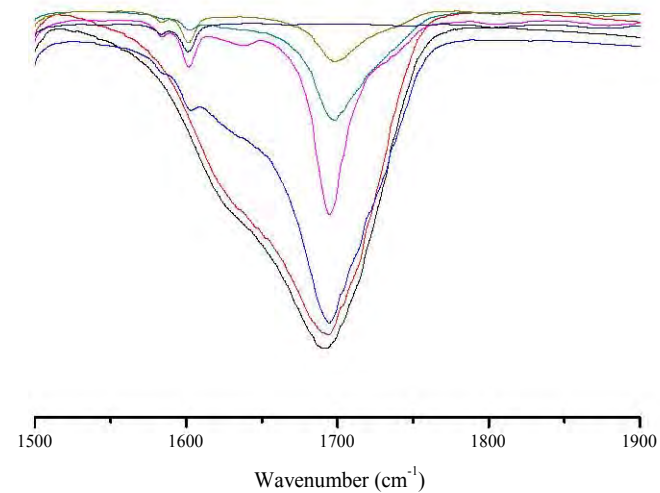
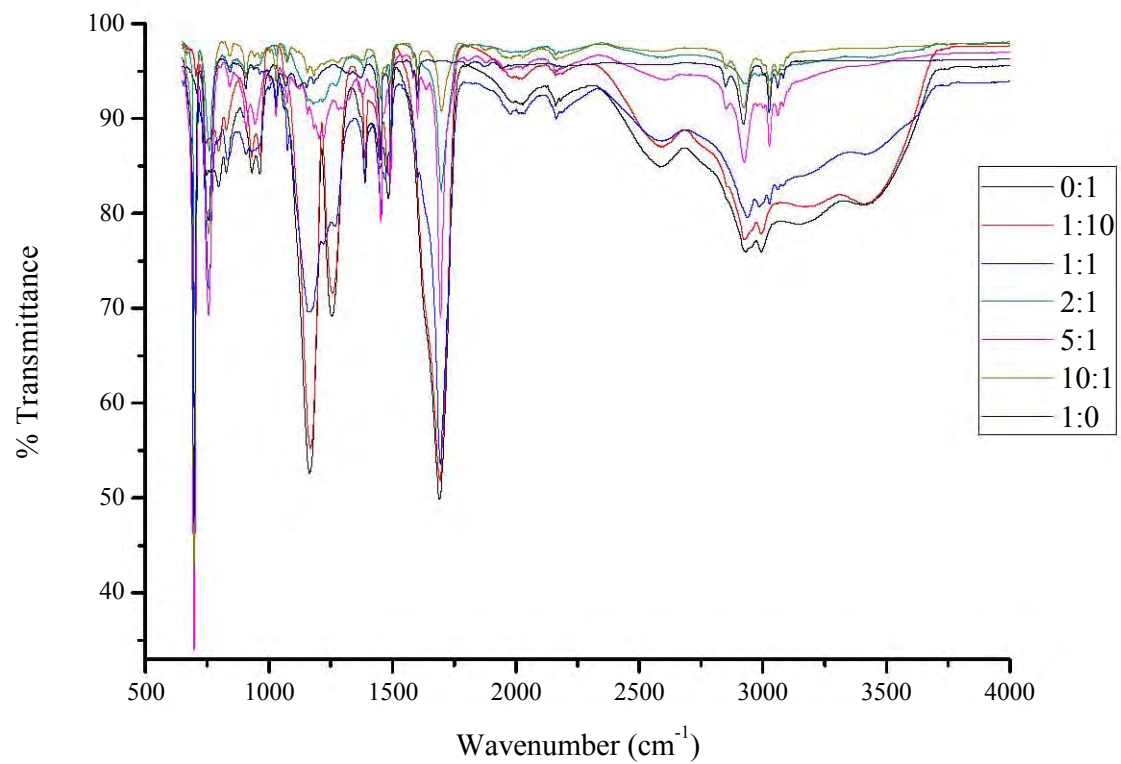


Fig.5.8 FTIR comparison of polystyrene copolymers synthesised from different mole ratios of styrene: methacrylic acid.

The FTIR spectra of polystyrene copolymers synthesized from mole ratios ranging from 0:1 (styrene: acrylamide) to 1:0 (styrene: acrylamide) are shown in Fig.5.9. Peaks around 3200 cm^{-1} (N-H stretching), 1650 cm^{-1} (C=O stretching), 1420 and 1105 cm^{-1} all characteristic of the acrylamide monomer [233] were observed. With the increase in the acrylamide content in the feed, the intensity of the peak at 1650 cm^{-1} was observed to gradually increase which provided confirmatory evidence of the successful incorporation of the amide group onto the polystyrene backbone. Most importantly, the presence of the carbonyl stretch at the mole ratio 10:1 confirmed the incorporation of the acrylamide functionality onto the polystyrene backbone, which was consistent with the prediction from the solubility experiments.

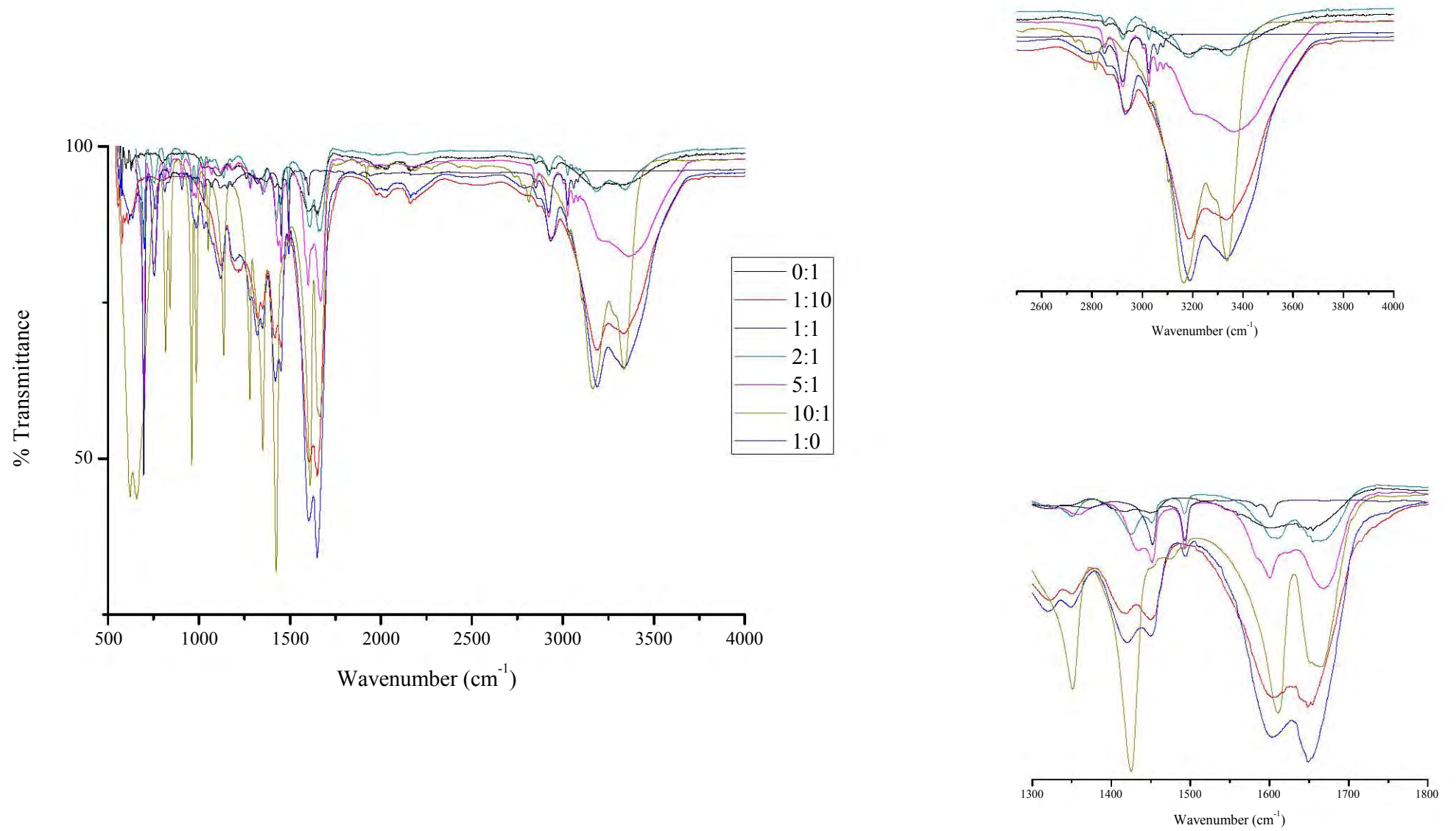


Fig.5.9 FTIR comparison of polystyrene copolymers synthesised from different mole ratios of styrene: acrylamide.

The FTIR spectra of polystyrene copolymers synthesized from various mole ratios ranging from 0:1 (styrene: *p*-sodium styrene sulfonate) to 1:0 (styrene: *p*-sodium styrene sulfonate) are shown in Fig.5.10. The broad peak at 3450 cm^{-1} is due to the O-H stretching vibration of residual water and the sulfonate group [234]. The peak becomes stronger and sharper with increasing *p*-sodium styrene sulfonate in the feed indicating its incorporation onto the polystyrene backbone. Most importantly, the presence of the characteristic peaks of sulfonate groups (around 1041 cm^{-1} representing symmetric stretching vibration of the SO_3 groups and 1182 cm^{-1} representing asymmetric stretching vibration of the SO_3 groups) at the mole ratios 10:1 to 20:1 confirmed the successful incorporation of the sulfonate functionality onto the polystyrene backbone, which was consistent with the prediction from the solubility experiments.

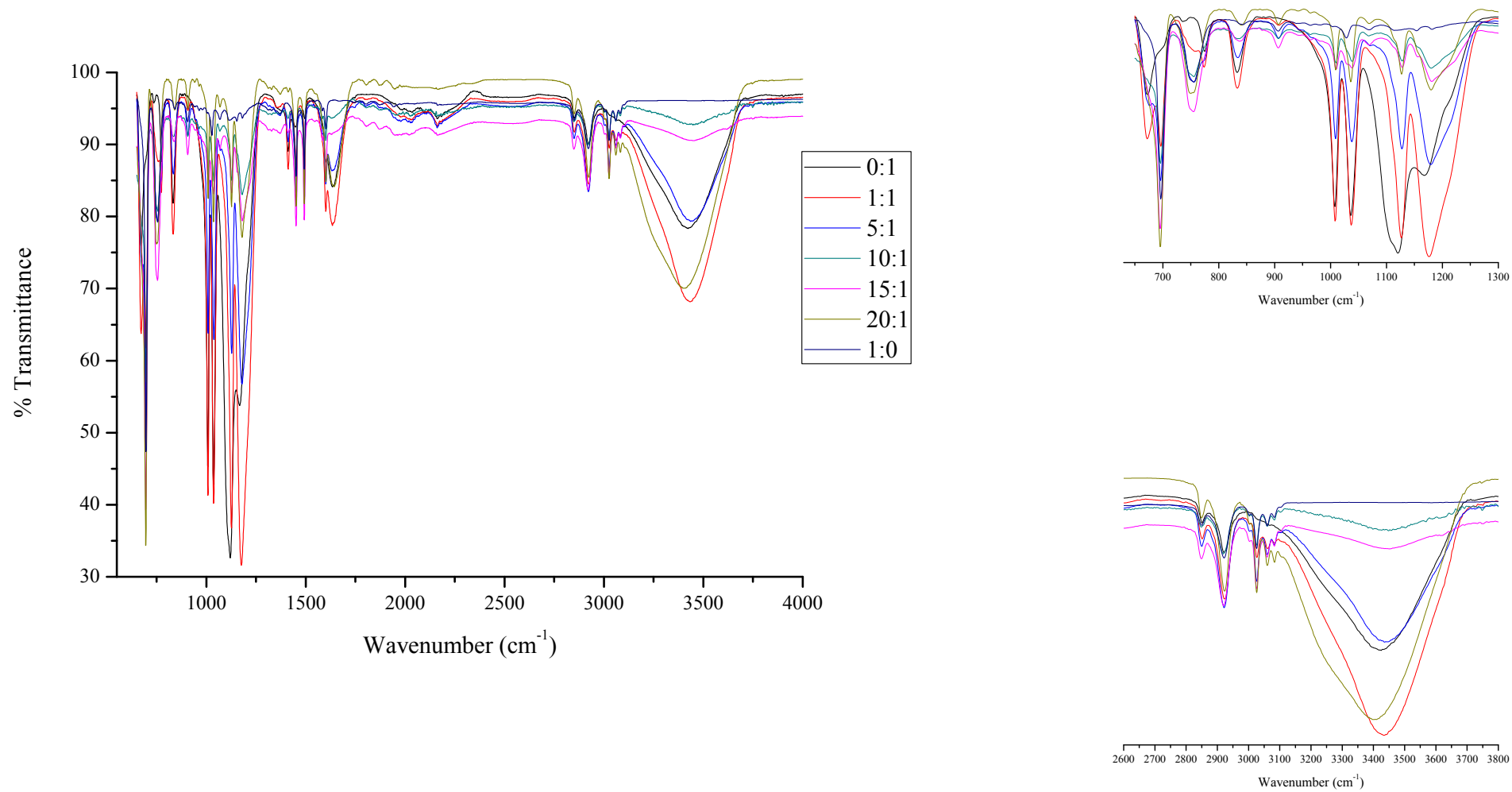


Fig.5.10 FTIR comparison of polystyrene copolymers synthesised from different mole ratios of styrene: *p*-sodium styrene sulfonate.

5.2.4 Thermogravimetric analysis of copolymers

In an effort to provide complementary evidence of the successful incorporation of functional groups onto the polystyrene backbone, thermogravimetric analysis was conducted. Thermogravimetric profiles of each of the copolymers at a mole ratio of 10:1 were compared to those of their respective homopolymers.

The TGA thermograms for polystyrene, poly (styrene-co-acrylamide) and polyacrylamide are shown in Fig.5.11. A weight loss around 100 °C was observed for the poly (styrene-co-acrylamide) and polyacrylamide. This was attributed to the absorbed moisture as a result of the hygroscopic nature of the acrylamide moieties. As expected, a larger weight loss around 100 °C was observed for the polyacrylamide homopolymer. A weight loss around 180 °C was attributed to the loss of NH₃ due to a side group cyclisation reaction of the amide functionalities, it was more pronounced for the polyacrylamide homopolymer as compared to the poly (styrene-co-acrylamide)[235]. The complete absence of the loss on the polystyrene thermogram as compared to the poly (styrene co-acrylamide) confirmed the successful incorporation of the acrylamide onto the polystyrene backbone. The complete decomposition of the polystyrene homopolymer around 350 °C as compared to that of poly (styrene co-acrylamide) at 450 °C confirmed the successful incorporation of acrylamide on to the polystyrene backbone.

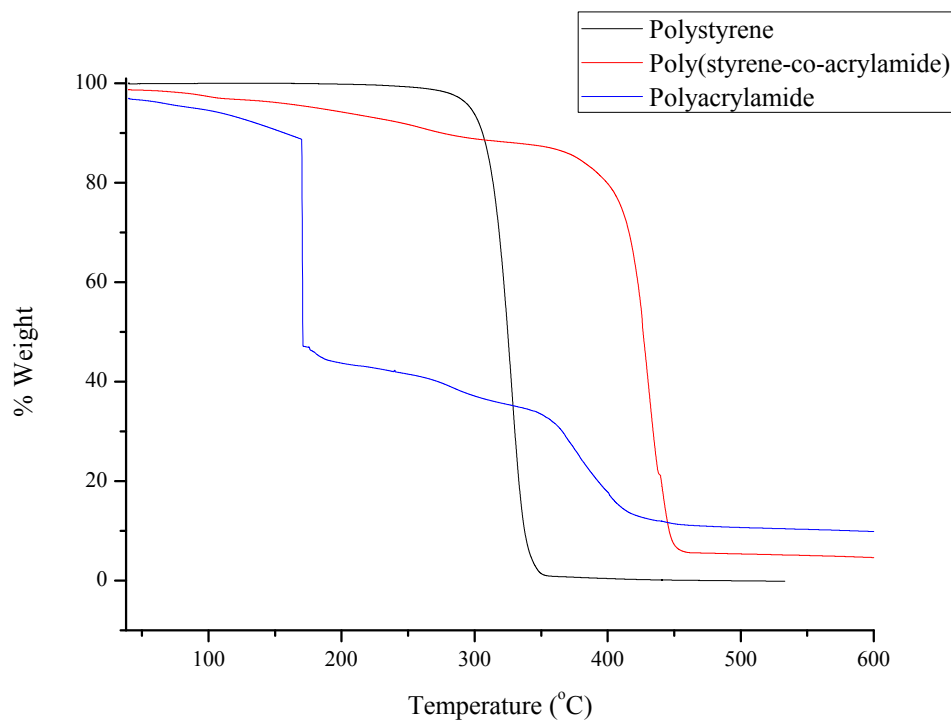


Fig.5.11 TGA thermograms of (a) polystyrene homopolymer (b) poly (styrene-co-acrylamide) synthesized from a mole ratio of 10:1 (styrene:acrylamide) and (c) polyacrylamide homopolymer.

The TGA thermograms for polystyrene, poly (styrene-co-*p*-sodium styrene sulfonate) and poly (*p*-sodium styrene sulfonate) are shown in Fig.5.12. A weight loss around 100 °C was observed for the poly (styrene-co-*p*-sodium styrene sulfonate) and poly (*p*-sodium styrene sulfonate) while for polystyrene it was not observed. This was attributed to the absorbed moisture as a result of the hygroscopic nature of the sulfonate moieties. As expected, a larger weight loss around 100 °C was observed for the poly (styrene-co-*p*-sodium styrene sulfonate) homopolymer. A major weight loss was observed around 350 °C for polystyrene and poly (styrene-co-*p*-sodium styrene sulfonate), while this loss was not observed for the poly (*p*-sodium styrene sulfonate). This was attributed to the decomposition of the hydrocarbon component of the polymers as a result of the polystyrene backbone. A complete decomposition of the polystyrene while the poly (styrene-co-*p*-sodium styrene sulfonate)

homopolymer experienced a weight loss up to 20% served to confirm that the sulfonate functionality was successfully bound onto the polystyrene backbone [236].

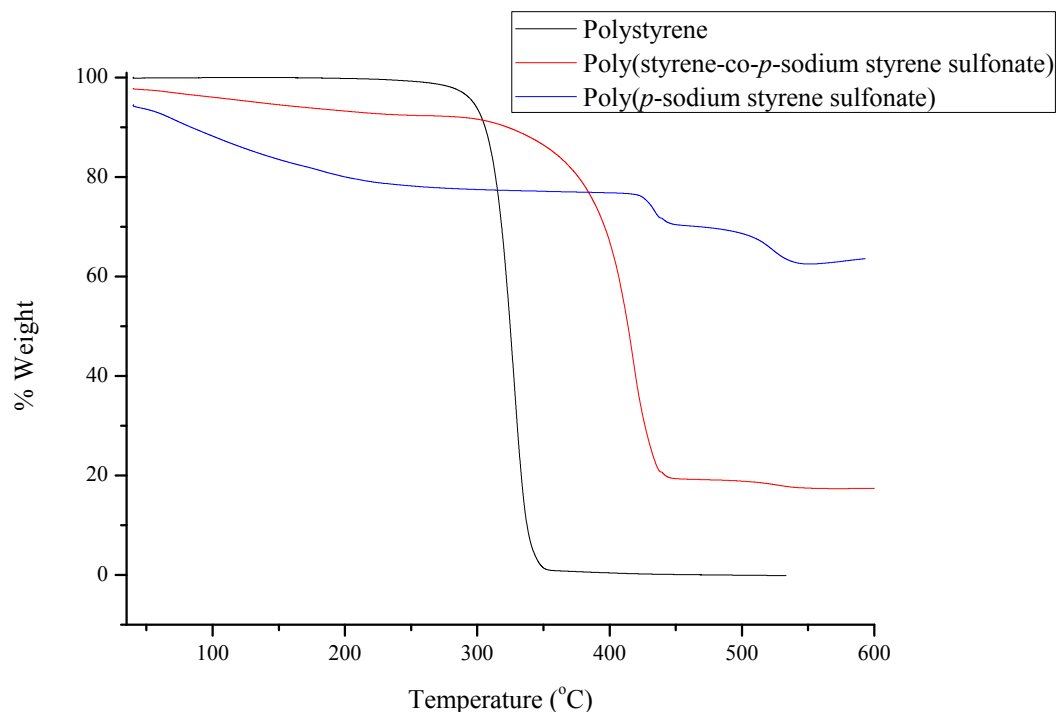


Fig.5.12 TGA thermograms of (a) polystyrene homopolymer (b) poly (styrene-co-*p*-sodium styrene sulphate) copolymer synthesized from a mole ratio of 10:1 (styrene:*p*-sodium styrene sulphate) and (c) *p*-sodium styrene sulphate homopolymer.

The TGA thermograms for polystyrene, poly (co-methacrylic acid) and poly (methacrylic acid) are shown in Fig.5.13. A weight loss at 100 °C attributed to water was observed for the polymethacrylic acid thermogram. Two losses were observed for the poly (styrene-co-methacrylic acid) thermogram. The first loss due to the styrene component of the polymer and the second due to the methacrylic acid component of the polymer. The fact that only one loss was observed for the polystyrene thermograms served to confirm the successful incorporation of the methacrylic acid monomer onto the polystyrene backbone [231, 237].

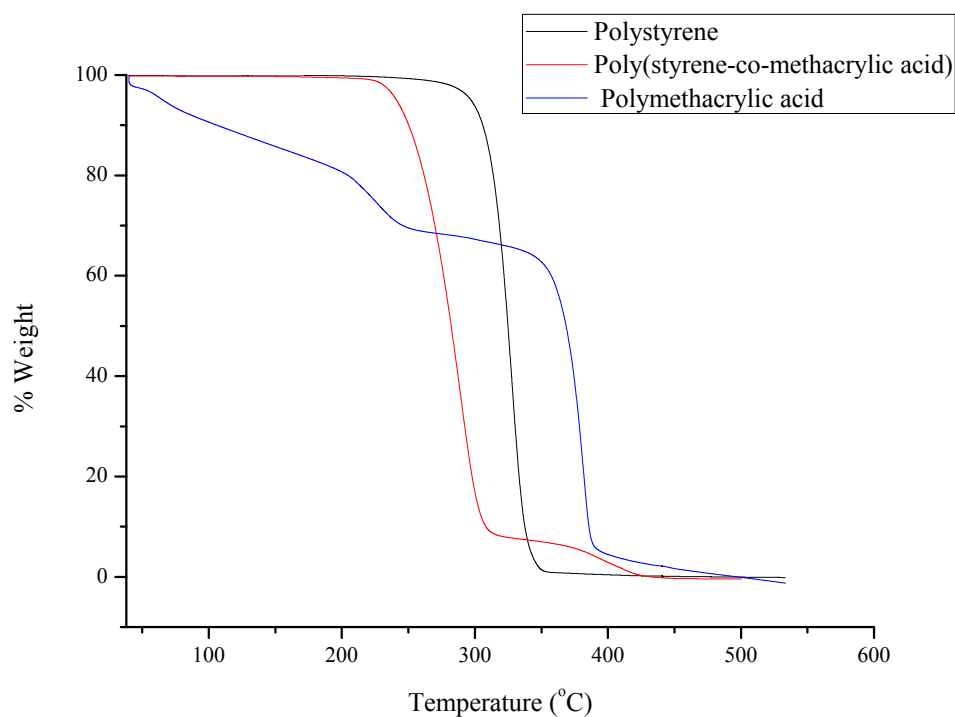


Fig.5.13 TGA thermograms of (a) polystyrene homopolymer (b) poly (styrene-co-methacrylic acid) copolymer synthesized from a mole ratio of 10:1 (styrene:methacrylic acid) and (c) polymethacrylic acid homopolymer.

5.3 Electrospinning of copolymers

5.3.1 Poly (styrene-co-methacrylic acid)

It was observed that all the mole ratios of poly (styrene-co-methacrylic acid) were spinnable as shown by the SEM images in Figs 5.14 and 5.15. Table 5.4 presents a summary of the SEM results obtained for all the fibers.

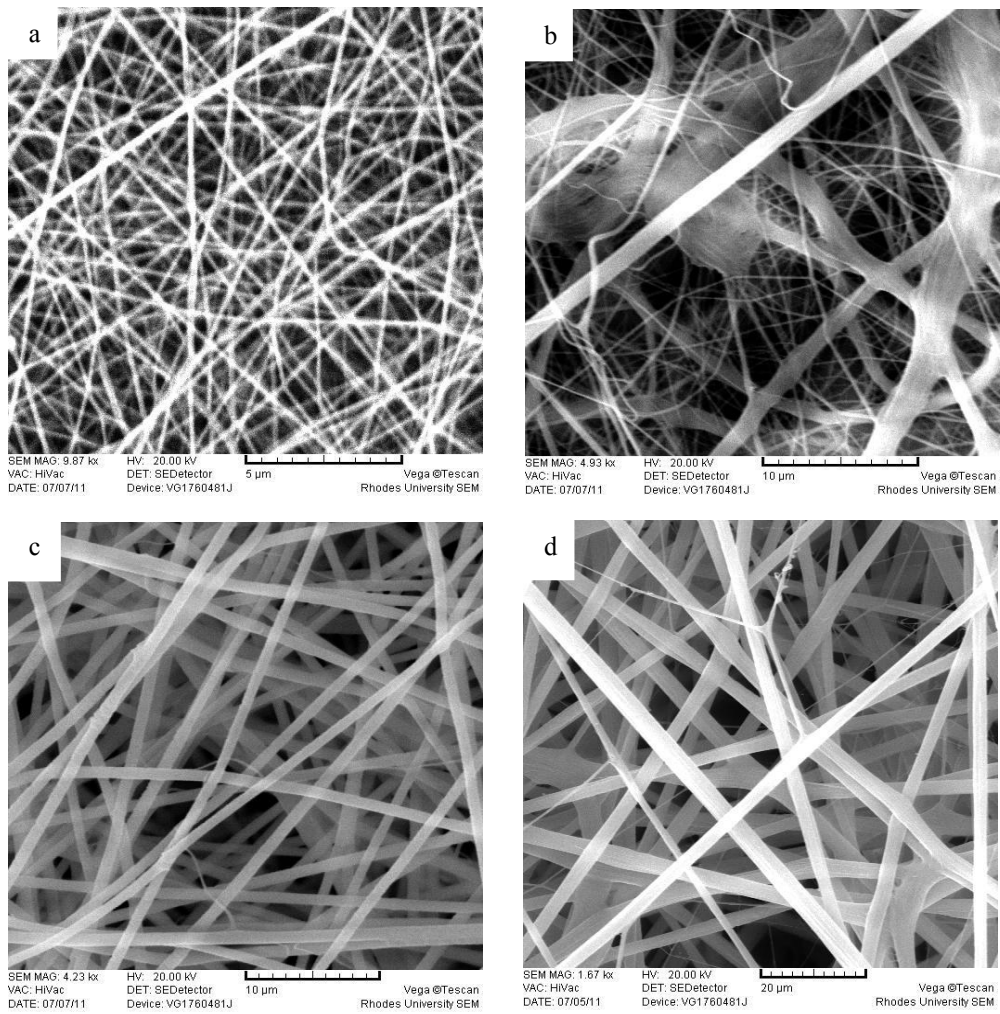


Fig.5.14 SEM images for poly (styrene-co-methacrylic acid) spun from copolymers of different mole ratios of styrene: methacrylic acid (a) 0:1 (b) 2:1 (c) 5:1 (d) 10: 1

Even though all mole ratios besides the homopolymer of methacrylic acid were spun from DMF: THF, mole ratios 1:10 to 5:1 displayed some degree of solubility in either methanol or water. This observation was consistent with the results obtained from the solubility studies of the polymer powders. An attempt was made to modify the solvent compatibility properties of the copolymers by employing heat induced β -cyclodextrin cross linking. Besides modifying the solvent compatibility of the copolymer fibers, it was an attempt to introduce the inclusion complex functionality of the β -cyclodextrin moieties [238-242].

Fig 5.15 shows SEM images of electrospun β -cyclodextrin doped poly (styrene-co-methacrylic acid) before and after heat treatment. As observed from the SEM images, the heat did not have a significant effect on altering the fiber morphology which suggested that heat induced β -cyclodextrin cross linking of poly (styrene-co-methacrylic acid) copolymers could be employed without posing the danger of deforming the fiber morphology.

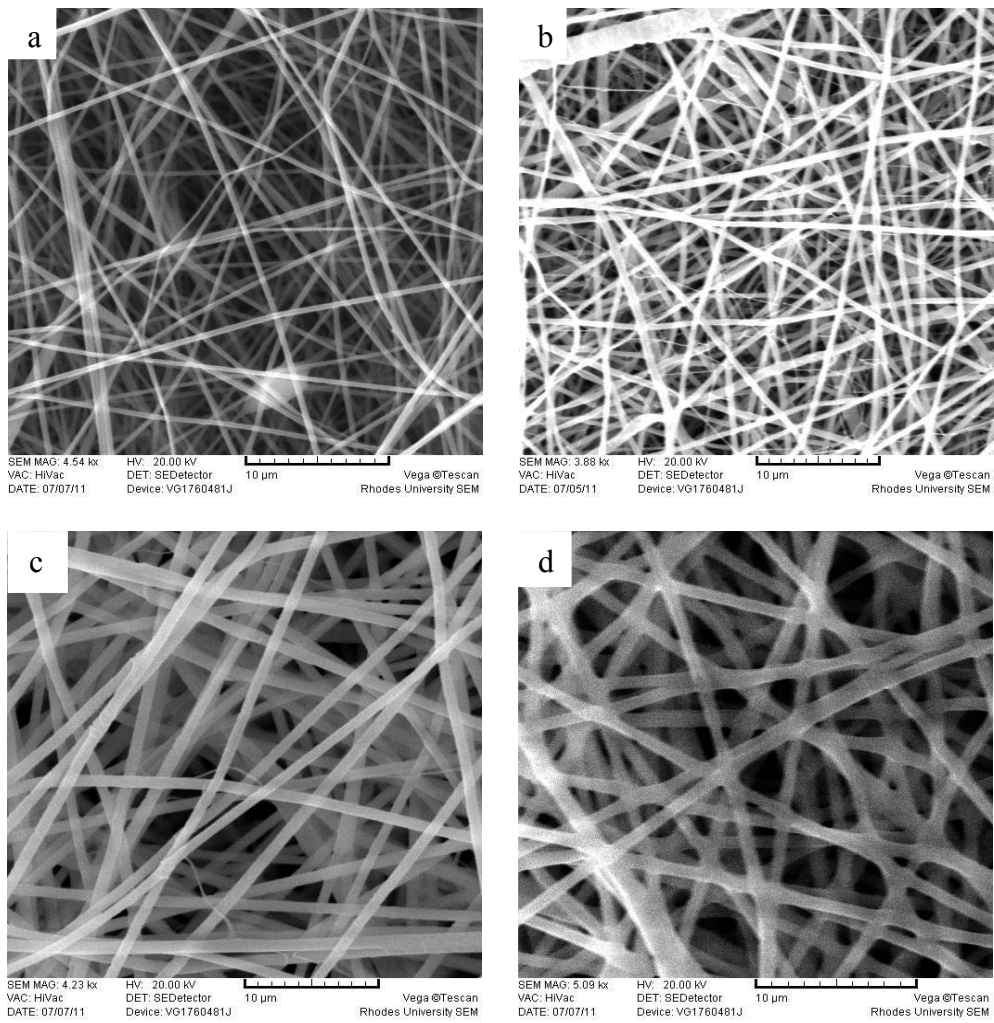


Fig.5.15 SEM images of electrospun poly (styrene-co-methacrylic acid) copolymers spun from different mole ratios of styrene:methacrylic acid doped with 10% β -cyclodextrin (a) 1:10 before heat treatment (b) 1:1 before heat treatment (c) 1:10 before heat treatment (d) 1:10 after heat treatment.

Table.5.4 SEM results summary for electrospun poly (styrene-co-methacrylic acid) fibers at different mole ratios.

Mole ratio	Average diameter (nm)	Range (nm)	Spinnability
0:1	192.02	119.37-322.29	Yes
1:10	471.42	225.04-769.77	Yes
1:1	572.49	455.99-775.03	Yes
2:1	-	-	Yes
5:1	924.75	849.34-1034.40	Yes
10:1	2880.95	1423.20-3752.99	Yes

Based on a report by Li and co-workers [243] who suggested a β -cyclodextrin cross linking mechanism that proceeds via ester bond formation to result in the structure depicted by Fig 5.16 (a), a structure depicted by Fig 5.16 (b) was proposed for the cross linked poly (styrene-co-methacrylic acid) copolymer.

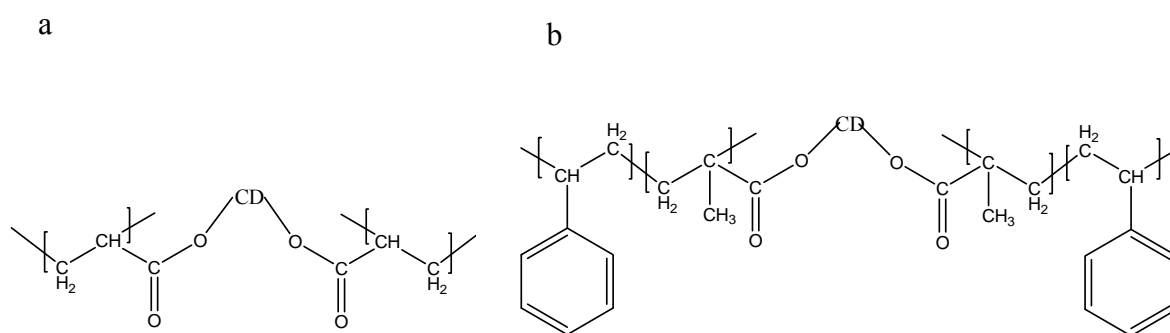


Figure.5.16 β -cyclodextrin cross linked structures of (a) poly (acrylic acid) and (b) poly (styrene co-methacrylic acid).

Table 5.5 shows the solubility properties of the β -cyclodextrin doped poly (styrene-co-methacrylic acid) before and after heat treatment. It was observed that cross linking improved the stability of the 1:10 mole ratio in methanol while the 1:1 mole ratio was observed to be

soluble. This could be attributed to the increased ester formation as a result of the increased content of methacrylic thus rendering the copolymer insoluble. Despite the fact that further optimisation experiments were not conducted, it can be said that β -cyclodextrin could be employed to impart insolubility on the soluble mole ratios of poly (styrene-co-methacrylic acid).

Table.5.5 Summary of the behaviour of β -cyclodextrin doped poly (styrene-co-methacrylic acid) fibers in methanol and water.

Mole ratio	Methanol	Water
1:10 (before heating)	Soluble	Swelling and becomes colourless
1:10 (after heating)	Swelling	Insoluble
1:1 (before heating)	Soluble	Insoluble
1:1 (after heating)	Soluble	Insoluble

Electrospun poly (styrene-co-methacrylic acid) fibers, by virtue of the carboxylic acid functionality and polystyrene backbone could be applied as a weak cation exchange sorbent bed material for the extraction of strongly basic and neutral analytes. A typical SPE procedure for in which a weak cation exchange sorbent is employed could involve the use of methanol, water, 2% formic acid and 5% ammonium hydroxide/methanol. Table 5.6 shows the results obtained when electrospun poly (styrene-co-methacrylic acid) fibers at a mole ratio of 10:1 and 5:1 were immersed in the SPE solvents. The results confirm suitability of the poly (styrene-co-methacrylic acid) at a mole ratio of 10: 1 for SPE application.

Table.5.6 Behaviour of selected mole ratios of electrospun poly (styrene-co-methacrylic acid) fibers in SPE solvents.

Mole ratio	Methanol	Water	2% Formic acid	5% NH₄OH/Methanol
10:1	Insoluble	Insoluble	Insoluble	Insoluble
5:1	Shrunk	Insoluble	Insoluble	Not completely soluble

In 2003, Fridrikh and co-workers [244] proposed a mathematical model for controlling fiber diameter as a function of surface tension and electrostatic charge repulsion. Investigation of the effect of polymer solution concentration (which influences surface tension and the extent of electrostatic charge repulsion) on fiber diameter was conducted by electrospinning poly(styrene-co-methacrylic acid) from 5-20 wt% DMF:THF solutions. As shown by Fig. 5.17, bead free fibers were obtained. However, a total control of the morphology and uniformity of fiber diameter was not achieved. A steady state electrospinning procedure where there is a precise control of the ambient conditions is proposed as it ensures reproducible electrospinning conditions [245, 246].

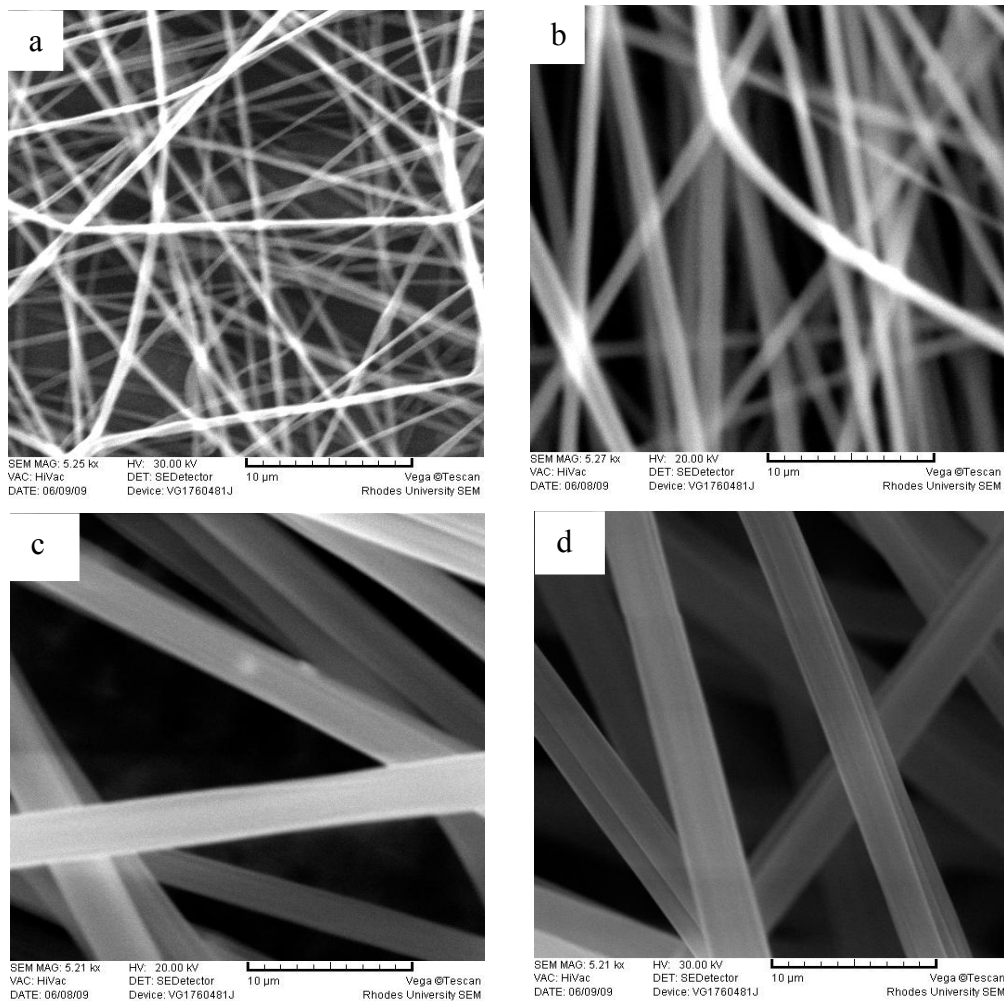


Fig.5.17 SEM images of electrospun poly (styrene-co-methacrylic acid) fibers spun from (a) 5 (b) 10 (c) 15 and (d) 20 wt% concentration in DMF: THF.

Fig.5.18 shows a graphical representation of the relationship between fiber diameter and poly (styrene-co-methacrylic acid) solution concentration. Given the fact that the fiber diameter was observed to vary from 500 nm to 3000 nm as a function of concentration, it is proposed that a similar strategy could be employed for all functionalised copolymers.

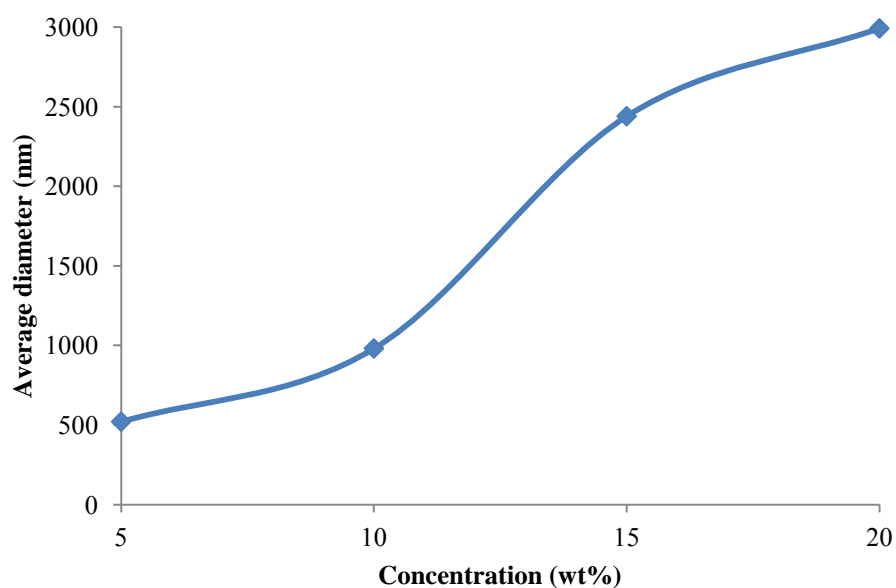


Fig.5.18 Effect of polymer solution concentration on fiber diameter.

5.3.2 Poly (styrene-co-*p*-sodium styrene sulfonate)

Fig 5.19 shows the SEM images of the spinnable mole ratios of poly (styrene-co-*p*-sodium styrene sulfonate). Bead free fibers were obtained at mole ratios 10:1, 15:1 and 20:1. Mole ratios 1:1 and 5:1 could not be spun as they were found to be insoluble in the solvents employed. However, it cannot be concluded with certainty that they are not spinnable as there could be other solvents that could be employed.

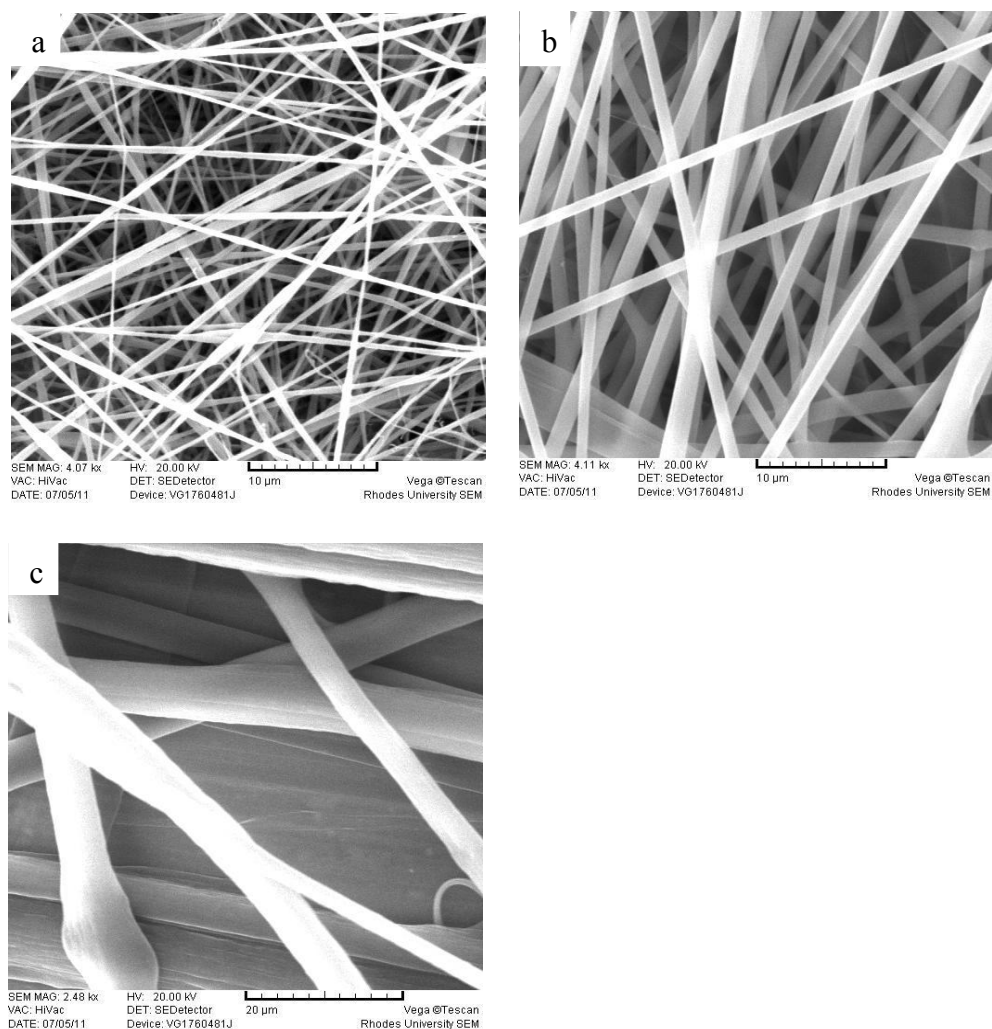


Fig.5.19 SEM images of electrospun poly (styrene-co-*p*-sodium styrene sulphonate) copolymers spun from different mole ratios of styrene:*p*-sodium styrene sulphonate (a) 10:1 (b) 15:1 (c) 20:1.

Table.5.7 SEM results summary for electrospun poly (styrene-co-*p*-sodium styrene sulphonate) fibers at different mole ratios.

Mole ratio	Average diameter (nm)	Range (nm)	Spinnability
0:1	-	-	?
1:1	-	-	?
5:1	-	-	?
10:1	602.96	216.88-817.90	Yes
15:1	1124.90	860.71-1828.66	Yes
20:1	4941.96	3018.71-6413.52	Yes

Electrospun poly (styrene-co-*p*-sodium styrene sulfonate) fibers, by virtue of the sulfonate functionality and polystyrene backbone could be applied as a strong cation exchange sorbent bed material for the extraction of weakly basic and neutral analytes. A typical SPE procedure for in which a strong cation exchange sorbent is employed could involve the use of methanol, water, 2% formic acid and 5% ammonium hydroxide/methanol. Table 5.8 shows the results obtained when electrospun poly (styrene-co-*p*-sodium styrene sulfonate) fibers at a mole ratios of 10:1, 15:1 and 20:1 were immersed in the SPE solvents. The results confirm suitability of the mole ratios for SPE application.

Table.1.8 Behaviour of selected mole ratios of electrospun poly (styrene-co-*p*-sodium styrene sulfonate) fibers in SPE solvents.

Mole ratio	Methanol	Water	2% Formic acid	5% NH₄OH/Methanol
10:1	Insoluble	Insoluble	Insoluble	Insoluble
15:1	Insoluble	Insoluble	Insoluble	Insoluble
20:1	Insoluble	Insoluble	Insoluble	Insoluble

5.3.3 Poly (styrene-co- acrylamide)

Fig 5.20 shows the SEM images of the spinnable mole ratios of poly (styrene-co-acrylamide). Bead free fibers were obtained at mole ratios 0:1, 1:10 and 10:1. Mole ratios 5:1 although categorized as spinnable, it was found to be very sticky such that the electrospinning jet seemed not to go through the bending instability stage. Mole ratios 1:1 and 2:1 could not be spun as they were found to be insoluble in the solvents employed. However, it cannot be concluded with certainty that they are not spinnable as there could be other solvents that could be employed.

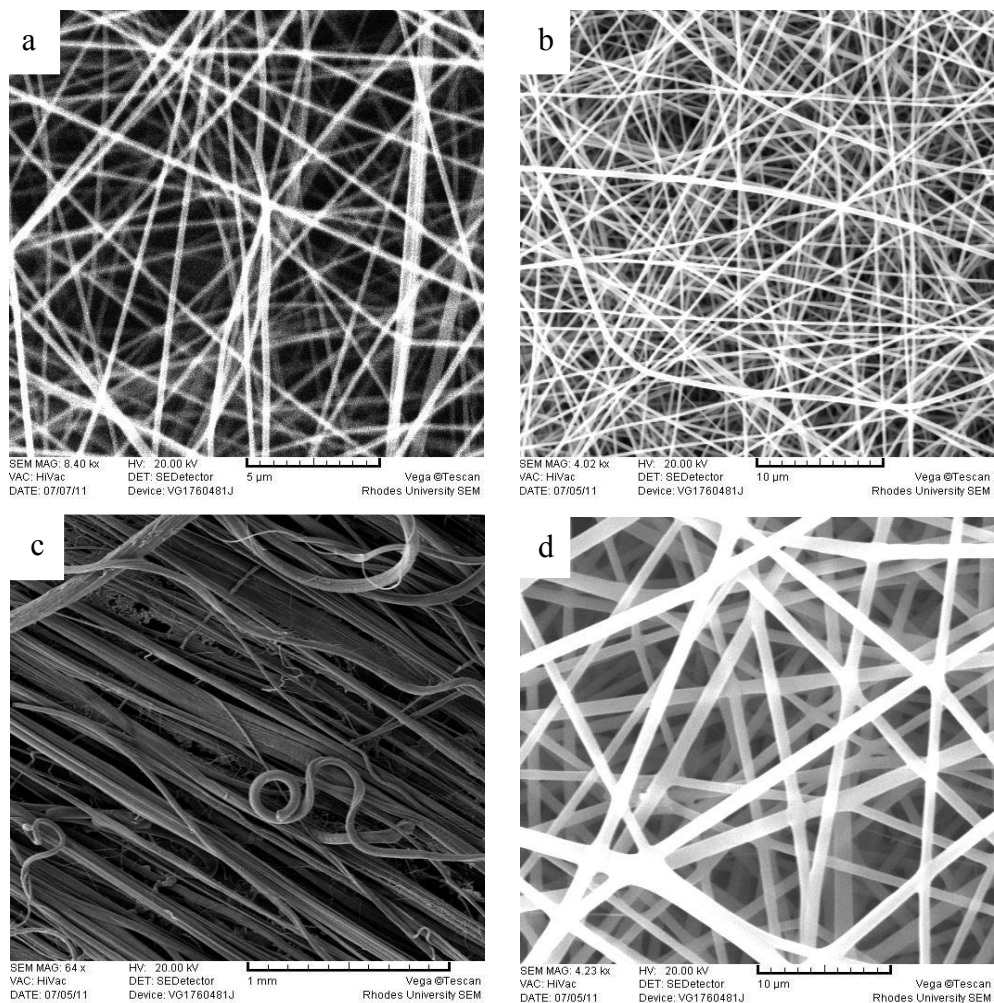


Fig.5.20 SEM images of electrospun poly (styrene-co-acrylamide) copolymers spun from different mole ratios of styrene:acrylamide (a) 0:1 (b) 1:10 (c) 5:1 and (d) 10:1.

Table.5.9 SEM results summary for electrospun poly (styrene-co-acrylamide) fibers at different mole ratios.

Mole ratio	Average diameter (nm)	Range (nm)	Spinnability
0:1	253.57	210.35-282.65	Yes
1:10	365.83	302.11-427.25	Yes
1:1	-	-	?
2:1	-	-	?
5:1	-	-	Yes
10:1	1159.92	985.69-1436.88	Yes

Electrospun poly (styrene-co-acrylamide) fibers, by virtue of the amide functionality and polystyrene backbone could be applied for the extraction of a broad range of analytes on the basis of hydrophobic interactions. Therefore, the fibers were immersed in methanol, water and well as let to stand in air. Table 5.10 shows the results obtained when electrospun poly (styrene-co-acrylamide) fibers at a mole ratios of 1:10 and 10:1 were immersed in water, methanol as well as left to stand in air. The results confirm suitability of the mole ratio 10:1 for SPE application.

Table.2.10 Behaviour of selected mole ratios of electrospun poly (styrene-co-acrylamide) fibers in SPE solvents.

Mole ratio	Methanol	Water	Air
1:10	Insoluble	Shrunk	Shrunk
10:1	Insoluble	Insoluble	No change

5.4 Solid phase extraction devices

5.4.1 Electrospun polystyrene fiber based solid phase extraction devices

Polystyrene fibers were employed as a representative sorbent bed material for all electrospun fibrous materials that could be easily rolled up to form a fiber clew (relatively low mechanical strength). The first SPE device that was fabricated is referred to as a micro column SPE device (see Fig. 5.21 (a)) [177]. In an effort to investigate the effect of the force applied on the sorbent bed in the manual packing process, the top side of the sorbent bed was viewed under SEM (see Fig. 5.21 (c-d)). It was confirmed that the force applied was not inducing any breakup or significant flattening of the electrospun fibers.

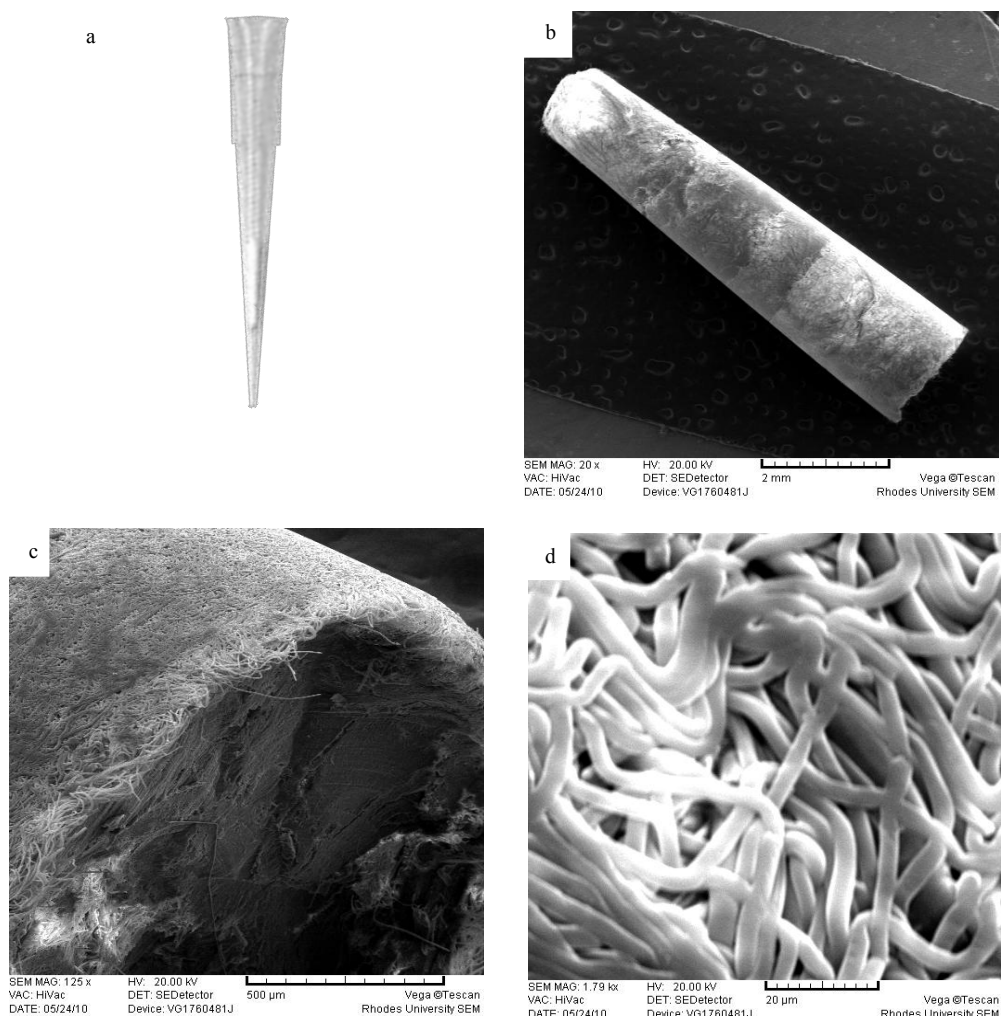


Fig.5.21 (a) Photograph of micro column SPE device, SEM images of (b) sorbent bed (c) magnification of top edge (d) zoomed in top surface.

The second SPE device that was fabricated is referred to as disk (I) SPE device (see Fig. 5.22) [180]. Unlike the micro column SPE device where a certain degree of flattening was observed, for this device, flattening was not observed as viewed under SEM. This suggested that the force applied in the packing process was lower compared to that applied for the micro column SPE device. A possible explanation could be that the wire (0.5 mm diameter) employed in the micro column SPE device fabrication procedure, by virtue of having a

smaller contact surface compared to the glass rod (5 mm diameter) employed in the disk (I) fabrication procedure, resulted in an increased pressure imposed.

Despite the observed slight flattening of the fibers, percolation of the solvents was not hindered which suggested that the packing procedure was plausible for fundamental experiments. Alternative polymers or packing procedures could be employed to address the challenge of slight flattening of fibers. More so, the thesis seeks to provide a platform for electrospun nanofiber sorbent based research, thus the primary focus at this stage was to have the electrospun fibers in a packed format for evaluation. Based on that thinking further experiments were conducted to evaluate the performance of the fabricated devices.

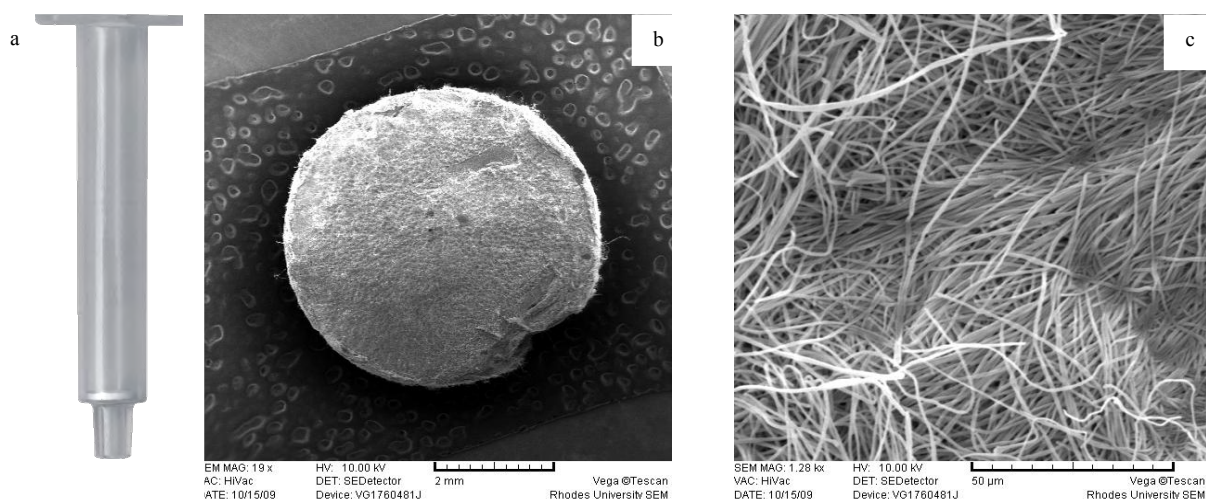


Fig.5.22 (a) Photograph of disk (I) SPE device, SEM images of (b) sorbent bed (c) zoomed in top surface [180].

An optimal sorbent is one that can provide a platform for fast analyte mass transfer kinetics and this is dependent on the sorbent physicochemical properties (surface area, pore structure and surface chemistry). Despite the fact that sorbent physicochemical properties can be used to predict SPE performance, a bias towards SPE method development sorbent characterisation is more effective as the contribution of solution physicochemical properties

and flow rate to analyte mass transfer kinetics is significant. On that basis, it may be said that initial evaluation of new sorbent materials for SPE application can be achieved without a complete characterisation of sorbent physicochemical properties. Progress can be made in getting a better understanding of new sorbent materials by relying on the theoretical prediction of sorbent physicochemical characteristics.

From the SPE method development perspective, the major sorption parameters characterizing a sorbent are recovery efficiency and breakthrough volume [50]. On that basis, the experimental design for fabrication and evaluation of SPE devices was divided into two stages. The first stage consisted of establishing a sorbent mass, packing format and SPE method at which quantitative recoveries (preferably above 80%) could be achieved. Based on the established sorbent mass and packing formats, the second stage consisted of determining breakthrough curves from which sorbent retention characteristics were determined.

The first part of the SPE experiments involved an investigation of the effect of the packing format on the recovery efficiency. Initial recovery studies were carried out on deionised water spiked with 500 ng ml⁻¹ of each of four corticosteroids. The choice of corticosteroids as the model analytes was based on the expected π - π interactions with the benzene rings of the polystyrene backbone [247, 248] (see Fig. 5.23).

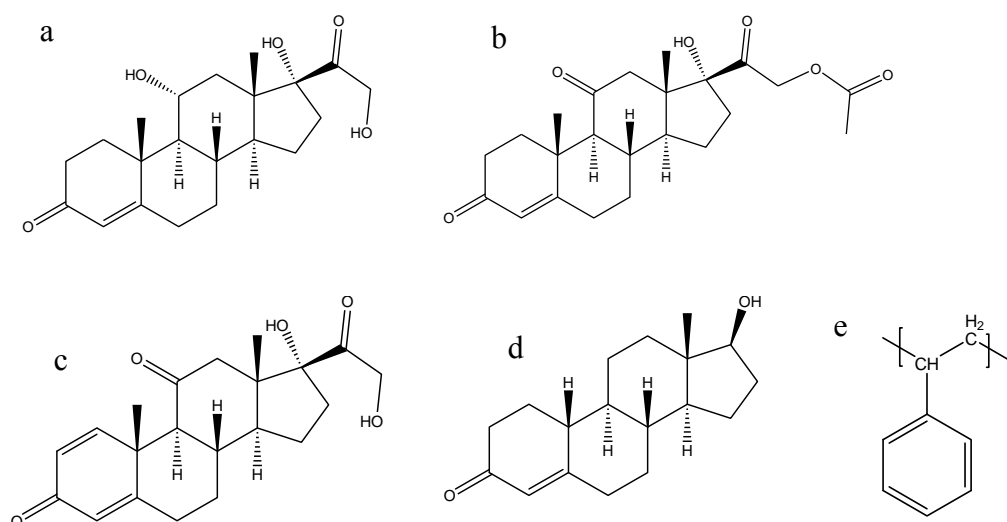


Fig.5.23 Chemical structures of corticosteroids (a) Hydrocortisone (b) Cortisone acetate (c) Prednisone (d) 19-nortestosterone and sorbent material (e) Polystyrene.

Fig. 5.24 shows the recoveries obtained for the micro column and disk (I) SPE devices at 5 mg and 10 mg sorbent bed masses. The recoveries for the disk format improved from 66.07-81.4% to 83.76-93.43% when the sorbent mass was increased from 5 mg to 10 mg. While slightly higher recoveries of 101.07-124.29% were obtained for the micro column sorbent bed format. This could be attributed mainly to the increased sorbent bed height.

It was established that 10 mg was optimal for achieving quantitative recoveries. Given the fact that the main objective of the study was to develop miniaturised SPE devices, an upper limit of 10 mg sorbent bed mass was set. Therefore, where quantitative recoveries (preferably above 80%) were achieved, the sorbent mass was considered suitable. On that basis 10 mg was used as a sorbent mass for all preceding experiments in which polystyrene was used as the sorbent bed for the micro column and disk (I) SPE devices.

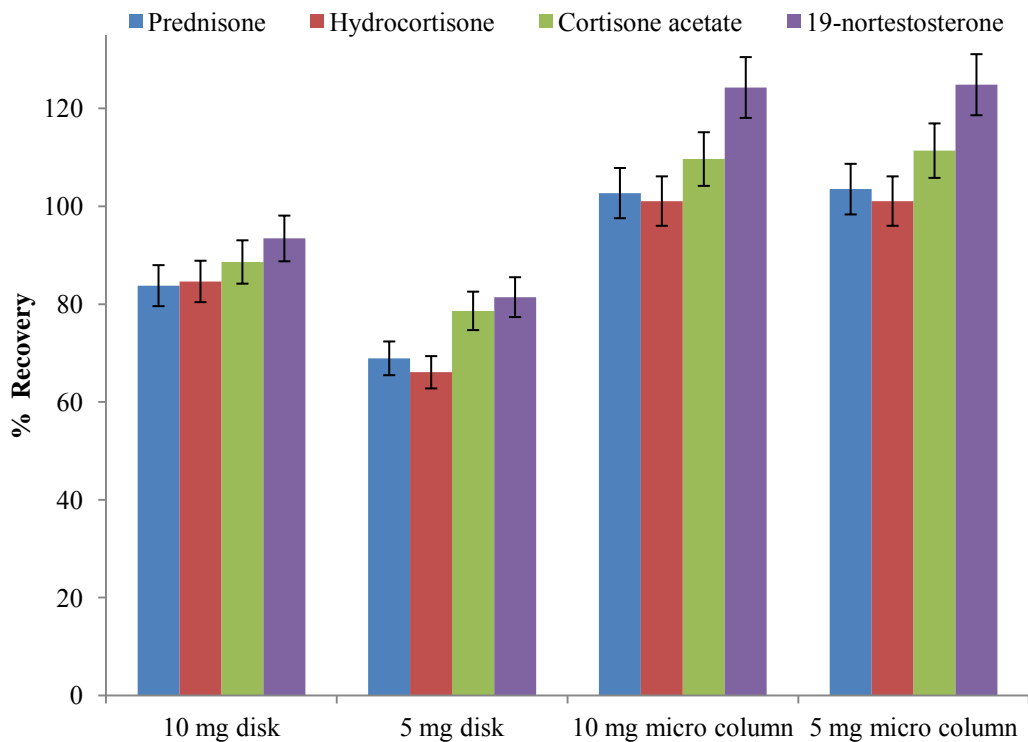


Fig.5.24 Effect of sorbent packing format and sorbent mass on recoveries in water for disk (I) and micro column SPE devices ($n=5$ at 500 ng ml^{-1}).

One of the driving forces for the experimental design was to explore the possibility of developing an electrospun fiber based disk SPE device. This was driven by the need to simplify the disk SPE fabrication procedure in order to provide a platform for widening disk sorbent chemistries. Disk sorbent chemistries are currently limited because of the complexity of the available fabrication procedures [103, 208].

Given the fact that analytical parameters for the micro column SPE device had already been reported by Kang and co-workers [178], further recovery experiments were focussed on the disk SPE device. The extraction ability of the polystyrene disk sorbent bed was further evaluated by determining the extraction recoveries of the analytes in spiked plasma at three

different concentrations (500, 125 and 31.25 ng ml⁻¹). The extraction recoveries ranged from 51.14 to 80.13% over the three concentration ranges (see Fig. 5.25).

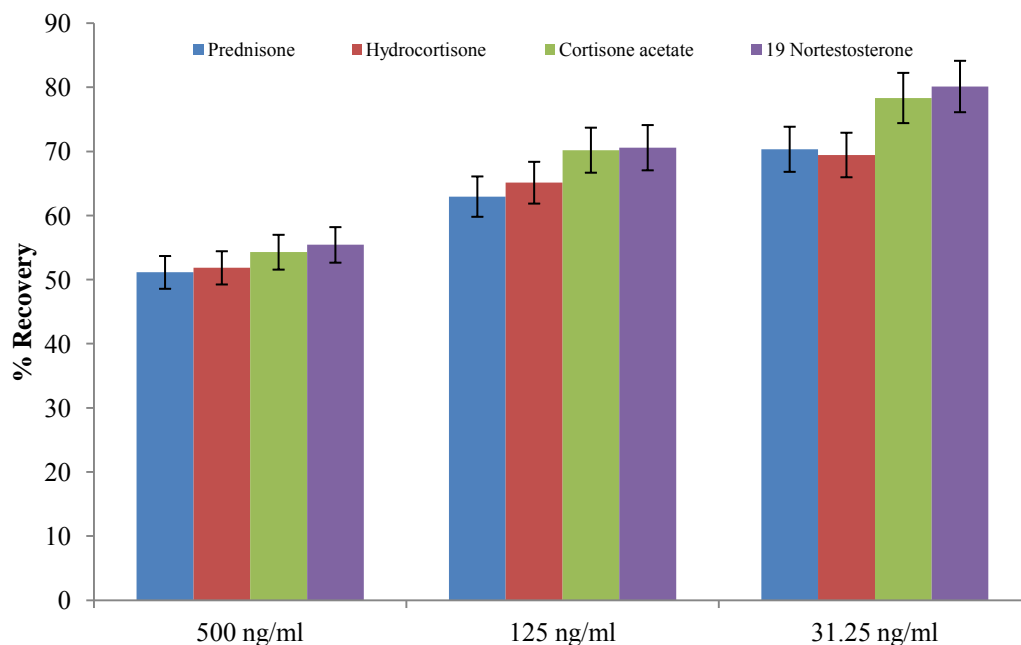


Fig.5.25 Disk sorbent bed recoveries in plasma at different concentrations (n=5).

The analytical parameters obtained for the disk (I) based SPE procedure are summarised in Table 5.11. Good linearity of the four analytes was achieved in the range 12.5-400 ng ml⁻¹ with correlation coefficients greater than 0.99. The detection limits were calculated at a signal to noise ratio of 3 and ranged from 0.75 to 1.29 ng ml⁻¹. The repeatability of the disk SPE procedure (expressed as relative standard deviation of the peak areas) was determined for five analyses of the same sample and it ranged from 2.81 to 8.92%.

Although there was a decrease in absolute recovery at 500 ng ml⁻¹, the results indicated the suitability of the disk SPE device for the trace determination of the target analytes. On the basis of the analytical parameters, it was successfully demonstrated that the disk SPE procedure was viable. Given the fact that a protocol for controlling the chemistry at the

surface of electrospun polystyrene copolymer fibers was successfully demonstrated as reported in sections 5.2 and 5.3, it can be said with confidence that a procedure for disk sorbent bed fabrication for broadening the range of sorbent chemistries has been developed.

Table.5.11 Analytical parameters for polystyrene microfiber disks.

Analyte	Linear range (ng ml ⁻¹)	Linearity (r ²)	Repeatability (%RSD)					Absolute recovery (plasma)		
			500 ng ml ⁻¹	125 ng ml ⁻¹	31.25 ng ml ⁻¹	LOD (ng ml ⁻¹)	LOQ (ng ml ⁻¹)	500 ng ml ⁻¹	125 ng ml ⁻¹	31.25 ng ml ⁻¹
Prednisone	12.5-400	0.9954	7.83	6.27	7.19	1.27	4.22	51.14	62.96	70.34
Hydrocortisone	12.5-400	0.9965	2.81	4.16	5.66	0.75	2.51	51.85	65.13	69.45
Cortisone acetate	12.5-400	0.9971	8.92	8.76	3.72	0.95	3.15	54.29	70.20	78.34
19-Nortestosterone	12.5-400	0.9958	7.11	2.7	7.44	1.29	4.29	55.43	70.59	80.13

One of the most important characteristic parameters in establishing the suitability of a SPE sorbent bed for extracting target analytes is the breakthrough volume (V_B) as it gives an indication of the sorbent's loading capacity for the target analytes. Assuming that there is a measurable analyte retention, the breakthrough curve forms a sigmoid shape that gives an indication of the analyte mass transfer kinetics as a function of the sorbent retention characteristics [50]. In addition to the breakthrough volume, two important parameters that are obtained from the breakthrough curve are the holdup volume (V_M) and retention volume (V_R). From these parameters chromatographic characteristics of the sorbent bed can then be calculated.

Theoretical and experimental methods have been proposed for determining breakthrough curves [249, 250]. Although experimental breakthrough curve determination by frontal analysis is more tedious, it is more useful for SPE device fabrication. This is due to the fact

that it serves as a guide for understanding the effect sorbent packing format, packing density and sorbent morphology on the flow characteristics of the sample phase.

In order to establish the breakthrough curves for the four steroidal analytes on the electrospun polystyrene sorbent bed, frontal analysis was conducted by loading 500 ng ml⁻¹ aliquots of spiked water samples ranging from 100 µl to 4000 µl and monitoring the eluates by HPLC-DAD. The breakthrough curves were plotted with the vertical axis representing the ratio of the eluted (C_e) to the inlet (C_i) analyte concentration and the horizontal axis representing volume fractions.

Under ideal conditions, the breakthrough curve forms a smooth sigmoid shape. However, experimentally the breakthrough curve is plotted by using the line of best fit.

The precise determination of breakthrough parameters is subject to debate as several methods have been proposed [251, 252]. Nevertheless, a mathematical modelling approach can be said to be more suitable for research purposes as it takes into consideration the actual shape of the breakthrough curve. In addition, interpreting observed experimental phenomena from the mathematical modelling perspective is invaluable as it provides a platform for linking up the various parameters influencing any system [253-257]. The choice of the curve fitting mathematical model depends on the shape of the breakthrough profile as a function of the retention characteristics of the sorbent bed. Due to the importance of accurate determination of breakthrough parameters, it was imperative to compare different mathematical models for each set of data points obtained in the experimental procedure. In addition, chromatographic characterisation of electrospun fiber based SPE sorbent beds has not been reported so it was necessary to explore the mathematical modelling approach with the hope that in future a point could be reached where the electrospinning procedure and retention characteristics of a sorbent bed could be related mathematically.

In an effort to determine chromatographic parameters of the polystyrene disk sorbent bed, two mathematical models were employed, the Boltzmann model (based on the Origin 8.0 curve fitting software) and the sigmoid three parameter model (based on the Sigma plot 11.0 curve fitting software).

The Boltzmann model has been used to fit experimental data as it has generally been accepted as an accurate method [252]. Thus it was the first model employed (see equation 5.2)

$$Y = A_2 + \frac{A_1 - A_2}{1 + e^{-\frac{x - x_0}{dx}}} \quad 5.2$$

Where Y represents the ratio of the eluted (C_e) to the inlet (C_i) analyte concentration ($\frac{C_e}{C_i}$), x is the volume of sample flowing through the sorbent, A_1 and A_2 are two regression parameters. The maximum value of ($\frac{C_e}{C_i}$) is (A_2) and it is obtained when $x \rightarrow \infty$, while the minimum value of ($\frac{C_e}{C_i}$) is approximately A_1 , obtained for $x \rightarrow 0$. The retention volume which corresponds to the point of inflexion on the breakthrough curve was obtained from the model and it corresponds to the $\left(\frac{C_e}{C_i}\right) = \frac{A_1 + A_2}{2}$

$$V_R = x_0 \quad 5.3$$

The hold-up volume (V_M) and the breakthrough volume (V_B) were calculated as the x values obtained from equating the following;

$$\left(\frac{99}{100}\right) * A_2 = A_2 + \frac{A_1 - A_2}{1 + e^{-\frac{x - x_0}{dx}}} \quad 5.4$$

$$\left(\frac{1}{100}\right) * A_2 = A_2 + \frac{A_1 - A_2}{1 + e^{-\frac{x - x_0}{dx}}} \quad 5.5$$

And by solving these equations, the formulae below were derived;

$$V_B = x_o + (dx) * \ln\left(\frac{100}{99} \left(1 - \frac{A_1}{A_2}\right) - 1\right) \quad 5.6$$

$$V_M = x_o + (dx) * \ln(99 - 100 * \frac{A_1}{A_2}) \quad 5.7$$

The number of theoretical plates (N) corresponds to the efficiency of the sorbent bed and was calculated from the breakthrough curve, using the relationship proposed by Werkhoheve-Goëwie and co-workers [258]

$$V_B = V_R * \left(\frac{\sqrt{N}-2}{\sqrt{N}}\right) \quad 5.8$$

The second method that can be applied is that proposed by Lökvist and Jönsson [259] who adopted a differential numerical solution to the breakthrough curve for analytes on a sorbent bed with a low number of theoretical plates

$$V_B = V_R \left(a_o + \frac{a_1}{N} + \frac{a_2}{N^2}\right)^{-1} \quad 5.9$$

Where $a_o = (1 - b)^2$, a_1 and a_2 are complex functions of b evaluated from tabular data [259] and b is the breakthrough level (the fraction of the total mass of analyte which has passed through the sorbent bed).

The retention factor (k) was calculated from the fundamental equation of chromatography expressed as;

$$V_R = V_M(1 + k) \quad 5.10$$

The experimental breakthrough curves for the disk sorbent packing format for the four analytes as plotted by the Boltzmann model are shown in Fig.5.26. Table 5.12 shows the calculated chromatographic parameters for the sorbent bed. It was observed that there was a

significant difference between the calculated and observed (based on the last point before breakthrough) breakthrough volumes for hydrocortisone and cortisone acetate (98.13 and 71.46 μl compared to 400 and 500 μl respectively). In addition, the hold-up volumes for prednisone and cortisone acetate were found to be above the sample volume, which showed that the Boltzmann model was not the best for fitting the data points. Thus the sigmoid three parameter model was employed.

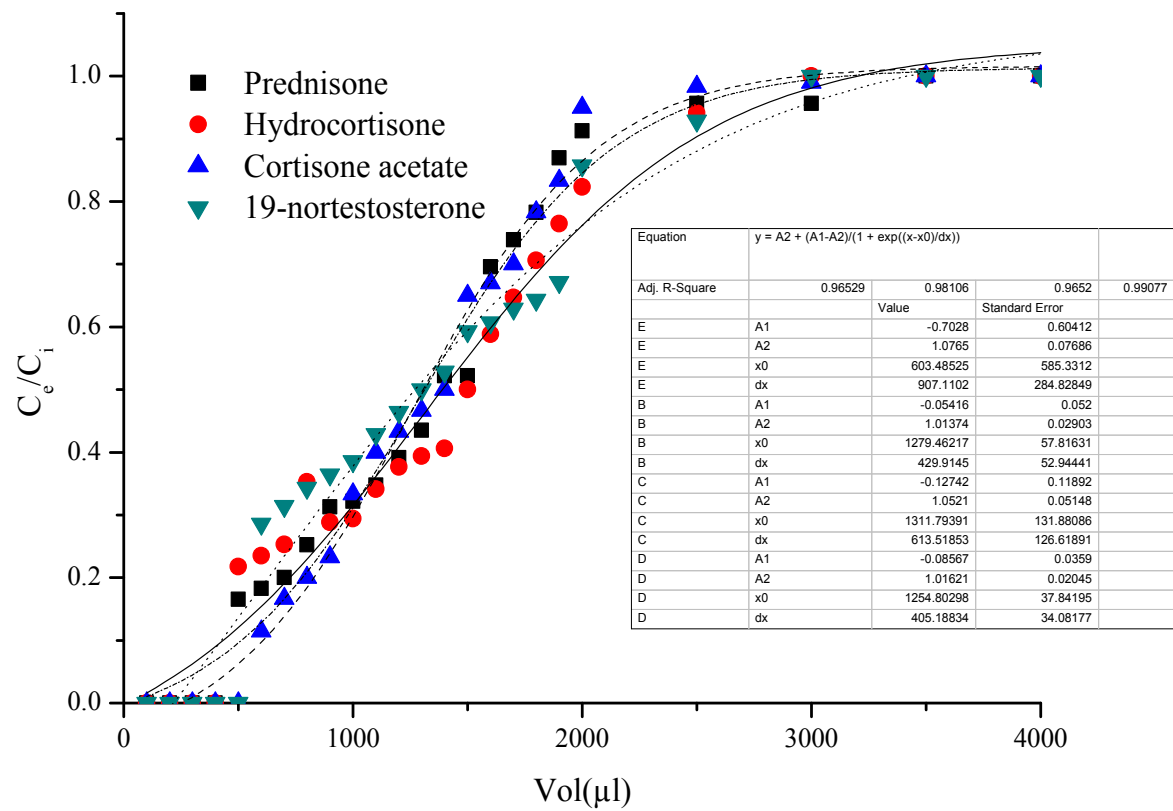


Fig.5.26 Breakthrough curves determined for four steroids on the electrospun polystyrene fiber disks plotted using the Boltzmann model.

Table.5.12 Chromatographic parameters of the electrospun polystyrene fiber based disk sorbent bed derived from the Boltzmann model.

	$V_B(\mu\text{l})$	$V_B(\mu\text{l})$					
Analyte	Observed	Calculated	$V_M(\mu\text{l})$	$V_R(\mu\text{l})$	N_{cal}	N_{obs}	k
Prednisone	400	239.601	5231.2	603.49	11.00	35.18	-0.88
Hydrocortisone	400	98.13	3277.57	1279.46	4.7	8.47	-0.61
Cortisone acetate	500	71.46	4201.79	1311.79	4.47	10.44	-0.69
19-nortestosterone	500	302.12	3149.81	1254.8	6.93	11.05	-0.60

For the sigmoid three parameter model (see equation 5.11)

$$Y = \frac{a}{1 + e^{-\frac{(x-x_0)}{b}}} \quad 5.11$$

Similar to the Boltzmann model, Y represents the ratio of the eluted (C_e) to the inlet (C_i) analyte concentration ($\frac{C_e}{C_i}$), x is the volume of sample flowing through the sorbent, a and b are two regression parameters. The maximum value of ($\frac{C_e}{C_i}$) is (a). Calculation of V_M and V_B was achieved by expressing ($\frac{C_e}{C_i}$) as a fraction of a as follows;

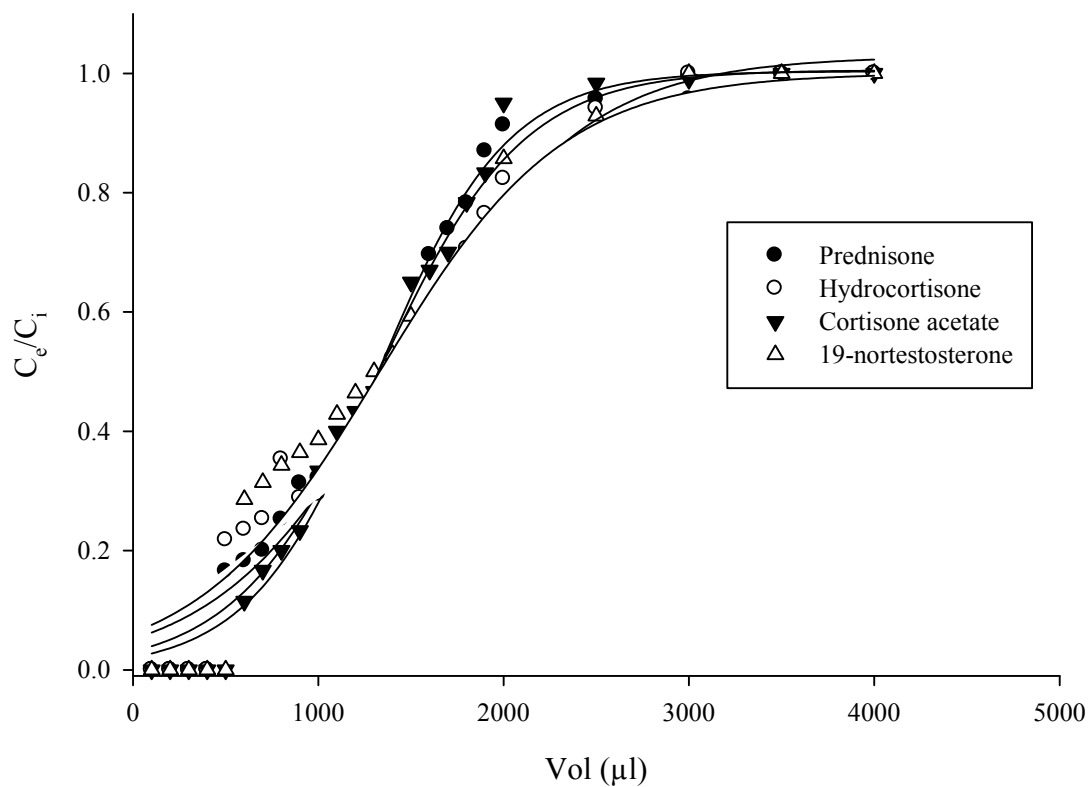
$$\left(\frac{C_e}{C_i}\right) = F * a \quad 5.12$$

Where $F = \frac{1}{1 + e^{-\frac{(x-x_0)}{b}}}$ and solving for x (corresponding to either V_M or V_B) resulted in the expression below

$$x = x_0 + b \ln \frac{F}{1-F} \quad 5.13$$

V_M and V_B were obtained from equation 5.13 at F values of 0.99 and 0.01 respectively.

The experimental breakthrough curves for the disk sorbent packing format for the four analytes as plotted by the Sigmoid three parameter model are shown in Fig.5.27. Table 5.13 shows the calculated chromatographic parameters for the sorbent bed. All the values of calculated breakthrough volumes were observed to be negative due to the fact that the curves pass through the origin above the observed breakthrough volume. Nevertheless, all values for the holdup volumes and retention volumes were realistic thus the sigmoid three parameter model was found to be more applicable as compared to the Boltzmann model.



Analyte	Coefficient			R ²
	a	b	x ₀	
Prednisone	1.0035 (0.02)	343.75 (21.23)	1325.85 (27.27)	0.9886
Hydrocortisone	1.0056 (0.03)	384.91 (27.73)	1329.39 (35.66)	0.9826
Cortisone acetate	1.0287 (0.04)	489.86 (46.27)	1442.09 (59.97)	0.9673
19-nortestosterone	1.0004 (0.048)	490.91 (58.28)	1331.15 (74.42)	0.9494

Fig.5.27 Breakthrough curves determined for the four steroids on the electrospun polystyrene fiber disk sorbent bed presented lines of best fit using sigmoid three parameter model.

Table.5.13 Chromatographic parameters of the electrospun polystyrene fiber based disk sorbent bed derived from the sigmoid three parameter model.

	$V_B(\mu\text{l})$	$V_B(\mu\text{l})$					
Analyte	Observed	Calculated	$V_M(\mu\text{l})$	$V_R(\mu\text{l})$	N_{cal}	N_{obs}	k
Prednisone	400	-253.72	2905.42	1325.85	2.82	8.20	-0.54
Hydrocortisone	400	-439.32	3098.1	1329.39	2.26	8.18	-0.57
Cortisone acetate	500	-808.88	3693.06	1442.09	1.64	9.37	-0.61
19-nortestosterone	500	-924.64	3586.94	1331.15	1.39	10.26	-0.63

The fact that all breakthrough volumes were well above the loading volume demonstrated that quantitative recovery (100%) could be achieved with the disk SPE device.

Theoretical plates of the sorbent bed determined based on the calculated breakthrough volumes ranged from 1.39-2.82 while those determined based on the observed breakthrough volume ranged from 8.18-10.26. Due to the fact that this is the first time that experiments have been conducted to determine the chromatographic parameters of an electrospun fiber based sorbent bed, there was no reference point to establish the exact range of theoretical plates. Even though there may be uncertainties regarding the theoretical plates, it can be said with confidence that the sorbent bed has a low number of theoretical plates between 1 and 10. The observed shape of the breakthrough profile and the range of theoretical plates is consistent with that reported by Lövkvist and Jönsson [259] in their discussion of alternative equations for breakthrough curves of short sampling columns.

In an effort to investigate the relationship between the theoretical plates of an electrospun fiber based SPE sorbent bed and retention capacity, the effect of packing format on the shape of breakthrough curve was investigated. The experiments were designed with three

objectives, the first was to demonstrate the applicability of the polystyrene sorbent bed for extraction of structurally related analytes thus betamethasone and dexamethasone were chosen as the model analytes where π - π interactions were expected to be the predominant extraction mechanism (see Fig. 5.28).

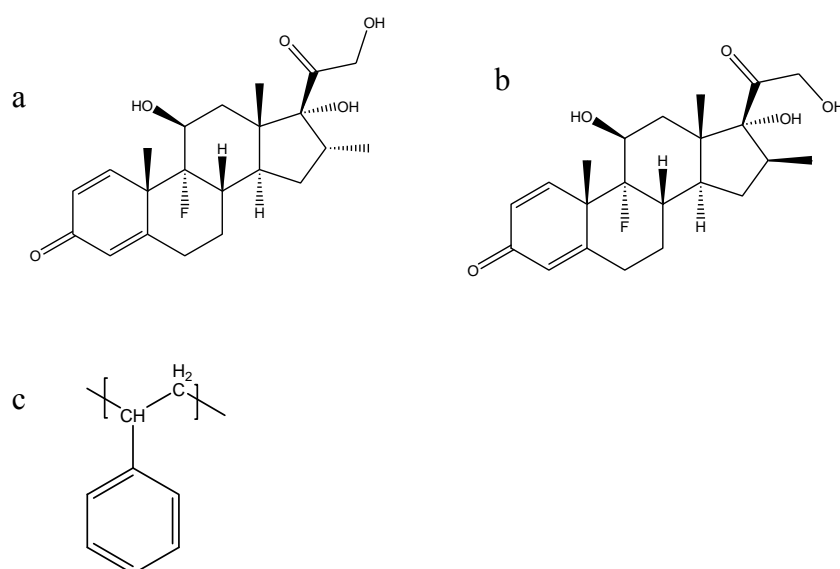


Fig.5.28 Chemical structures for corticosteroids (a) dexamethasone (b) betamethasone and polymer (c) polystyrene.

The second objective was to simplify the breakthrough experimental set-up by employing a syringe pump driven semi-automated system (as reported in section 4.6.2). The third objective was to investigate the relationship between the packing format, theoretical plates and the sorbent retention capacity.

Unlike in the initial set of breakthrough experiments where a vacuum manifold was employed to force solvents through the sorbent bed, a syringe was used to deliver a continuous flow of water spiked at 500 ng ml^{-1} through the sorbent bed at 0.1 ml min^{-1} . Fig. 5.29 shows comparative scatter plots of the breakthrough curves obtained for the disk (I) and micro column SPE devices. By inspection it can be seen that the packing format had an effect on the retention characteristics of a sorbent as shown by a higher breakthrough volume for

the micro column SPE device (1400 μ l) compared to a lower breakthrough volume (400 μ l) for the disk packing format. The increase in breakthrough volume can be attributed to the increased sorbent bed height that had a direct effect on the mass transfer kinetics as there was an increased sample sorbent contact time.

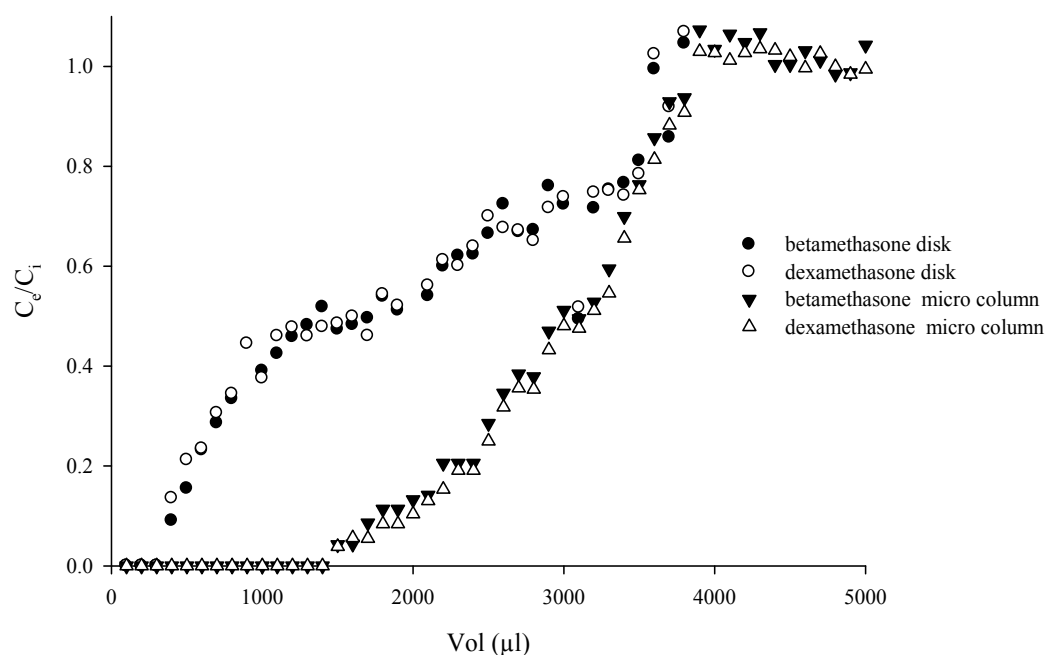


Fig.5.29 Comparison of breakthrough curves (presented as scatter plots) determined for two steroids on electrospun polystyrene fibers packed as (a) disk I and (b) micro column sorbent bed formats.

Despite the fact that the observed breakthrough volume for the disk sorbent bed was similar to that observed in the initial breakthrough experiments, the exact shape of the breakthrough curves was not the same. The Boltzmann and sigmoid three parameter models were found not to fit the data points in the same way as the first set of experiments. Nevertheless, the fact that the logP values (2.07, 1.79, 2.35 and 4.23) for (prednisone, hydrocortisone, cortisone acetate and 19-nortestosterone) and (1.93 and 1.93) for (betamethasone and dexamethasone) are closely related led to the conclusion that chromatographic parameters obtained for the disk

sorbent bed in the first set of experiments could be used for approximate comparative studies with the micro column sorbent bed.

Unlike the disk sorbent bed where the sigmoid three parameter model was found to be more suitable, for the micro column SPE device, the Weibull five parameter model was found to be more appropriate.

Equation 5.14 shows an expression for the Weibull five parameter model;

$$Y = Y_o + a \left[1 - e^{-\left(\frac{x-x_o+b \ln 2^{\frac{1}{c}}}{b}\right)^c} \right] \quad 5.14$$

Y_o and a correspond to the maximum and minimum points on the breakthrough curve, x_o corresponds to the point of inflexion while b and c are regression parameters.

As $x \rightarrow \infty$, Y approaches the maximum value of $\left(\frac{C_e}{C_i}\right) = Y_o + a$ thus, $\left(\frac{C_e}{C_i}\right)$ at any point of the breakthrough curve can be expressed as a fraction (F) of the maximum value of $\left(\frac{C_e}{C_i}\right)$.

If the maximum value of $\left(\frac{C_e}{C_i}\right)$ is expressed as

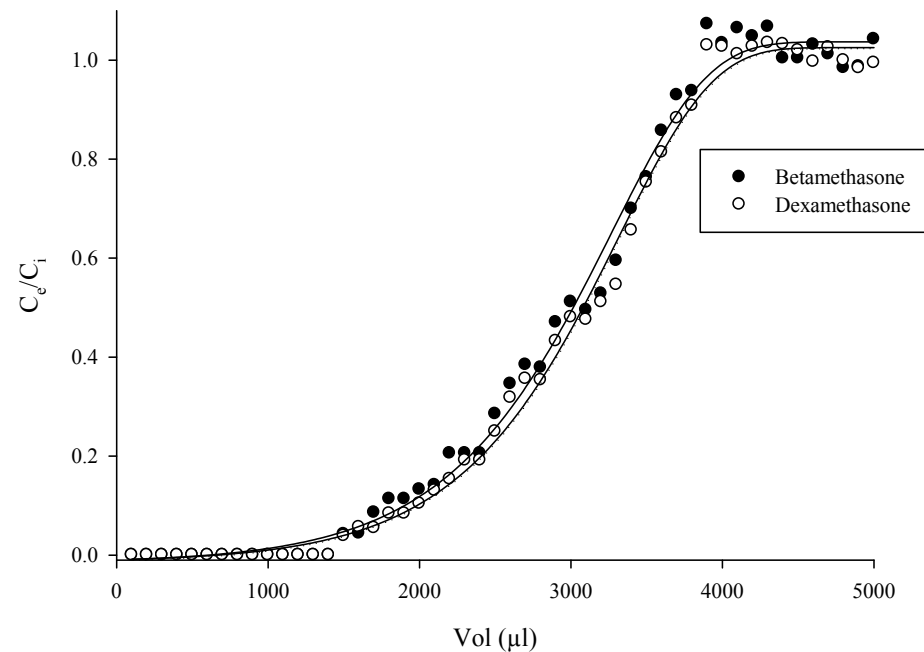
$$F * (Y_o + a) = Y_o + a \left[1 - e^{-\left(\frac{x-x_o+b \ln 2^{\frac{1}{c}}}{b}\right)^c} \right] \quad 5.15$$

Solving for x results in the expression below;

$$x = x_o - b \ln 2^{\frac{1}{c}} + b \left[\ln \left[\left(\frac{Y_o}{a} + 1\right)^{-1} (1 - F)^{-1} \right] \right]^{\frac{1}{c}} \quad 5.16$$

Therefore, V_M and V_B can be calculated at F values corresponding to $\frac{99}{100}$ and $\frac{1}{100}$ respectively.

The values of chromatographic parameters presented in Tables 5.14 and 5.15 show that the Weibull five parameter model was more accurate than the Boltzmann model on the basis of the holdup volumes.



Analyte	Coefficient					R^2
	a	b	c	x_0	y_0	
Betamethasone	1.0396(0.01)	545252504.47 (0.30)	879140.39 (7.94)	3088.50 (40.73)	-0.0143(0.0094)	0.9953
Dexamethasone	1.0528(0.02)	15042770.75 (8.91)	23676.51 (7.37)	3032.19(34.33)	-0.0159 (0.0110)	0.9943

Fig.5.30 Breakthrough curves determined for two steroids on electrospun polystyrene fibers packed in micro column sorbent bed format presented as lines of best fit using the sigmoid Weibull five parameter model.

Table.5.14 Chromatographic parameters of the electrospun polystyrene fiber based micro column sorbent bed format derived from the sigmoid Weibull five parameter model.

	$V_B(\mu\text{l})$	$V_B(\mu\text{l})$					
Analyte	Observed	Calculated	$V_M(\mu\text{l})$	$V_R(\mu\text{l})$	N_{cal}	N_{obs}	k
Betamethasone	1400	901	4250	3088.5	7.98	13.38	- 0.27
Dexamethasone	1400	1020	4240	3032.2	9.1	13.80	- 0.28

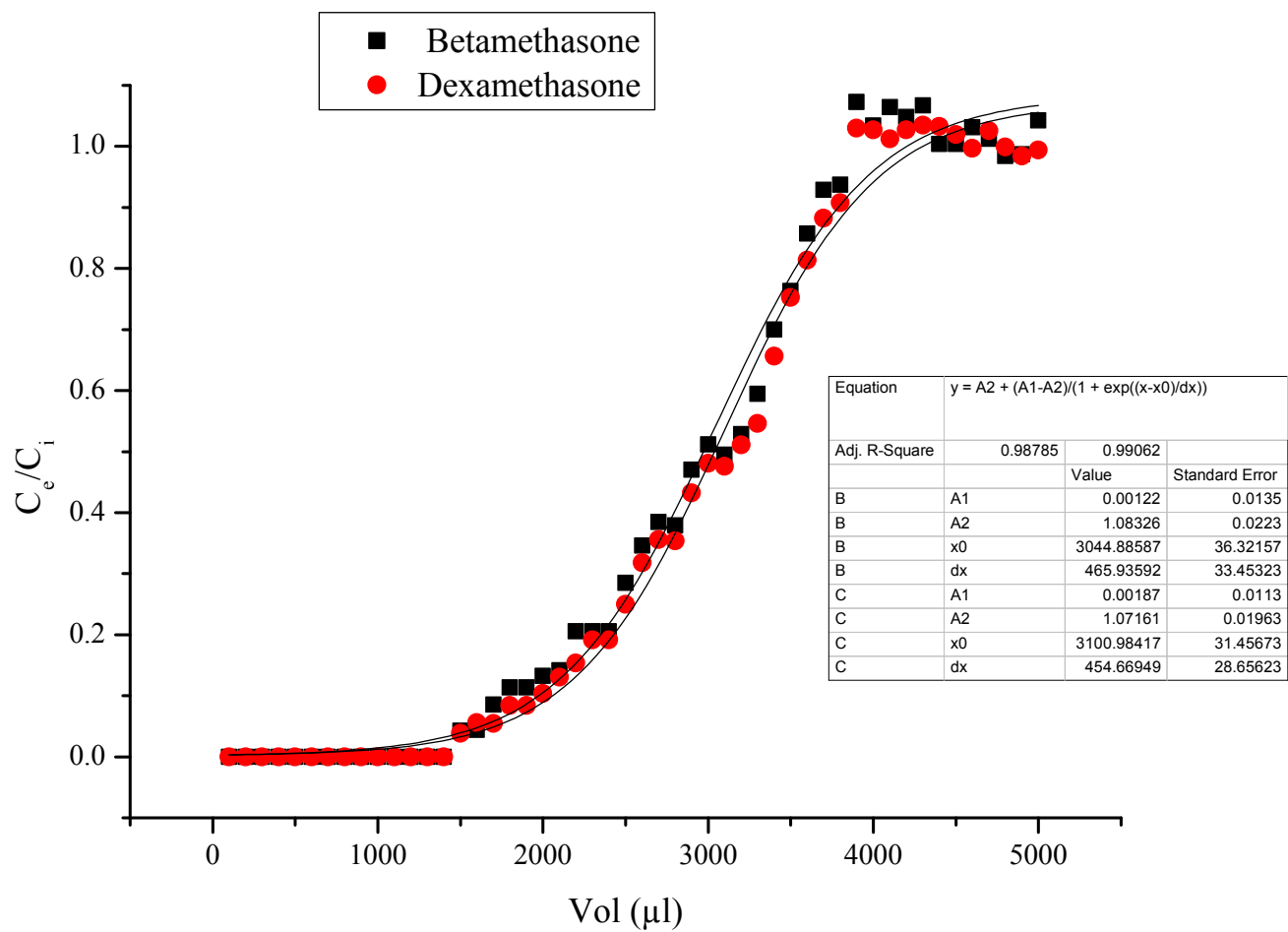


Fig.5.31 Breakthrough curves determined for two steroids on electrospun polystyrene fibers packed in micro column sorbent bed format presented as lines of best fit using the sigmoid Boltzmann model.

Table.5.15 Chromatographic parameters of the electrospun polystyrene fiber based micro column sorbent bed format derived from the sigmoid Boltzmann model.

	$V_B(\mu\text{l})$	$V_B(\mu\text{l})$					
Analyte	Observed	Calculated	$V_M(\mu\text{l})$	$V_R(\mu\text{l})$	N_{cal}	N_{obs}	k
Betamethasone	1400	848.18	5185.39	3044.89	7.69	13.71	- 0.41
Dexamethasone	1400	924.53	5189.44	3100.98	8.12	13.29	- 0.40

The breakthrough volumes, equilibrium volumes, retention volumes, theoretical plates and retention factor values for betamethasone and dexamethasone were very close which was consistent with the closeness of their logP values. This consistency was observed for the breakthrough curves fitted using both the Boltzmann and the Weibull five parameter model. On that basis, it may be concluded that these mathematical models would be suitable for characterisation of any electrospun fiber sorbent-analyte system that follows a similar profile.

Comparison of the calculated theoretical plates for the disk (1.39-2.82) and the micro column (7.98-9.1) SPE devices revealed that the shape of the breakthrough curve could be related to the theoretical plates [259, 260]. In addition, the observed breakthrough volumes for the disk (400-500 μl) and micro column (1400 μl) respectively were consistent with the theoretical plates. This demonstrates that theoretical plates are important for the retention characteristics of a SPE sorbent bed.

Given the fact that theoretical plates are a function of the available surface area for analyte interaction, it can be concluded that a sorbent material with a larger surface area may exhibit a larger number of theoretical plates and consequently a large retention capacity as mass transfer kinetics would be enhanced. Therefore, a larger number of theoretical plates would

correspond to a steeper slope of the breakthrough curve as a result of fast mass transfer kinetics.

Given the fact that surface chemistry of a sorbent material has an influence on the retention characteristics of a sorbent material [261] by virtue of enhancing analyte mass transfer kinetics, it is expected that screening of electrospun nanofiber based sorbents on the basis of the shape of the breakthrough curves could be achieved.

5.4.2 Electrospun nylon 6 nanofiber based solid phase extraction devices

Nylon 6 fibers were employed as a representative sorbent bed material for all electrospun fibrous materials of a relatively high mechanical strength. A SPE device referred to as disk (II) was fabricated by cutting out electrospun nylon 6 nanofibers (disk sorbent bed format) directly from the aluminium foil collector. It was observed that after electrospinning for 6 h, disks that were cut out from the area within a distance of approximately 7 cm on either side of the point directly opposite the counter electrode had a thickness of approximately 350 μm . Disks cut out from the area beyond 7 cm from the central part of the collector exhibited thicknesses below 350 μm (Fig. 5.32).

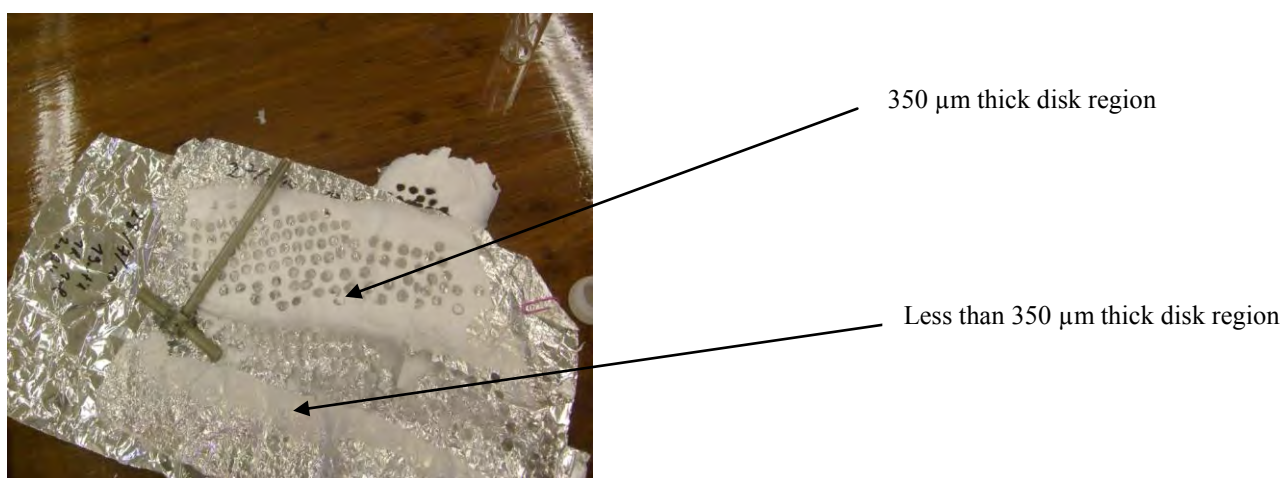


Fig.5.32 Photograph of an electrospun nylon 6 nanofiber mat showing regions from which disks were cut out.

A possible explanation for the observation could be that the converging electric field lines in addition to enhanced charge dissipation introduced by the counter electrode contributed to the focussed deposition of the fibers resulting in a thick sheet.

It was also observed that the thickness of the nanofiber sheet played a significant role in maintaining the integrity of the sorbent bed. This is due to the fact that cutting out or stacking up thinner (less than 350 μm) disk sorbent beds was a challenge as they were observed to warp. Therefore, all disk sorbent beds employed in the study were fabricated on the basis of an electrospinning procedure that consisted of focussed sheet deposition for 6 h. Given the fact that control of electrospun nanofiber mat thickness is of paramount significance for disk (II) SPE device fabrication, multiple counter-electrode [224], moving collector[262] or moving spinneret[263] electrospinning set-ups could be employed in future.

Fabrication of an optimal SPE device was guided by establishing quantitative recoveries as a function of sorbent mass (number of disks stacked) and stacking configuration of the disks. Corticosteroids were employed as model analytes due to the expected non-polar interactions between the hydrophobic portions of the steroids and the methylene chains of nylon (Fig. 5.33). The hydrophilic amide groups were expected to enhance analyte mass transfer to the sorbent bed as they facilitated contact between the aqueous sample phase and the hydrophobic part of the nylon structure [264-266].

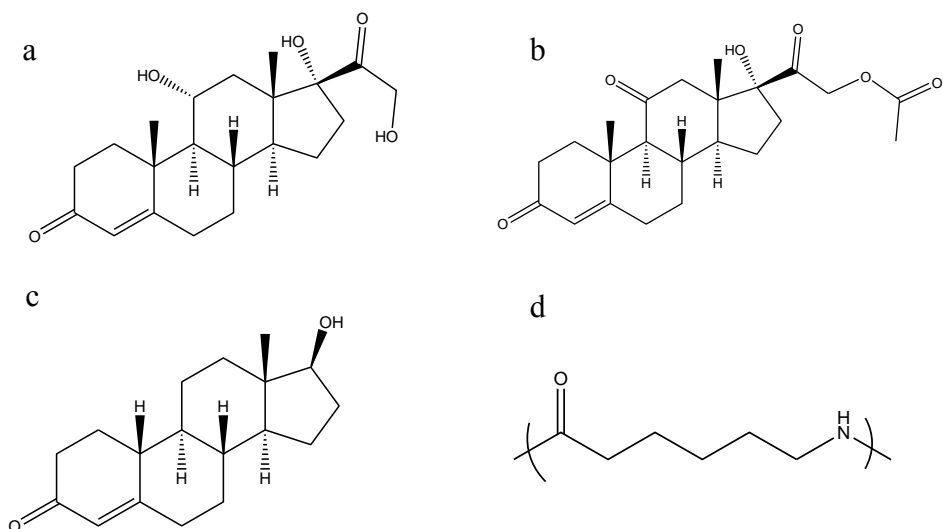


Fig.5.33 Chemical structures for corticosteroids (a) Hydrocortisone (b) Cortisone acetate (c) 19-Nortestosterone and polymer (d) Nylon 6.

In addition to the electrospun nylon 6 fiber disk sorbent beds, 5 mm disks of a polyamide HPLC filtration membrane were employed for comparative studies. However, the exact details of the fabrication procedure of the filtration membrane are not known due to company intellectual property restrictions. All that is known is that it is part of the anopore membrane range. In addition, it was not known whether the primary structure of the polyamide was based on nylon 6 or nylon 6,6. Nevertheless, comparative studies were conducted on the assumption that the flow through characteristics of the sorbent material would have a more significant effect on the retention characteristics in comparison to the surface chemistry. Fig. 5.34 (a) shows the fabricated disk SPE device while Fig. 5.34 (b-c) show the SEM images for the sorbent beds employed in the study.

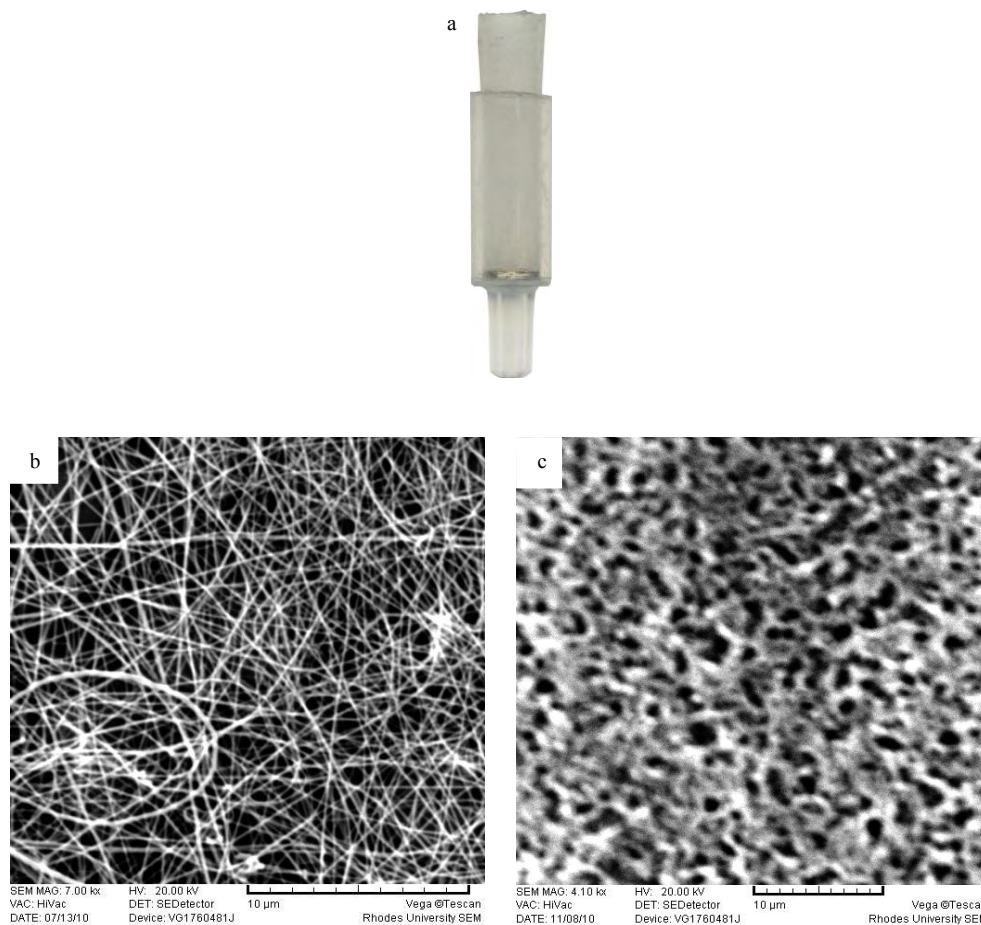


Fig.5.34 (a) Photograph of disk (II) SPE device zoomed in top surface SEM images of (b) electrospun nylon nanofiber sorbent bed (c) polyamide filtration membrane.

Investigation of the relationship between the sorbent bed (mass and stacking configuration of the disks), flow rate, elution time and recovery efficiency was carried out using deionised water spiked with 500 ng ml^{-1} of each of three corticosteroids. Fig. 5.35 shows the SPE curve profile and recovery efficiencies obtained when five disks (4.6 mg) of the polyamide filtration membrane were sandwiched between two stainless steel frits. Recoveries ranged from 10.69-21.71% in a total SPE time of 3 min. Fig. 5.36 shows the SPE curve profile and recovery efficiencies obtained when five disks (4.6 mg) of the polyamide filtration membrane

were stacked at the base of the polypropylene barrel. Unlike the sandwich stacking configuration, improved recoveries (40-76.09%) were obtained in a total SPE time of 40.5 min. It was also observed that as the SPE curve profile tended towards a pattern that can be likened to overlapping sine waves such that when the flow rate is at peak maxima, the elution time is at the peak minima, it corresponds to quantitative recoveries. Packing density is proposed to be the most significant attribute to the improved recovery efficiencies observed when the disks were stacked at the base. This is in light of the fact that when the disks were sandwiched, solvents leaked between the sorbent bed and the inner lining of the SPE barrel resulting in low recoveries. However, when the disks were stacked at the base, all the solvents pass through the sorbent bed due to tight packing. Simplification of the disk (II) fabrication procedure aimed at quantitative recoveries can be achieved by employing a similar procedure to commercially available 96-well plate SPE formats.

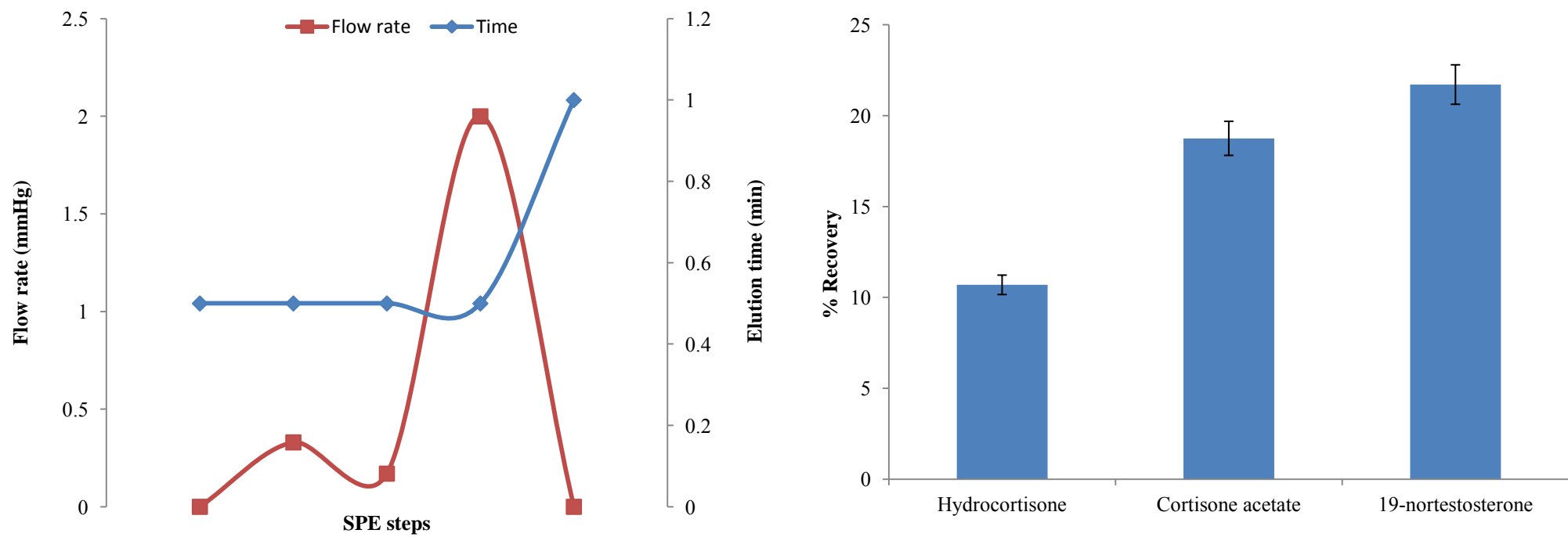


Fig.5.35 SPE curve profile and analyte recoveries for a total SPE time of 3 min on polyamide filtration membrane disk sorbent bed 5 disks (4.6 mg) arranged in sandwich format.

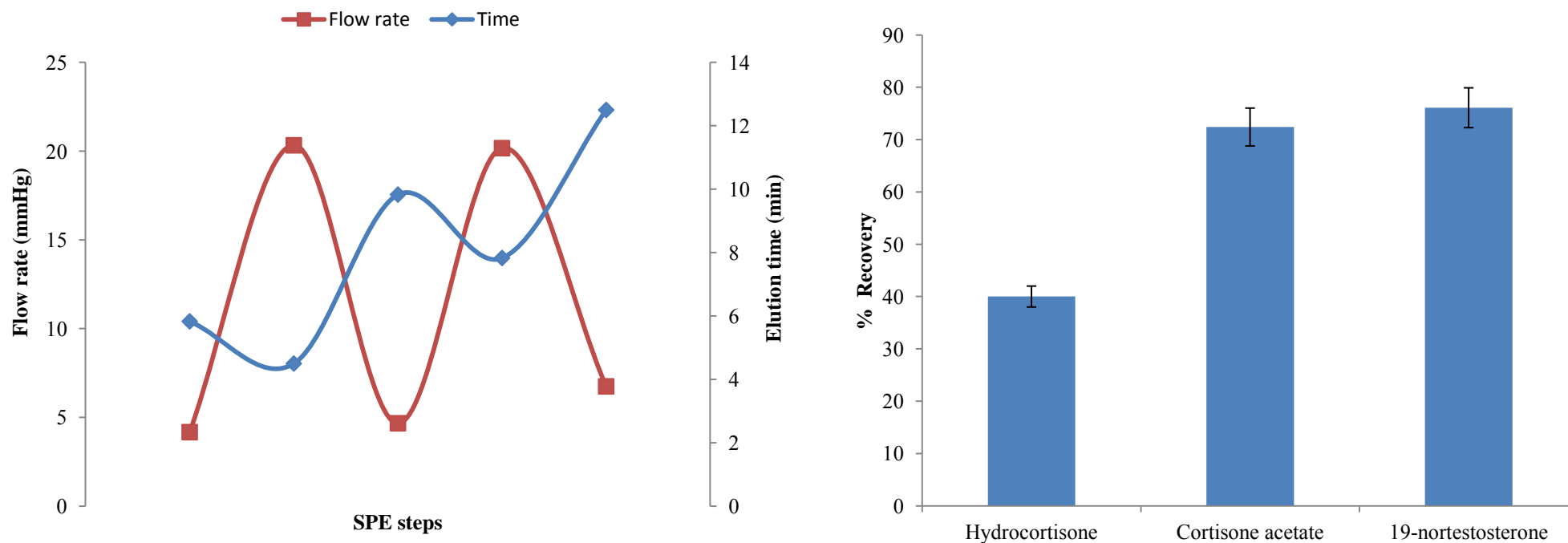


Fig.5.36 SPE curve profile and analyte recoveries for a total SPE time of 40.5 min on polyamide filtration membrane disk sorbent bed 5 disks (4.6 mg) arranged in base format.

Fig. 5.37 shows the SPE curve profile and recovery efficiencies obtained when three disks (2 mg) of electrospun nylon 6 nanofibers were sandwiched between two stainless steel frits. Recoveries ranged from 6.14-11.87% in a total SPE time of 1.25 min. Improved recoveries of 19.34-47.26% were achieved in a total SPE time of 7.17 min when the base packing configuration was employed (see Fig. 5.38). On increasing the number of disks to five and maintaining the base stacking configuration, recoveries of 45.4-97.72% were achieved in total SPE time of 48 min (Fig. 5.39). Similar to the polyamide membrane bed experiments, the variation of the SPE curve profile corresponded to quantitative recoveries. Given the fact that a common challenge with SPE method development is its empirical nature as it relies on experimental trial and error procedures [50], standardisation of SPE devices poses a challenge. Unlike HPLC columns where a standard chromatogram and method are documented, there is no standardisation for SPE sorbent beds. Therefore, it is proposed that SPE curves in relation to recoveries could be employed as a guide for standardising electrospun nanofiber based solid phase extraction devices. In addition, Bierman and co-workers [267] explored a SPE method development software, the knowledge could be expanded by relating the electrospinning procedure and electrospun nanofiber sorbent bed physicochemical characteristics to quantitative recovery.

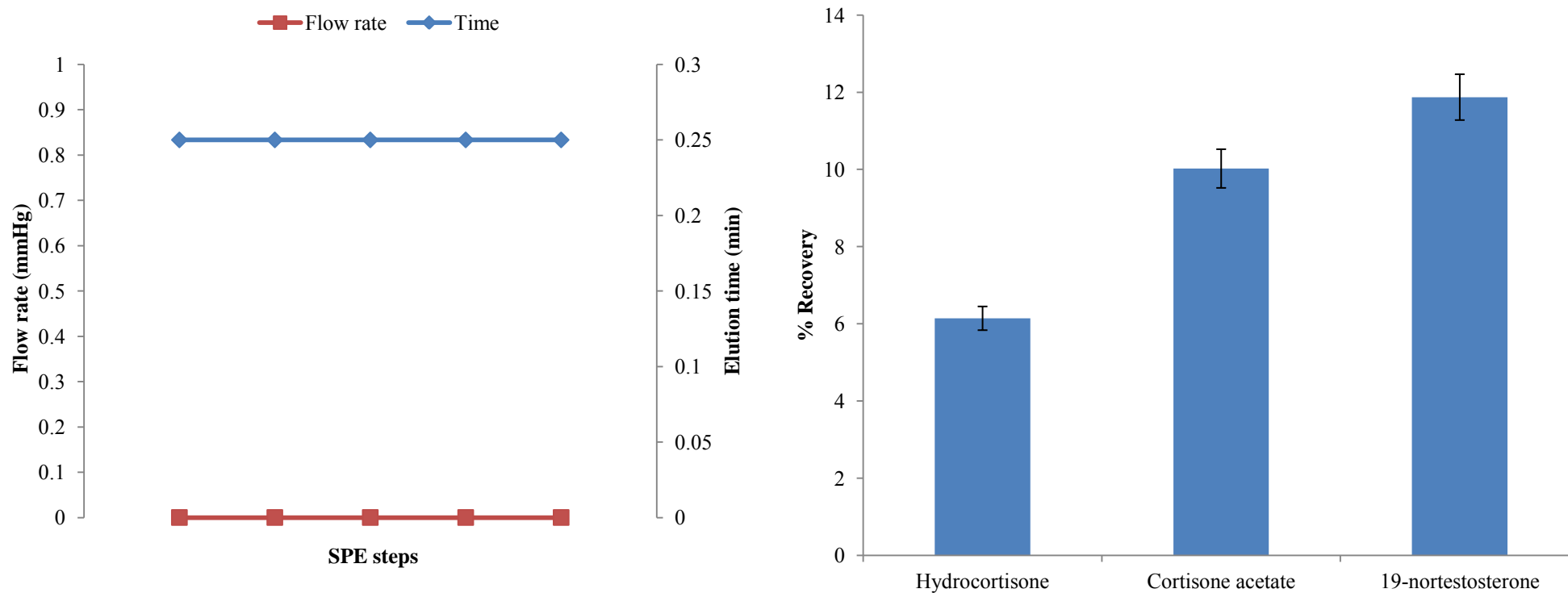


Fig.5.37 SPE curve profile and analyte recoveries for a total SPE time of 1.25 min on nylon 6 nanofiber disk sorbent bed 3 disks (2 mg) arranged in sandwich format.

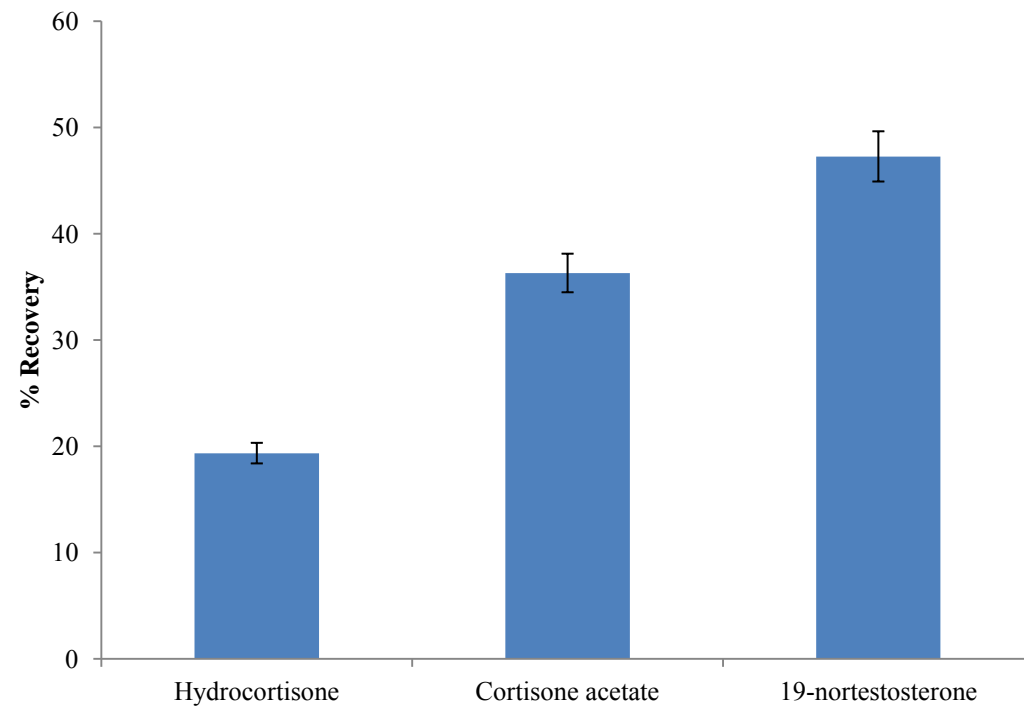
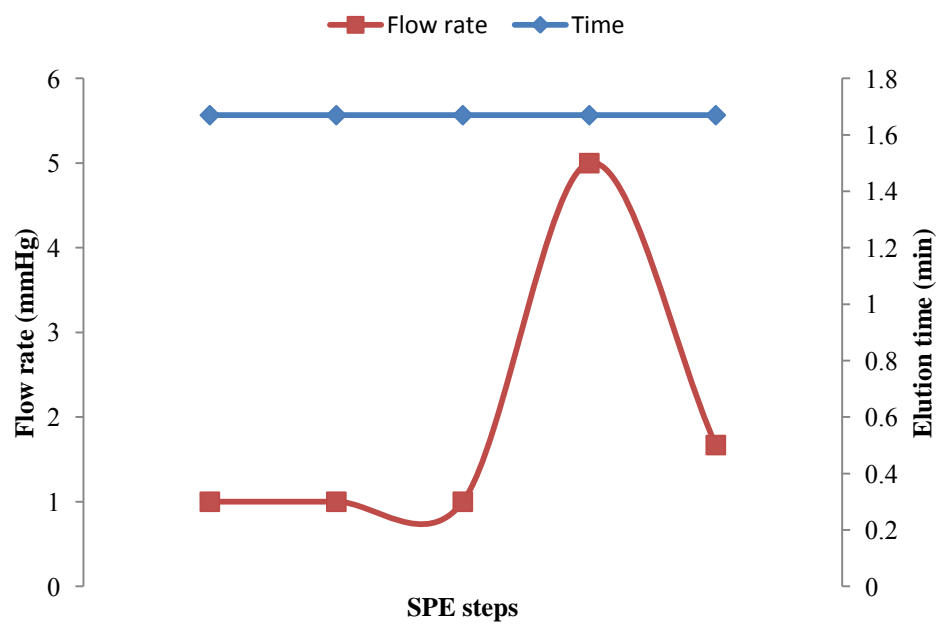


Fig.5.38 SPE curve profile and analyte recoveries for a total SPE time of 7.17 min on nylon 6 nanofiber disk sorbent bed 3 disks (2 mg) arranged in base format.

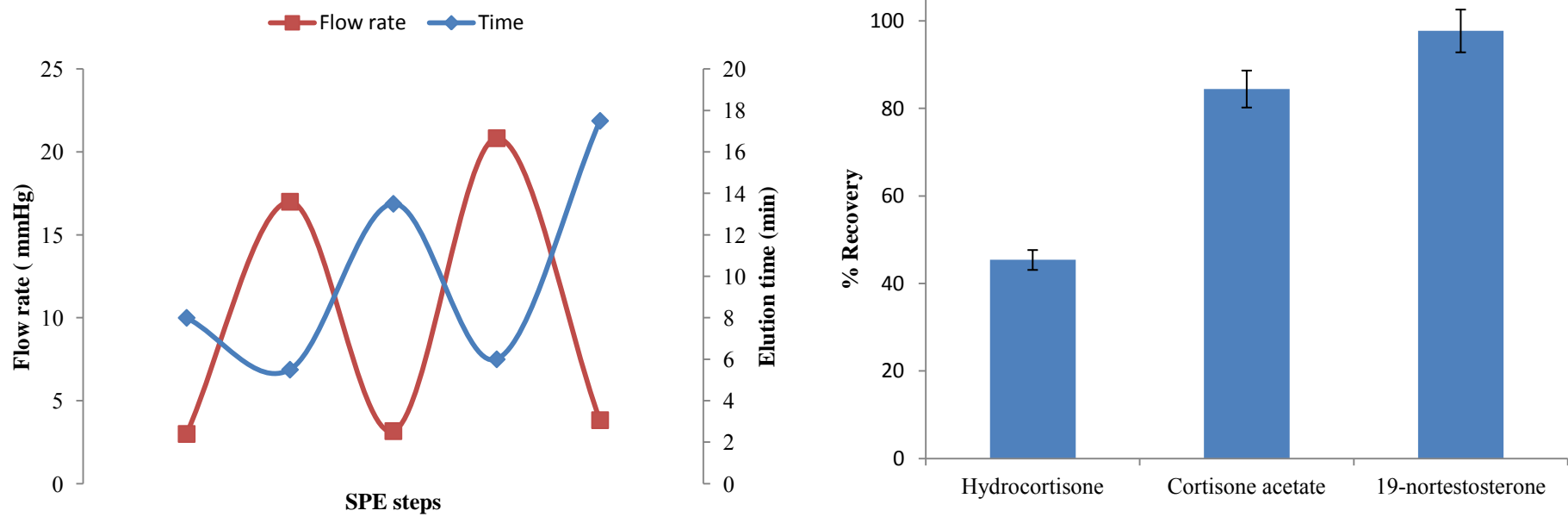
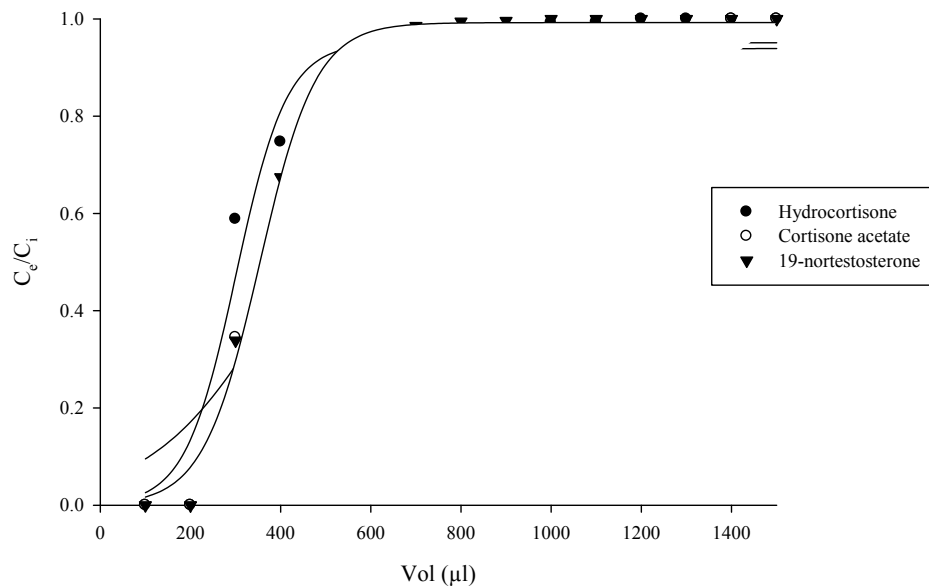


Fig.5.39 SPE curve profile and analyte recoveries for a total SPE time of 48 min on nylon 6 nanofiber disk sorbent bed 5 disks (4.4 mg) arranged in base format.

Having fabricated a device that could achieve quantitative recoveries, it was imperative to establish the chromatographic parameters of the sorbent bed. In order to establish the breakthrough curves for the three steroidal analytes on the electrospun nylon 6 nanofiber and polyamide membrane sorbent beds, frontal analysis was conducted by manually loading 500 ng ml⁻¹ aliquots of spiked water samples and monitoring the eluates by HPLC-DAD.

The experimental breakthrough curves for the polyamide disk sorbent bed for the three steroids were fitted by the sigmoid three parameter model (Fig. 5.40). Table 5.16 shows the calculated chromatographic parameters for the sorbent bed. It was observed that there was a difference between the calculated and observed (based on the last point before breakthrough) breakthrough volumes for all analytes (42.73, -253.25 and 66.42 µl compared to 200 µl respectively). This is not surprising as the calculated breakthrough volume was based on a point at 1% of the maximum value of $\left(\frac{C_e}{C_i}\right)$. The fact that all observed breakthrough volumes were above the loading volume (100 µl) demonstrated that quantitative recovery (100%) could be achieved with the disk SPE device. Theoretical plates in relation to the shape of the breakthrough curve were not consistent with theoretical predictions [259, 260] suggesting that the relationship between breakthrough profiles and theoretical plates may only be applicable to fibrous or spherical particle beds. The steep slope which could be a result of fast analyte mass transfer kinetics and saturation of all the sorptive sites on the sorbent as the breakthrough curve plateaued just after the breakthrough point.



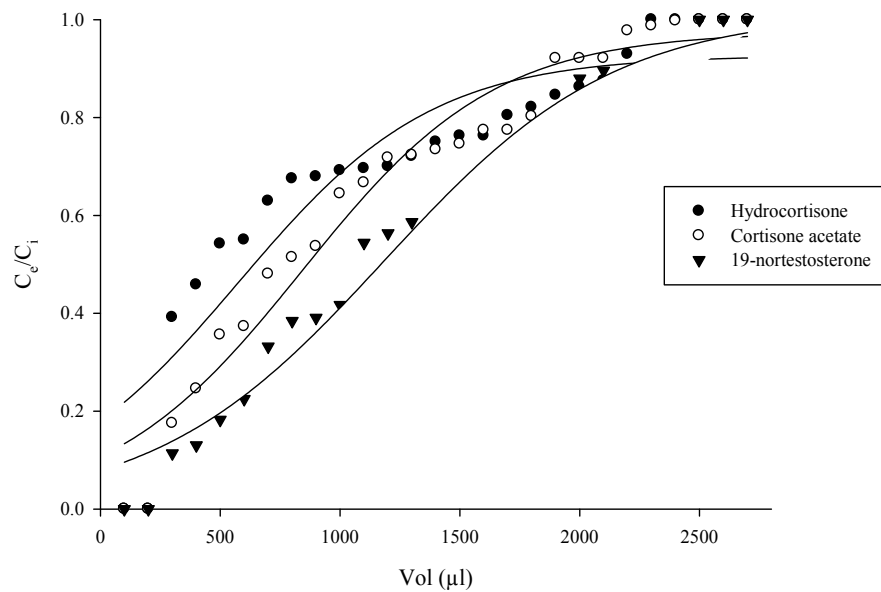
Analyte	Coefficient			R ²
	a	b	x ₀	
Hydrocortisone	0.9509 (0.02)	56.29 (15.11)	301.39 (16.84)	0.9476
Cortisone acetate	0.9399 (0.04)	146.76 (30.37)	420.39 (33.22)	0.9386
19-nortestosterone	0.9924 (0.01)	62.42 (5.18)	353.25 (5.99)	0.9945

Fig.5.40 Breakthrough curves determined for 3 steroids on commercial polyamide membrane disk sorbent bed format represented as lines of best fit using the sigmoid three parameter model.

Table.5.16 Chromatographic parameters for the polyamide filtration membrane disk sorbent bed.

	$V_B(\mu\text{l})$	$V_B(\mu\text{l})$					
Analyte	Observed	Calculated	$V_M(\mu\text{l})$	$V_R(\mu\text{l})$	N_{cal}	N_{obs}	k
Hydrocortisone	200	42.73	560.05	301.39	5.43	35.35	- 0.46
Cortisone acetate	200	-253.25	1094.77	420.29	1.55	14.55	- 0.62
19-nortestosterone	200	66.42	640.08	353.25	6.07	21.25	- 0.45

The experimental breakthrough curves for the electrospun nylon 6 nanofiber disk sorbent bed for the three steroids were fitted by the sigmoid three parameter model (Fig. 5.41). In contrast to the polyamide disk sorbent bed, the electrospun nylon 6 nanofiber disk sorbent bed exhibited a relatively flat slope indicating slower analyte mass transfer kinetics. In addition, the nature of the pores of the polyamide membrane which are formed through the membrane (Fig. 5.34 (c)) are such that there is no restriction to solvent flow minimising the contact time. However, the nanofiber sorbent bed provided improved sample-sorbent contact primarily because of the 3D structure as a result of the intertwining nature of the fibers resulting in multiple flow paths (Fig. 5.34(a)). Table 5.20 shows the calculated chromatographic parameters for the sorbent bed.



Analyte	Coefficient			R ²
	a	b	x ₀	
Hydrocortisone	0.9267 (0.04)	404.56 (82.25)	576.33 (72.94)	0.8625
Cortisone acetate	0.9753 (0.02)	403.45 (45.27)	842.82 (47.93)	0.9578
19-nortestosterone	1.0146 (0.04)	479.89 (41.48)	1184.28 (53.83)	0.9780

Fig.5.41 Breakthrough curves determined for 3 steroids on electrospun nylon 6 nanofiber disk sorbent bed format represented as lines of best fit using the sigmoid three parameter model.

Table.5.17 Chromatographic parameters for the electrospun nanofiber disk sorbent bed.

	$V_B(\mu\text{l})$	$V_B(\mu\text{l})$					
Analyte	Observed	Calculated	$V_M(\mu\text{l})$	$V_R(\mu\text{l})$	N_{cal}	N_{obs}	k
Hydrocortisone	200	-1282.7	2435.33	576.33	0.38	9.38	- 0.76
Cortisone acetate	200	-1011.1	2696.72	842.82	0.83	6.88	- 0.69
19-nortestosterone	200	-1020.9	3389.43	1184.28	1.15	5.79	- 0.65

Chapter 6

6. Conclusions and further work

6.1 Conclusions

6.1.1 Electrospinning

The experimental results obtained demonstrated that for any electrospinning set-up, the control of nanofiber deposition can be influenced by three major factors which are the magnetic field, electric field and mechanical forces. On that basis, it may be said that electrospinning research with the intent of controlling nanofiber deposition should be focussed on getting a better understanding of the influences of each of these factors.

6.1.2 Copolymers

The experimental results obtained demonstrated that emulsion polymerisation could be used as a method of polymer synthesis with the intent of controlling nanofiber functionality. It can be concluded that emulsion polymerisation could be employed for the synthesis of a wide range of polystyrene copolymers on the basis of varying the vinylic comonomer. In addition, the extent of functionality as well as spinnability of the resultant polymers can be controlled by varying the mole ratio in the polymerisation feed.

6.1.2 SPE devices

The experimental results obtained demonstrated that the electrospun nanofiber based SPE device fabrication strategies that could be employed are governed by the nanofiber mechanical strength and the electrospinning deposition procedure. The devices fabricated in the study resulted in a classification of polymers in to two as polystyrene type (relatively low mechanical strength) and nylon type (relatively high mechanical strength).

It was demonstrated that breakthrough and recovery experiments were sufficient to evaluate or predict the performance of electrospun nanofiber based SPE devices. Therefore, a similar experimental procedure can be employed to evaluate future electrospun nanofiber based SPE devices as well as screening of electrospun nanofiber based sorbent.

6.2 Further work

6.2.1 Electrospinning

The effect of the ambient environment to the electrospinning process was not investigated in this study. It is recommended that further studies be carried out on the effect of the magnetic field, electric field in a controlled environment. These experiments could be conducted in a vacuum tight Perspex box where humidity could be controlled by a fan driven draft of air from a saturated salt solution.

6.2.2 Copolymers

Surface analysis of the copolymer fibers was not conducted in this study. It is recommended that x-ray photoelectron spectroscopy (XPS) and time of flight-secondary ion mass spectrometry (ToF-SIMS) be employed to establish the extent of surface functionality of the electrospun fibers. This could give an idea of the available functional groups on the surface of the fibers. It is also recommended that molecular weight determination of the copolymers be established by gel permeation chromatography (GPC) as well as either matrix assisted laser desorption ionisation –time of flight mass spectrometry (MALDI-ToF) and nuclear magnetic resonance spectroscopy (NMR) to get an understanding of the molecular weight range as well as the type of copolymers (block, random or alternate).

6.2.3 SPE devices

It is recommended that a relationship be established with commercial companies involved in the development of chromatographic sorbent beds with the view of fabricating electrospun nanofiber based sorbents chromatographic devices. That would go a long way in simplifying and making the fabrication process more reproducible as well as the employment of automated systems for SPE. In addition, a complete characterisation of the physical properties (pore structure and surface area) in relation to an electrospinning procedure conducted in a controlled environment is recommended as the physical properties of fibers are depended on the electrospinning procedure. The development of an online breakthrough curves determination set-up is recommended. This would consist of a HPLC pump directly connected to a detection system and a computer monitor such that a plot of the frontal chromatogram can be obtained without manual collection of eluate fractions.

References

1. S. Chigome N. Torto, *Anal. Chim. Acta* 706 (2011) 25-36.
2. S. Mounicou R. Lobinski, *Pure Appl. Chem.* 80 (2008) 2565-2575.
3. J. Wang, *Acc. Chem. Res.* 35 (2002) 811-6.
4. D. M. Spence, *Analyst* 129 (2004) 102-104.
5. D. Pappas K. Wang, *Anal. Chim. Acta* 601 (2007) 26-35.
6. M. A. Martin, A. I. Olives, C. B. Del, J. C. Menendez, *An. R. Acad. Nac. Farm.* 69 (2003) 513-530.
7. C. Kranz, D. C. Eaton, B. Mizaikoff, *Anal. Bioanal. Chem.* 399 (2011) 2309-2311.
8. J. Durner, *Angew. Chem., Int. Ed.* 49 (2010) 1026-1051.
9. K. A. Cissell, S. Shrestha, S. K. Deo, *Anal. Chem.* 79 (2007) 4754-4761.
10. S. K. Sia C. D. Chin, *Nat. Chem.* 3 (2011) 659-660.
11. A. Rios, A. Escarpa, M. C. Gonzalez, A. G. Crevillen, *TrAC, Trends Anal. Chem.* 25 (2006) 467-479.
12. L. He C.-S. Toh, *Anal. Chim. Acta* 556 (2006) 1-15.
13. G. Q. Lu X. S. Zhao, *Ser. Chem. Eng.* 4 (2004) 1-13.
14. V. Chawla, S. Prakash, B. S. Sidhu, *Mater. Manuf. Processes* 22 (2007) 469-473.
15. J. Zeleny, *Physical Review* 3 (1914) 69-91.
16. T. Asefa, C. T. Duncan, K. K. Sharma, *Analyst* 134 (2009) 1980.
17. A. Vaseashta D. Dimova-Malinovska, *Sci. Technol. Adv. Mater.* 6 (2005) 312-318.
18. R. Lucena, B. M. Simonet, S. Cárdenas, M. Valcárcel, *J. Chrom A* 1218 (2011) 620-637.
19. J. Shi, Y. Zhu, X. Zhang, W. R. G. Baeyens, A. M. Garcia-Campana, *TrAC, Trends Anal. Chem.* 23 (2004) 351-360.
20. M. Valcárcel, B. M. Simonet, S. Cárdenas, *Anal. Bioanal. Chem.* 391 (2008) 1881-1887.
21. K. Scida, P. W. Stege, G. Haby, G. A. Messina, C. D. García, *Anal. Chim. Acta* 691 (2011) 6-17.
22. D. Sykora, V. Kasicka, I. Miksik, P. Rezanka, K. Zaruba, P. Matejka, V. Kral, *J. Sep. Sci.* 33 (2010) 372-387.
23. A.-H. Duan, S.-M. Xie, L.-M. Yuan, *TrAC Trends Anal. Chem.* 30 (2011) 484-491.
24. Z. Zhang, Z. Wang, Y. Liao, H. Liu, *J. Sep. Sci* 29 (2006) 1872-1878.
25. C. Nilsson, S. Birnbaum, S. Nilsson, *J. Chromatogr., A* 1168 (2007) 212-224.
26. H. Kataoka, *Anal. Bioanal. Chem.* 396 339-364.
27. H. Kataoka, *TrAC, Trends Anal. Chem.* 22 (2003) 232-244.
28. H. Kataoka, A. Ishizaki, Y. Nonaka, K. Saito, *Anal. Chim. Acta* 655 (2009) 8-29.
29. W. Wardencki, J. Curylo, J. Namiesnik, *J. Biochem. Biophys. Methods* 70 (2007) 275-288.
30. M. C. Hennion, *J. Chromatogr., A* 856 (1999) 3.
31. N. Fontanals, R. M. Marce, F. Borrull, *J. Chromatogr., A* 1152 (2007) 14.
32. N. Fontanals, R. M. Marce, F. Borrull, *Adv. Chem. Res.* 4 (2010) 107-142.
33. K. Ensing, C. Berggren, R. E. Majors, *LC-GC Eur.* 15 (2002) 16,18-20,22,24-25.
34. L. A. Berrueta, B. Gallo, F. Vicente, *Chromatographia* 40 (1995) 474-83.
35. A. Zwir-Ferenc M. Biziuk, *Pol. J. Environ. Stud.* 15 (2006) 677-690.
36. A. R. Turker, *Clean: Soil, Air, Water* 35 (2007) 548-557.
37. D.H. Everett, *Pure Appl. Chem.* 31 (1972) 577-638.

38. R. P. Schwarzenbach, P. M. Gschwend, D. M. Imboden, *Environmental Organic Chemistry*. 1992: Wiley. 681 pp.
39. B. S. Bahl, G. D. Tuli, A. Bahl, *Essentials of Physical Chemistry, 24th Edition*. 2000: S. Chand & Co. Ltd. 880 pp.
40. J. Fraissard, C. W. Conner, Editors, *Physical Adsorption: Experiment, Theory and Applications. (Proceedings of the NATO Advanced Study Institute, held 19 May-1 June 1996, in La Colle sur Loup, France.) [In: NATO ASI Ser., Ser. C, 1997; 491]*. 1997: Kluwer. 619 pp.
41. K.-U. Goss R. P. Schwarzenbach, *Environ. Sci. Technol.* 35 (2001) 1-9.
42. P. W. Lankford, W. W. Eckenfelder, Jr., Editors, *Toxicity Reduction in Industrial Effluents*. 1990: Van Nostrand Reinhold. 350 pp.
43. W. J. Thomas B. Crittenden, *Adsorption Technology and Design*. 1997: Butterworth-Heinemann. 176 pp.
44. S. Mitra J. D. Winefordner, *Sample Preparation Techniques in Analytical Chemistry*. 2003: John Wiley & Sons Inc. 400 pp.
45. H. Braus, F. M. Middleton, G. Walton, *Anal. Chem.* 23 (1951) 1160-4.
46. I. Liska, *J. Chromatogr., A* 885 (2000) 3.
47. J. K. Lokhnauth, *Solid phase microextraction and stir bar sorptive extraction coupled to ion mobility spectrometry*. 2005. p. 201 pp.
48. J. S. Fritz M. Macka, *J. Chromatogr., A* 902 (2000) 137-166.
49. J. S. Fritz, *Analytical Solid-Phase Extraction*. 1999: Wiley. 210 pp.
50. C. F. Poole, A. D. Gunatilleka, R. Sethuraman, *J. Chromatogr., A* 885 (2000) 17-39.
51. E. Matisova S. Skrabakova, *J. Chromatogr., A* 707 (1995) 145.
52. C. Crescenzi, C. A. Di, R. Samperi, A. Marcomini, *Anal. Chem.* 67 (1995) 1797-804.
53. C. A. Di M. Marchetti, *Anal. Chem.* 63 (1991) 580-5.
54. G. D'Ascenzo, A. Gentili, S. Marchese, A. Marino, D. Perret, *Environ. Sci. Technol.* 32 (1998) 1340.
55. J. H. Knox, B. Kaur, G. R. Millward, *J. Chromatogr.* 352 (1986) 3.
56. K. K. Unger, *Anal. Chem.* 55 (1983) 361A-362A, 364A, 366A, 370A, 372A, 375A.
57. K. Unger, P. Roumeliotis, H. Mueller, H. Goetz, *J. Chromatogr.* 202 (1980) 3-14.
58. J. H. Knox, K. K. Unger, H. Mueller, *J. Liq. Chromatogr.* 6 (1983) 1-36.
59. M. T. Gilbert, J. H. Knox, B. Kaur, *Chromatographia* 16 (1982) 138-46.
60. H. Colin, C. Eon, G. Guiochon, *J. Chromatogr.* 119 (1976) 41-54.
61. H. Colin, C. Eon, G. Guiochon, *J. Chromatogr.* 122 (1976) 223-42.
62. W. Golkiewicz, C. E. Werkhoven-Goewie, U. A. T. Brinkman, R. W. Frei, H. Colin, G. Guiochon, *J. Chromatogr. Sci.* 21 (1983) 27-33.
63. V. Coquart M. C. Hennion, *J. Chromatogr.* 600 (1992) 195.
64. M. C. Hennion, *J. Chromatogr., A* 885 (2000) 73-95.
65. S. Iijima, *Nature* 354 (1991) 56-8.
66. L. M. Ravelo-Pérez, A. V. Herrera-Herrera, J. Hernández-Borges, M. Á. Rodríguez-Delgado, *J. Chrom A* 1217 (2010) 2618-2641.
67. Q. Zhou, J. Xiao, W. Wang, G. Liu, Q. Shi, J. Wang, *Talanta* 68 (2006) 1309.
68. L. M. Ravelo-Perez, J. Hernandez-Borges, M. A. Rodriguez-Delgado, *J. Sep. Sci.* 31 (2008) 3612.
69. A. H. El-Sheikh, J. A. Sweileh, Y. S. Al-Degs, *Anal. Chim. Acta* 604 (2007) 119.
70. C. M. Hussain, C. Saridara, S. Mitra, *Analyst* 134 (2009) 1928-1933.
71. Y.-Q. Cai, G.-B. Jiang, J.-F. Liu, Q.-X. Zhou, *Anal. Chim. Acta* 494 (2003) 149-156.
72. Y. Cai, G. Jiang, J. Liu, Q. Zhou, *Anal. Chem.* 75 (2003) 2517-2521.
73. C. F. Poole, *TrAC, Trends Anal. Chem.* 22 (2003) 362-373.
74. P. Veverka K. Jerabek, *React. Funct. Polym.* 59 (2004) 71-79.

75. V. A. Davankov M. P. Tsyurupa, *React. Polym.* 13 (1990) 27.
76. V. Davankov, M. Tsyurupa, M. Ilyin, L. Pavlova, *J. Chromatogr., A* 965 (2002) 65-73.
77. M. P. Tsyurupa V. A. Davankov, *React. Funct. Polym.* 53 (2002) 193-203.
78. N. Masque, R. M. Marce, F. Borrull, *TrAC, Trends Anal. Chem.* 17 (1998) 384.
79. C. W. Huck G. K. Bonn, *J. Chromatogr., A* 885 (2000) 51-72.
80. I. Rodriguez, M. P. Llompert, R. Cela, *J. Chromatogr., A* 885 (2000) 291-304.
81. N. Fontanals, R. M. Marce, F. Borrull, *Curr. Anal. Chem.* 2 (2006) 171-179.
82. M. E. Leon-Gonzalez L. V. Perez-Arribas, *J. Chromatogr., A* 902 (2000) 3-16.
83. E. Caro, R. M. Marce, F. Borrull, P. A. G. Cormack, D. C. Sherrington, *TrAC, Trends Anal. Chem.* 25 (2006) 143.
84. O. Rbeida, B. Christiaens, P. Hubert, D. Lubda, K. S. Boos, J. Crommen, P. Chiap, *J. Chromatogr., A* 1030 (2004) 95.
85. O. Rbeida, B. Christiaens, P. Chiap, P. Hubert, D. Lubda, K. S. Boos, J. Crommen, *J. Pharm. Biomed. Anal.* 32 (2003) 829.
86. P. Chiap, O. Rbeida, B. Christiaens, P. Hubert, D. Lubda, K. S. Boos, J. Crommen, *J. Chromatogr., A* 975 (2002) 145.
87. M. Walles, J. Borlak, K. Levsen, *Anal. Bioanal. Chem.* 374 (2002) 1179-1186.
88. D. T. Rossi N. Zhang, *J. Chromatogr., A* 885 (2000) 97-113.
89. E. M. Thurman M. S. Mills, *Solid-Phase Extraction: Principles and Practice. [In: Chem. Anal. (N. Y.), 1998; 147]*. 1998: Wiley. 344 pp.
90. V. Pichon, H. Rogniaux, N. Fischer-Durand, S. B. Rejeb, G. F. Le, M. C. Hennion, *Chromatographia* 45 (1997) 289.
91. A. Martin-Esteban, P. Fernandez, C. Camara, *Fresenius' J. Anal. Chem.* 357 (1997) 927.
92. V. Pichon, L. Chen, M. C. Hennion, R. Daniel, A. Martel, G. F. Le, J. Abian, D. Barcelo, *Anal. Chem.* 67 (1995) 2451.
93. I. Ferrer, M.-C. Hennion, D. Barcelo, *Anal. Chem.* 69 (1997) 4508.
94. B. Sellergren, *Anal. Chem.* 66 (1994) 1578.
95. L. I. Andersson, *Analyst* 125 (2000) 1515.
96. C. Chassaing, J. Stokes, R. F. Venn, F. Lanza, B. Sellergren, A. Holmberg, C. Berggren, *J. Chromatogr., B: Anal. Technol. Biomed. Life Sci.* 804 (2004) 71-81.
97. A. Berezki, A. Tolokan, G. Horvai, V. Horvath, F. Lanza, A. J. Hall, B. Sellergren, *J. Chromatogr., A* 930 (2001) 31-38.
98. W. M. Mullett E. P. C. Lai, *J. Pharmaceut. Biomed. Anal.* 21 (1999) 835-843.
99. C. Berggren, S. Bayouth, D. Sherrington, K. Ensing, *J. Chromatogr., A* 889 (2000) 105-110.
100. G. Theodoridis P. Manesiotis, *J. Chromatogr., A* 948 (2002) 163-169.
101. K. M. Li, L. P. Rivory, S. J. Clarke, *Curr. Pharm. Anal.* 2 (2006) 95-102.
102. L. I. Andersson, *J. Chromatogr., B: Biomed. Sci. Appl.* 739 (2000) 163-173.
103. E. M. Thurman K. Snavely, *TrAC, Trends Anal. Chem.* 19 (2000) 18-26.
104. F. E. Ahmed, *TrAC, Trends Anal. Chem.* 20 (2001) 649-661.
105. D. D. Blevins D. O. Hall, *LC GC: Liquid Chromatography, Gas Chromatography* 16 (1998) S16.
106. M. Abdel-Rehim, *J. Chromatogr., A* 1217 (2010) 2569-2580.
107. M. Abdel-Rehim, *Method and apparatus for sample preparation using solid phase microextraction*. 2003, Astrazeneca AB, Swed. . p. 16 pp.
108. L. Kovatsi, K. Rentifis, D. Giannakis, S. Njau, V. Samanidou, *J. Sep. Sci.* 34 (2011) 1716-1721.
109. R. P. Belardi J. B. Pawliszyn, *Water Pollut. Res. J. Can.* 24 (1989) 179.

110. S. Risticovic, V. H. Niri, D. Vuckovic, J. Pawliszyn, *Anal. Bioanal. Chem.* 393 (2009) 781.
111. F. M. Musteata J. Pawliszyn, *TrAC Trends Anal. Chem.* 26 (2007) 36-45.
112. D. Vuckovic, X. Zhang, E. Cudjoe, J. Pawliszyn, *J. Chrom. A* 1217 (2010) 4041-4060.
113. L. Muller. *Field analysis by SPME*. 1999: Royal Society of Chemistry.
114. Z. Zhouyao, J. Poerschmann, J. Pawliszyn, *Anal. Commun.* 33 (1996) 219-221.
115. M. F. Alpendurada, *J Chromatogr A* 889 (2000) 3-14.
116. J. Pawliszyn Editor, *Applications of Solid Phase Microextraction*. 1999: Royal Soc. Chem. 655 pp.
117. L. Cardenes, J. H. Ayala, A. M. Afonso, V. Gonzalez, *J. Chromatogr., A* 1030 (2004) 87-93.
118. A. Westberg, D. Momcilovic, F. Bjoerk, S. Karlsson, *Polym. Degrad. Stab.* 94 (2009) 914-920.
119. E. B. Razote, R. G. Maghirang, L. M. Seitz, I. J. Jeon, *Trans. ASAE* 47 (2004) 1231-1238.
120. V.-S. Wang M.-Y. Lu, *J. Chromatogr., B: Anal. Technol. Biomed. Life Sci.* 877 (2009) 24-32.
121. M. Abalos, J. M. Bayona, F. Ventura, *Anal. Chem.* 71 (1999) 3531-3537.
122. W. S. A. Scheppers Editor, *Solid Phase Microextraction: A Practical Guide*. 1999: Dekker. 257 pp.
123. A. Kumar, Gaurav, A. Malik, D. Tewary, B. Singh, *Anal. Chim. Acta* 610 (2008) 1-14.
124. S. L. Chong, D. Wang, J. D. Hayes, B. W. Wilhite, A. Malik, *Anal. Chem.* 69 (1997) 3889-3898.
125. S. Bigham, J. Medlar, A. Kabir, C. Shende, A. Alli, A. Malik, *Anal. Chem.* 74 (2002) 752-761.
126. A. L. Lopes F. Augusto, *J. Chrom A* 1056 (2004) 13-19.
127. W. M. Mullett, P. Martin, J. Pawliszyn, *Anal. Chem.* 73 (2001) 2383-2389.
128. E. H. M. Koster, C. Crescenzi, H. W. den, K. Ensing, J. G. J. de, *Anal. Chem.* 73 (2001) 3140-3145.
129. E. Baltussen, P. Sandra, F. David, C. Cramers, *J. Microcolumn Sep.* 11 (1999) 737-747.
130. J. Vercauteren, C. Peres, C. Devos, P. Sandra, F. Vanhaecke, L. Moens, *Anal. Chem.* 73 (2001) 1509-1514.
131. T. Hyotylainen M.-L. Riekkola, *Anal Chim Acta* 614 (2008) 27-37.
132. H. Kataoka, *Anal. Bioanal. Chem.* 396 (2010) 339-364.
133. J. A. Koziel, M. Odziemkowski, J. Pawliszyn, *Anal. Chem.* 73 (2001) 47-54.
134. A. Wang, F. Fang, J. Pawliszyn, *J. Chromatogr., A* 1072 (2005) 127-135.
135. I. Eom, *J. Chrom. A* 1196-1197 (2008) 3-9.
136. I. Bruheim, X. Liu, J. Pawliszyn, *Anal. Chem.* 75 (2003) 1002-1010.
137. L. Bragg, Z. Qin, M. Alae, J. Pawliszyn, *J. Chromatogr. Sci.* 44 (2006) 317-323.
138. F. Augusto, E. Carasek, R. G. C. Silva, S. R. Rivellino, A. D. Batista, E. Martendal, *J. Chromatogr., A* 1217 2533-2542.
139. E. Turiel A. Martín-Esteban, *Anal. Chim. Acta* 668 (2010) 87-99.
140. W. E. Teo S. Ramakrishna, *Nanotechnology* 17 (2006) R89-R106.
141. G. Taylor, *Proceedings of the Royal Society of London. A. Mathematical and Physical Sciences* 313 (1969) 453-475.
142. J. Doshi D. H. Reneker, *J. Electrostat.* 35 (1995) 151.
143. T. Ondarcuhu C. Joachim, *Europhys. Lett.* 42 (1998) 215.

144. L. Feng, S. Li, H. Li, J. Zhai, Y. Song, L. Jiang, D. Zhu, *Angew. Chem., Int. Ed.* 41 (2002) 1221.
145. P. X. Ma R. Zhang, *J. Biomed. Mater. Res.* 46 (1999) 60.
146. J. D. Hartgerink, E. Beniash, S. I. Stupp, *Science* 294 (2001) 1684.
147. F.-L. Zhou, R.-H. Gong, I. Porat, *Polym. Int* 58 (2009) 331-342.
148. S. A. Theron, A. L. Yarin, E. Zussman, E. Kroll, *Polymer* 46 (2005) 2889-2899.
149. J. Bowman, M. Taylor, V. Sharma, A. Lynch, S. Chadha, *Mater. Res. Soc. Symp. Proc.* 752 (2003) 15-19.
150. Y. Yamashita, A. Tanaka, H. Miyake, A. Higashiyama, H. Kato. *Establishment of nano fiber preparation technique for nanocomposite.* 2007.
151. Y. Yang, Z. Jia, Q. Li, L. Hou, H. Gao, L. Wang, Z. Guan. *Multiple jets in electrospinning.* 2007.
152. H.-y. Kim, *A bottom-up electrospinning devices, and nanofibers prepared by using the same.* 2005, Raisio Chemicals Korea Inc., S. Korea .
153. O. Jirsak, F. Sanetnik, D. Lukas, V. Kotek, L. Martinova, J. Chaloupek, *Process and apparatus for producing nanofibers from polymer solution by electrostatic spinning.* 2004, Technicka Univerzita v Liberci, Czech Rep. . p. 13 pp.
154. S. Petrik M. Maly, *Mater. Res. Soc. Symp. Proc.* 1240E (2010) Paper #: 1240-WW03-07.
155. A. Frenot I. S. Chronakis, *Curr. Opin. Colloid Interface Sci.* 8 (2003) 64.
156. S. Ramakrishna, K. Fujihara, W.-E. Teo, T. Yong, Z. Ma, R. Ramaseshan, *Mater. Today* 9 (2006) 40.
157. A. Greiner J. H. Wendorff, *Angew. Chem., Int. Ed.* 46 (2007) 5670.
158. M. Valcárcel, S. Cárdenas, B. M. Simonet, Y. Moliner-Martínez, R. Lucena, *TrAC Trends Anal. Chem* 27 (2008) 34-43.
159. C.-K. Liu, K. Lai, W. Liu, M. Yao, R.-J. Sun, *Polym Int* 58 (2009) 1341-1349.
160. G.-Y. Oh, Y.-W. Ju, M.-Y. Kim, H.-R. Jung, H. J. Kim, W.-J. Lee, *Sci. Tot. Environ* 393 (2008) 341-347.
161. W. G. Shim, C. Kim, J. W. Lee, J. J. Yun, Y. I. Jeong, H. Moon, K. S. Yang, *J. Appl. Polym. Sci* 102 (2006) 2454-2462.
162. N.-N. Bui, B.-H. Kim, K. S. Yang, M. E. Dela Cruz, J. P. Ferraris, *Carbon* 47 (2009) 2538-2539.
163. L. Y. Yeo J. R. Friend, *J. Exp. Nanosci.* 1 (2006) 177.
164. E. T. Thostenson, C. Li, T.-W. Chou, *Compos. Sci. Technol.* 65 (2005) 491.
165. R. Sen, B. Zhao, D. Perea, M. E. Itkis, H. Hu, J. Love, E. Bekyarova, R. C. Haddon, *Nano Lett.* 4 (2004) 459.
166. F. Ko, Y. Gogotsi, A. Ali, N. Naguib, H. Ye, G. Yang, C. Li, P. Willis, *Adv. Mater.* 15 (2003) 1161.
167. C. Shao, H. Kim, J. Gong, D. Lee, *Nanotechnology* 13 (2002) 635.
168. S.-S. Choi, S. G. Lee, S. S. Im, S. H. Kim, Y. L. Joo, *J. Mater. Sci. Lett.* 22 (2003) 891.
169. A. C. Patel, S. Li, C. Wang, W. Zhang, Y. Wei, *Chem. Mater.* 19 (2007) 1231.
170. H. Guan, C. Shao, S. Wen, B. Chen, J. Gong, X. Yang, *Inorg. Chem. Commun.* 6 (2003) 1302.
171. S. Madhugiri, B. Sun, P. G. Smirniotis, J. P. Ferraris, K. J. Balkus, *Microporous Mesoporous Mater.* 69 (2004) 77.
172. C. Shao, H. Guan, Y. Liu, J. Gong, N. Yu, X. Yang, *J. Cryst. Growth* 267 (2004) 380.
173. H. Dai, J. Gong, H. Kim, D. Lee, *Nanotechnology* 13 (2002) 674.
174. P. K. Panda S. Ramakrishna, *J. Mater. Sci* 42 (2007) 2189-2193.

175. D. Qi, X. Kang, L. Chen, Y. Zhang, H. Wei, Z. Gu, *Anal. Bioanal. Chem.* 390 (2008) 929.
176. Z. Liu, X. Kang, F. Fang, *Microchim. Acta* 168 59.
177. X. Kang, C. Pan, Q. Xu, Y. Yao, Y. Wang, D. Qi, Z. Gu, *Anal. Chim. Acta* 587 (2007) 75-81.
178. Y. Zhang, X. Kang, L. Chen, C. Pan, Y. Yao, Z.-Z. Gu, *Anal. Bioanal. Chem* 391 (2008) 2189-2197.
179. X.-j. Kang, L.-q. Chen, Y.-y. Zhang, Y.-w. Liu, Z.-z. Gu, *J. Sep. Sci* 31 (2008) 3272-3278.
180. S. Chigome, G. Darko, U. Buttner, N. Torto, *Anal. Methods* 2 (2010) 623.
181. L.-Q. Chen, X.-J. Kang, J. Sun, J.-J. Deng, Z.-Z. Gu, Z.-H. Lu, *J. Sep. Sci.* 33 2369.
182. Y. Wang, L. Chen, X. Kang, Q. Xu, Z. Gu, *Zhongguo Yaolixue Tongbao* 23 (2007) 832.
183. X. Kang, H. Wei, Y. Zhang, L. Chen, Z. Gu. *Proceedings of the International Forum on Post-Genome Technologies* (2006), 241-245.
184. F. Fang, X. J. Kang, Z. Y. Liu, Y. Q. Ma, Z. Z. Gu, *Chin. Chem. Lett* 20 (2009) 1491-1494.
185. Q. Xu, S.-Y. Wu, M. Wang, X.-Y. Yin, Z.-Y. Wen, W.-N. Ge, Z.-Z. Gu, *Chromatographia* 71 487.
186. Q. Xu, X. Yin, S. Wu, M. Wang, Z. Wen, Z. Gu, *Microchim. Acta* 168 (2010) 267-275.
187. Q. Xu, N. Zhang, X. Yin, M. Wang, Y. Shen, S. Xu, L. Zhang, Z. Gu, *J. Chromatogr., B: Anal. Technol. Biomed. Life Sci.* 878 2403.
188. K. Yoshimatsu, L. Ye, J. Lindberg, I. S. Chronakis, *Biosens. Bioelectron* 23 (2008) 1208-1215.
189. C.-h. Zheng, F.-g. Meng, X.-r. Mo, D.-y. Zhao, M.-m. Yang, *Fenxi Shiyanshi* 29 (2010) 80.
190. C. Zheng, L. Yang, Z. Yao, D. Zhao, M. Yang, *Fenxi Ceshi Xuebao* 28 (2009) 926.
191. Z. Yao, L. Yang, C. Zheng, M. Yang, *Huaxue Tongbao* 72 (2009) 845.
192. L. Zhang Y.-L. Hsieh, *Nanotechnology* 17 (2006) 4416.
193. C. L. Casper, J. S. Stephens, N. G. Tassi, D. B. Chase, J. F. Rabolt, *Macromolecules* 37 (2004) 573.
194. A. Gupta, C. D. Saquing, M. Afshari, A. E. Tonelli, S. A. Khan, R. Kotek, *Macromolecules* 42 (2009) 709.
195. Q. Shi, N. Vitchuli, L. Ji, J. Nowak, M. McCord, M. Bourham, X. Zhang, *J. Appl. Polym. Sci* 120 (2011) 425-433.
196. N. Fontanals, R. M. Marcé, F. Borrull, *TrAC Trends. Anal. Chem* 24 (2005) 394-406.
197. A. Kloskowski, M. Pilarczyk, A. Przyjazny, J. Namieśnik, *Critical Reviews in Analytical Chemistry* 39 (2009) 43-58.
198. L.-S. Wan, J. Wu, Z.-K. Xu, *Macro. Rapid. Comm* 27 (2006) 1533-1538.
199. C. E. Kibbey M. E. Meyerhoff, *J. Chromatogr.* 641 (1993) 49.
200. S. Y. Oh, K. P. Kim, M. W. Jung, D. J. Baek, H. B. Li, K. J. Paeng, *Chromatographia* 57 (2003) 665.
201. D.-G. Kim, M.-W. Jung, I. R. Paeng, J.-S. Rhee, K.-J. Paeng, *Microchem. J.* 63 (1999) 134.
202. A. M. Alak, *Cyclodextrin stationary phases: synthesis, characterization and applications in liquid chromatography*. 1986. p. 138 pp.
203. T. Uyar, R. Havelund, Y. Nur, J. Hacaloglu, F. Besenbacher, P. Kingshott, *J. Membr. Sci.* 332 (2009) 129.
204. C. Yao, X. Li, K. G. Neoh, Z. Shi, E. T. Kang, *J. Membr. Sci.* 320 (2008) 259.

205. Z. Ma, K. Masaya, S. Ramakrishna, J. Membr. Sci 282 (2006) 237-244.
206. J. H. T. Luong A. L. Nguyen, Adv. Biochem. Eng./Biotechnol. 47 (1992) 137.
207. I. S. Chronakis, B. Milosevic, A. Frenot, L. Ye, Macromolecules 39 (2006) 357.
208. J. S. Fritz J. J. Masso, J. Chromatogr., A 909 (2001) 79.
209. X.-J. Kang, L.-Q. Chen, Y. Wang, Y.-Y. Zhang, Z.-Z. Gu, Biomed. Microdevices 11 (2009) 723-729.
210. J. W. Zewe, J. K. Steach, S. V. Olesik, Anal. Chem. 82 5341.
211. K. H. Choi, S. Khan, H. W. Dang, Y. H. Doh, S. J. Hong, Jpn. J. Appl. Phys. 49 05EC08/1.
212. S. Zhang K. Kawakami, Int. J. Pharm. 397 211.
213. D. Pliszka, S. Sundarrajan, A. Jaworek, A. Krupa, M. Lackowski, S. Ramakrishna, Adv. Sci. Technol. 60 (2008) 117.
214. J. A. Ajao, A. A. Abiona, S. Chigome, A. Y. Fasasi, G. A. Osinkolu, M. Maaza, J. Mater. Sci 45 (2010) 2324-2329.
215. A. A. Abiona, S. Chigome, J. A. Ajao, A. Y. Fasasi, N. Torto, G. A. Osinkolu, M. Maaza, Int. J. Polym. Mater. 59 (2010) 818-827.
216. A. A. Abiona, J. A. Ajao, S. Chigome, J. B. K. Kana, G. A. Osinkolu, M. Maaza, J. Sol-Gel Sci. Technol. 55 (2010) 235-241.
217. J. A. Ajao, A. Abiona, S. Chigome, K. J. B. Kana, M. Maaza, J. Mater. Sci. 45 (2010) 713-718.
218. S. Chigome, A. A. Abiona, J. A. Ajao, J. K. Kana, L. Guerbous, N. Torto, M. Maaza, Int. J. Polym. Mater. 59 (2010) 863-872.
219. P. Katta, M. Alessandro, R. D. Ramsier, G. G. Chase, Nano Lett 4 (2004) 2215-2218.
220. D. H. Reneker, A. L. Yarin, H. Fong, S. Koombhongse, J. Appl. Phys. 87 (2000) 4531-4547.
221. T. A. Kowalewski, S. BŁoński, S. Barral, Bulletin of the Polish Academy of Sciences: Technical Sciences 53 (2005) 385-394.
222. Y. Wu, J. Y. Yu, J. H. He, Y. Q. Wan, Chaos, Solitons and Fractals 32 (2007) 5-7.
223. D. Li, Y. Wang, Y. Xia, Nano Lett. 3 (2003) 1167-1171.
224. Y. Wu, L. A. Carnell, R. L. Clark, Polymer 48 (2007) 5653-5661.
225. Z.-Z. Gu, H. Chen, S. Zhang, L. Sun, Z. Xie, Y. Ge, Colloids Surf., A 302 (2007) 312-319.
226. H. A. van B. Gilbert. *Emulsion polymerisation*. 2005: Blackwell Publishing Ltd.
227. D. Birkett, Chem. Ind. (London, U. K.) (2006) 24.
228. F. R. Mayo F. M. Lewis, J. Am. Chem. Soc. 66 (1944) 1594-1601.
229. W. Z. Xu P. A. Charpentier, Ind. Eng. Chem. Res. 48 (2009) 1384-1390.
230. G. Odian, *Principles of Polymerization, 4th Edition*. 2004: Wiley. 768 pp.
231. P. Govindaiah, J. M. Lee, Y. J. Jung, S. J. Lee, J. H. Kim, J. Mater. Chem. 19 (2009) 3529-3537.
232. Y. Tran P. Auroy, J. Am. Chem. Soc. 123 (2001) 3644-3654.
233. E. Teixeira-Neto, C. A. P. Leite, A. H. Cardoso, d. S. M. d. C. V. Medeiros, M. Braga, F. Galembeck, J. Colloid Interface Sci. 231 (2000) 182-189.
234. S. B. Brijmohan, S. Swier, R. A. Weiss, M. T. Shaw, Ind. Eng. Chem. Res. 44 (2005) 8039-8045.
235. R. Chen, F. Peng, S. Su, J. Appl. Polym. Sci. 108 (2008) 2712-2717.
236. D. Arunbabu, Z. Sanga, K. M. Seenimeera, T. Jana, Polym. Int. 58 (2009) 88-96.
237. A. Habi S. Djadoun, Thermochim. Acta 469 (2008) 1-7.
238. J.-Y. Moon, H.-J. Jung, M. H. Moon, B. C. Chung, M. H. Choi, Steroids 73 (2008) 1090-1097.
239. M. E. Davis M. E. Brewster, Nat. Rev. Drug Discovery 3 (2004) 1023-1035.

240. G. Crini M. Morcellet, *J. Sep. Sci.* 25 (2002) 789-813.
241. E. Bednarek, W. Bocian, J. Poznanski, J. Sitkowski, N. Sadlej-Sosnowska, L. Kozerski, *J. Chem. Soc., Perkin Trans. 2* (2002) 999-1004.
242. S. Li W. C. Purdy, *Chem. Rev.* 92 (1992) 1457-70.
243. L. Li Y.-L. Hsieh, *Polymer* 46 (2005) 5133-5139.
244. S. V. Fridrikh, J. H. Yu, M. P. Brenner, G. C. Rutledge, *Phys. Rev. Lett.* 90 (2003) 144502/1-144502/4.
245. S. De Vrieze, B. De Schoenmaker, Ö. Ceylan, J. Depuydt, L. Van Landuyt, H. Rahier, G. Van Assche, K. De Clerck, *J. Appl. Polym. Sci* 119 (2011) 2984-2990.
246. O. Hardick, B. Stevens, D. G. Bracewell, *J. Mater. Sci* 46 (2011) 3890-3898.
247. H.-J. Cho, J. D. Kim, W.-Y. Lee, B. C. Chung, M. H. Choi, *Anal. Chim. Acta* 632 (2009) 101-108.
248. C. S. Sychov, V. A. Davankov, N. A. Proskurina, A. J. Mikheeva, *LC-GC Eur.* 22 (2008) 20, 22-24, 26-27.
249. K. Bielicka-Daszkiwicz A. Voelkel, *Talanta* 80 (2009) 614-621.
250. R. Ferrer, J. L. Beltran, J. Guiteras, *Anal. Chim. Acta* 346 (1997) 253-258.
251. M. Mihaly, E. S. Andreiadis, E. Pincovschi, *Sci. Bull. - Univ. "Politeh." Bucharest, Ser. B* 67 (2005) 57-64.
252. E. Bacalum, M. Radulescu, E.-E. Iorgulescu, V. David, *Rev. Roum. Chim.* 56 (2011) 137-143.
253. S. V. Romanenko A. G. Stromberg, *J. Anal. Chem.* 55 (2000) 1024-1028.
254. W. D. Hillis, *Curr Biol* 3 (1993) 79-81.
255. S. D. Kolev, *Anal. Chim. Acta* 229 (1990) 183-9.
256. V. F. Pozhidaev, Y. B. Rubinshtein, G. Y. Golberg, S. A. Osadchii, *Chem. Pet. Eng.* 45 (2009) 460-467.
257. M. Ramirez C, M. Pereira da Silva, S. G. Ferreira L, O. Vasco E, *Journal of Hazardous Materials* 146 (2007) 86-90.
258. C. E. Werkhoven-Goewie, U. A. T. Brinkman, R. W. Frei, *Anal. Chem.* 53 (1981) 2072-80.
259. P. Lövkvist J. Å. Jönsson, *Anal. Chem* 59 (1987) 818-821.
260. G. I. Senum, *Environ. Sci. Technol.* 15 (1981) 1073-5.
261. P. J. Dumont J. S. Fritz, *J. Chromatogr., A* 691 (1995) 123-31.
262. T. J. Sill R. H. A. von, *Biomaterials* 29 (2008) 1989-2006.
263. X. Li, B. Ding, J. Lin, J. Yu, G. Sun, *J. Phys. Chem. C* 113 (2009) 20452-20457.
264. S. A. Bortolato, J. A. Arancibia, G. M. Escandar, *Anal. Chim. Acta* 613 (2008) 218-227.
265. M. S. Scandrett E. J. Ross, *Clin. Chim. Acta* 72 (1976) 165-9.
266. Q. Xu, S.-Y. Wu, M. Wang, X.-Y. Yin, Z.-Y. Wen, W.-N. Ge, Z.-Z. Gu, *Chromatographia* 71 (2009) 487-492.
267. J. S. Bierman M. V. Campognone, *LCGC North Am.* 27 (2009) 24-26.